



AD

JANSKY & BAILEY ENGINEERING DEPARTMENT

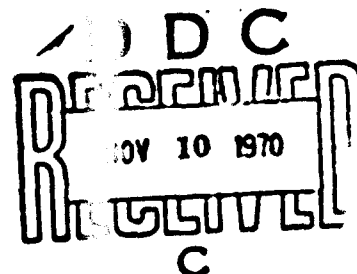
AD 714300

TROPICAL PROPAGATION RESEARCH (U) FINAL REPORT, VOLUME II

Prepared by
Richard G. Robertson
John J. Hicks
Charles B. Sykes
Per A. Anti

Submitted to
U. S. ARMY ELECTRONICS COMMAND
Fort Monmouth, New Jersey

Contract No.
DA 36-039 SC-90889



Sponsored by
ADVANCED RESEARCH PROJECTS AGENCY
Department of Defense
ARPA Order 371
and
U. S. ARMY ELECTRONICS COMMAND

This document has been approved for public release and sale; its distribution is unlimited.

ATLANTIC  RESEARCH

A DIVISION OF THE SUSQUEHANNA CORPORATION

Manufactured by
NATIONAL TECHNICAL
INFORMATION SERVICE
Springfield, Va. 22904

133

TROPICAL PROPAGATION RESEARCH (U)

FINAL REPORT, VOLUME III

Prepared by
Richard G. Robertson
John J. Hicks
Charles B. Sykes
Per A. Anti

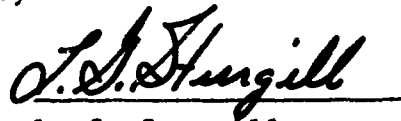
Submitted to
U. S. ARMY ELECTRONICS COMMAND
Fort Monmouth, New Jersey

Contract No.
DA 36-039 SC-90889

Sponsored by
ADVANCED RESEARCH PROJECTS AGENCY
Department of Defense
ARPA Order 371
and
U. S. ARMY ELECTRONICS COMMAND

This document has been approved for public release
and sale, its distribution is unlimited.

Approved by:


L. G. Sturgill
Project Director

The Jansky & Bailey Engineering Department
Atlantic Research Corporation
A Division of The Susquehanna Corporation
Shirley Highway at Edsall Road
Alexandria, Virginia 22314

SUMMARY

This Final Report Volume III is sequential to Volumes I and II previously prepared on an extensive experimental and theoretical research program on the propagation of radio signals in tropical jungle environments. The over-all objective of this program is to collect and analyze radio propagation data from actual representative environments needed to advance the state-of-the-art in the design and development of improved radio communication systems in these environments.

The previous two reports are concerned primarily with CW measurements, and analysis of the data resulting therefrom. Generally speaking, the models obtained from these results may be classed as CW, or narrowband, results. The derived models, such as the slab model of the jungle, yield average, or mean, predictions of radio path loss.

This Final Report summarizes the results of a series of specialized measurements, using pulse and swept-frequency transmitted signals. Various types of amplitude, frequency, and phase displays were recorded at the test receiver locations. The objective of these measurements was to obtain data which exhibit the multipath characteristics of the jungle path.

This report discusses the methods of making these measurements, and the results of a limited analysis of the data. The probability distributions of signal amplitude at VHF in the tropical rain forest test area in Thailand are presented. These distributions are generally a prerequisite to the practical estimation of error rate performance of digital, or wideband, systems in this type of environment. An example

is given in which the experimental probability distributions are used to obtain the error rate in an FSK modulation system in this type of environment.

TABLE OF CONTENTS

	<u>Page</u>
SUMMARY.....	i
LIST OF FIGURES.....	v
LIST OF TABLES.....	ix
1. INTRODUCTION.....	1
2. GENERAL DISCUSSION.....	5
3. DATA COLLECTION AND ANALYSIS - CW.....	7
3.1 Experimental Area.....	8
3.2 Equipment and Measurement Procedures.....	16
3.3 Analysis and Discussion.....	26
3.4 Probability of Error for Digital Transmission..	69
4. DATA COLLECTION AND ANALYSIS - SWEPT FREQUENCY.....	81
4.1 Experimental Equipment and Procedures.....	81
4.2 Data Analysis and Discussion.....	90
5. REFERENCES.....	121
DOCUMENT CONTROL DATA FORM DD 1473	
DISTRIBUTION LIST	

LIST OF FIGURES

<u>Figure No.</u>	<u>Page</u>
3.1.1	Locations of Thailand Test Areas..... 9
3.1.2	Sketch of Area II Test Site..... 10
3.1.3	Terrain and Tree Profiles Along Main Access Trail..... 12
3.2.1	Block Diagram of Transmitter and Receiver..... 17
3.2.2	Star Field-Point Measurement Paths Within 200-Foot Diameter Circle..... 19
3.3.1	Probability Distribution Curves..... 34
3.3.2	Probability Distribution Curves..... 35
3.3.3	Signal Recording at Star Field-Point FP-14 (50, 80, H, d, 6)..... 36
3.3.4	Plot of Experimental Probability Distribution for Data of Figure 3.3.3..... 38
3.3.5a	Signal Recording at Star Field-Point Y-20 (100, 80, V, d, 6)..... 39
3.3.5b	Signal Recording at 0.45° Relative to Radial, Y-20 (100, 80, V, d, 6)..... 40
3.3.5c	Signal Recording at 090° (Transverse) (100, 80, V, d, 6)..... 41
3.3.5d	Signal Recording at 135° Relative to Radial (100, 80, V, d, 6)..... 42
3.3.6	Plot of Experimental Probability Distribution for Data of Figure 3.3.5..... 43
3.3.7	Cumulative Probability Distribution of Long Spatial Variations About Deterministic Mean..... 53
3.3.8	Amplitude Spread Between Probability Limits Versus γ_F for Rician Distribution..... 57

LIST OF FIGURES (continued)

<u>Figure No.</u>		<u>Page</u>
3.3.9	Cumulative Distribution of γ_F and m for Data in Table 3.3.5.....	61
3.3.10	Plot of m_i Versus γ_F for Data from Table 3.3.5.....	62
3.3.11	Plot of $m/\sqrt{2} \sigma$ Versus γ_F for a Rician Distribution.....	65
3.3.12	Plot of $\sqrt{2} \sigma$, A, and Terrain Elevation Over Main Access Trail.....	67
3.4.1	Probability of Error for Noncoherent, Binary, FSK System.....	71
3.4.2	Probability of Error for a Noncoherent FSK System in a Rician Fading Channel.....	74
3.4.3	Average Probability of Error for Noncoherent FSK System Operating at 50 MHz in Area II....	77
3.4.4	Average Probability of Error at 100 MHz.....	78
3.4.5	Average Probability of Error at 150 MHz.....	79
4.1.1	Transmitter Instrumentation Block Diagram for Amplitude and Phase vs. Swept- Frequency Measurements.....	83
4.1.2	Receiver Instrumentation Block Diagram for Amplitude vs. Swept-Frequency Measurements....	84
4.1.3	Receiver Instrumentation Block Diagram for Amplitude and Phase vs. Swept-Frequency Measurements.....	85
4.2.1	Signal Amplitude as a Function of Distance and Frequency.....	91
4.2.2	Diagram of Configurations of Swept-Frequency Runs Analyzed.....	93
4.2.3	Illustration of Transmitted Amplitude Versus Frequency.....	98

LIST OF FIGURES (continued)

<u>Figure No.</u>	<u>Page</u>
4.2.4	Normalized Frequency Correlation Coefficient... 101
4.2.5	Normalized Frequency Correlation Coefficient... 102
4.2.6	Normalized Frequency Correlation Coefficient... 103
4.2.7	Normalized Frequency Correlation Coefficient... 104
4.2.8	Normalized Frequency Correlation Coefficient... 105
4.2.9	Normalized Frequency Correlation Coefficient... 106
4.2.10	Normalized Frequency Correlation Coefficient... 107
4.2.11	Normalized Frequency Correlation Coefficient... 108
4.2.12	Normalized Frequency Correlation Coefficient... 109
4.2.13	Normalized Frequency Correlation Coefficient... 110
4.2.14	Normalized Frequency Correlation Coefficient... 111
4.2.15	Normalized Frequency Correlation Coefficient... 112
4.2.16	Normalized Frequency Correlation Coefficient... 113
4.2.17	Normalized Frequency Correlation Coefficient... 114
4.2.18	Normalized Frequency Correlation Coefficient... 115
4.2.19	Normalized Frequency Correlation Coefficient... 116
4.2.20	Normalized Frequency Correlation Coefficient... 117
4.2.21	Normalized Frequency Correlation Coefficient... 118
4.2.22	Normalized Frequency Correlation Coefficient... 119

LIST OF TABLES

<u>Table No.</u>		<u>Page</u>
3.1.1	Measurement Trails for Long Trail Runs.....	11
3.1.2	Environmental Characteristics of Star Field-Points.....	13
3.1.3	Environmental Description of Long Trails.....	15
3.2.1	Combination of Test Parameters for Star Field Points Measurements.....	21
3.2.2	Combinations of Test Parameters for High Antenna Measurements.....	24
3.2.3	Combinations of Test Parameters for Long Trail Measurements.....	27
3.3.1	Time in Seconds That the Signals of Figure 3.3.3 Exceed Given Amplitude Levels.....	37
3.3.2	Time in Seconds That the Signals of Figure 3.3.5 Exceed Given Amplitude Levels.....	44
3.3.3	The Parameter γ_F for Star Field-Point Measurements.....	46
3.3.4	The Parameter γ_F for High Antenna Measurements.....	47
3.3.5	Characteristics of Signal Along Main Access Trail (50, 20, H, d, 10).....	60

1. INTRODUCTION

This Final Report Volume III contains the results from the third phase of an extensive experimental and theoretical program on radio propagation in a tropical jungle environment. This program is sponsored by the Advanced Research Projects Agency, and is contractually and technically directed by the U. S. Army Electronics Command, Fort Monmouth, New Jersey. The purpose of this program is to obtain basic experimental and theoretical data, and related information, which will be useful to the improvement of presently available radio equipment, as well as in the design and development of new equipment for tactical communications in such environments. While this program is aimed primarily at the problems encountered in ground-based, tactical radio communications systems, the measured data and the results deduced therefrom are general enough to also be applicable to many problems in the fields of electromagnetic surveillance and intrusion detection.

The first phase of this program involved an extensive series of propagation measurements in a tropical forested area in central Thailand. In terms of its climate and the character of its vegetation, this area is characterized as a wet-dry, or monsoon, semi-evergreen type of tropical forest. In order to correlate the measured radio propagation data with the natural characteristics of the environment that influence propagation, the environmental characteristics have been measured in a variety of ways. The total compilation of the radio propagation and environmental data from this first phase of measurements is, therefore, representative of radio wave behavior in one type of tropical vegetated environment that is common to much of southeast Asia, as well as other regions of the world.

The second phase of field measurements was carried out in a selected test area in southern Thailand having the environmental characteristics of a tropical rain forest. Here, the annual rainfall is greater than in central Thailand, and the physical characteristics of the vegetation per unit of land area are correspondingly different. Careful environmental measurements were also included in the second phase experiment.

The first two phases of effort primarily addressed the gross behavior of radio propagation in forested environments. That is, an extended amount of experimental and theoretical work was required to arrive at a model which would predict mean, or average, values of radio path loss. The first two phases of effort resulted in the development of a theoretical model, known as the slab, or lateral wave, model which gives satisfactory predictions of mean, or average, radio path loss when the correct values of forest dielectric constant, conductivity, and height are used.

This report summarizes the results from the third phase of measurements conducted in the tropical rain forest area in Thailand. This third phase of measurements actually consisted of a series of specialized experiments. Prompted by a growing need for data and other information that would be useful to more sophisticated digital, or wideband, systems, the third phase of this program branched into a new avenue of investigations. A series of specialized measurements, using pulse and swept-frequency transmissions, were conducted in the rain forest test area in Thailand, herein identified as Area II. The objective of these measurements, and analysis of the resulting data, was to gain some insight into the multipath characteristics for ground-to-ground terminals in this type of environment. This report summarizes the results of this third phase of effort.

The general environmental characteristics of the test area are described in Section 3, followed by a description of experimental equipment and procedures used in conducting the measurements. The results of a limited amount of analysis are presented in the next section. With the methods used to obtain the experimental data, considerably more data was obtained than could be reduced and analyzed under the scope of the present contract. However, the analysis that was accomplished has produced some important findings, and strongly suggest that the reduction and analysis of this data should be continued.

To illustrate the application of the results of this analysis to a general type of system problem, Section 3.4 presents an example of the theoretical calculation of the error rate for a typical FSK system in this type of environment.

THIS PAGE INTENTIONALLY BLANK

2. GENERAL DISCUSSION

This report is concerned mainly with the results from a specialized series of measurements, using pulse, or digital, and swept frequency transmissions to quantitatively examine the distortions introduced by the jungle vegetation through multipath phenomena.

The phenomena of short spatial fading experimentally observed in forested environments in the earlier part of this program have established that such environments are multipath channels at HF and above. It is well known that multipath channels place restrictions on the design and operation of communications systems, especially digital or wideband systems. However, there has been limited data available with which to assess the multipath effects of a forested environment upon such systems. Therefore, one of the major objectives of the work reported in this report is to obtain and analyze this type of data, and to investigate the ways of using the results to predict communication performance in tropical forested environments.

Measurements were made at carrier frequencies of 50, 100, and 150 MHz with both antennas stationary and with the receiving antenna mobile. Semiannual Report No. 11 illustrated the effects of multipath upon pulse amplitude and spectrum for various combinations of antenna heights, vertical and horizontal polarization, etc. This report extends these results by means of data obtained from swept-frequency transmissions. However, some of the statistical data needed to characterize the multipath behavior of forested environments are obtained from CW measurements. These measurements are also described in this report.

Under the scope of the present contract it has not been possible to complete analysis of all of the experimental data collected during this third phase of the experimental program. However, as shown in this report, even a limited analysis of this data gives considerable insight into the multipath character of forested channels, and suggests important new directions of investigation to undertake. For example, a more complete analysis of the data holds hope of developing a more realistic and useful scatter model with which to predict the performance of both wideband and narrowband systems in vegetated, or partially vegetated, terrains.

3. DATA COLLECTION AND ANALYSIS - CW

The data collected during this phase of the program may be broken into two classes: (1) data obtained by using continuous-wave type measurements, (2) data obtained by measurements using swept-frequency transmitted signals. This section is concerned with the first type of measurement, and the analyses of the resulting CW data.

The general physical characteristics of the test area (Area II), as they pertain to the specific measurements discussed in this report, are presented. Earlier reports have presented the general environmental characteristics of Area II in some detail, and the reader is referred to these earlier reports for such information as rainfall, temperature, etc.

Next the test equipment and measurement procedures used for the CW measurements are described. A general block diagram of the test set-up is shown in Figure 3.2.1.

The results of the analysis of the CW data are presented in Section 3.3. Here the cumulative probability distribution functions for long and short spatial signal variations are discussed in relation to operational parameters. The probability functions obtained from the data are examined.

Finally, in this Section, an example of the application of the results of this data are used to calculate the probability of error for a typical FSK digital system.

3.1 Experimental Area

The measurements were taken in Area II in the Satun province of southern Thailand (see Figure 3.1.1). The environment of Area II, discussed briefly in Final Volume II [Hicks, et al., 1969], may be grossly characterized as a tropical rain forest region having relatively smooth terrain. Figure 3.1.2 is a map of Area II showing the locations and extent of the measurement trails and field points used for this report. Specifically, four trails and seven field points were utilized. The locations and lengths of the four trails are listed in Table 3.1.1. Two of the trails, the main access trail and radial Z, have been used for previous propagation measurements and extend in an approximately radial direction from the respective transmitter locations. The remaining two trails, transverse A and transverse B, were newly cut to provide measurements in transverse directions, or at approximately constant ranges from the transmitter.

The trails were surveyed in both bearing and elevation, and marker stakes were placed at regular intervals of 100 or 200 feet along the trails.

The forest is not homogeneous throughout Area II. In general, the forest on the north side of the site, in which radial Z, transverse B, and field point Y-20 are located, consists of very large and tall trees having a visual average canopy height (height of tallest trees forming the canopy) of about 120 feet. The forest to the south, however, is relatively heavy and tall in the vicinity of the site, but its density and height diminish gradually with distance southward from the site. The lightest forest is found at one mile from the site, along the main access trail. Beyond one mile, the

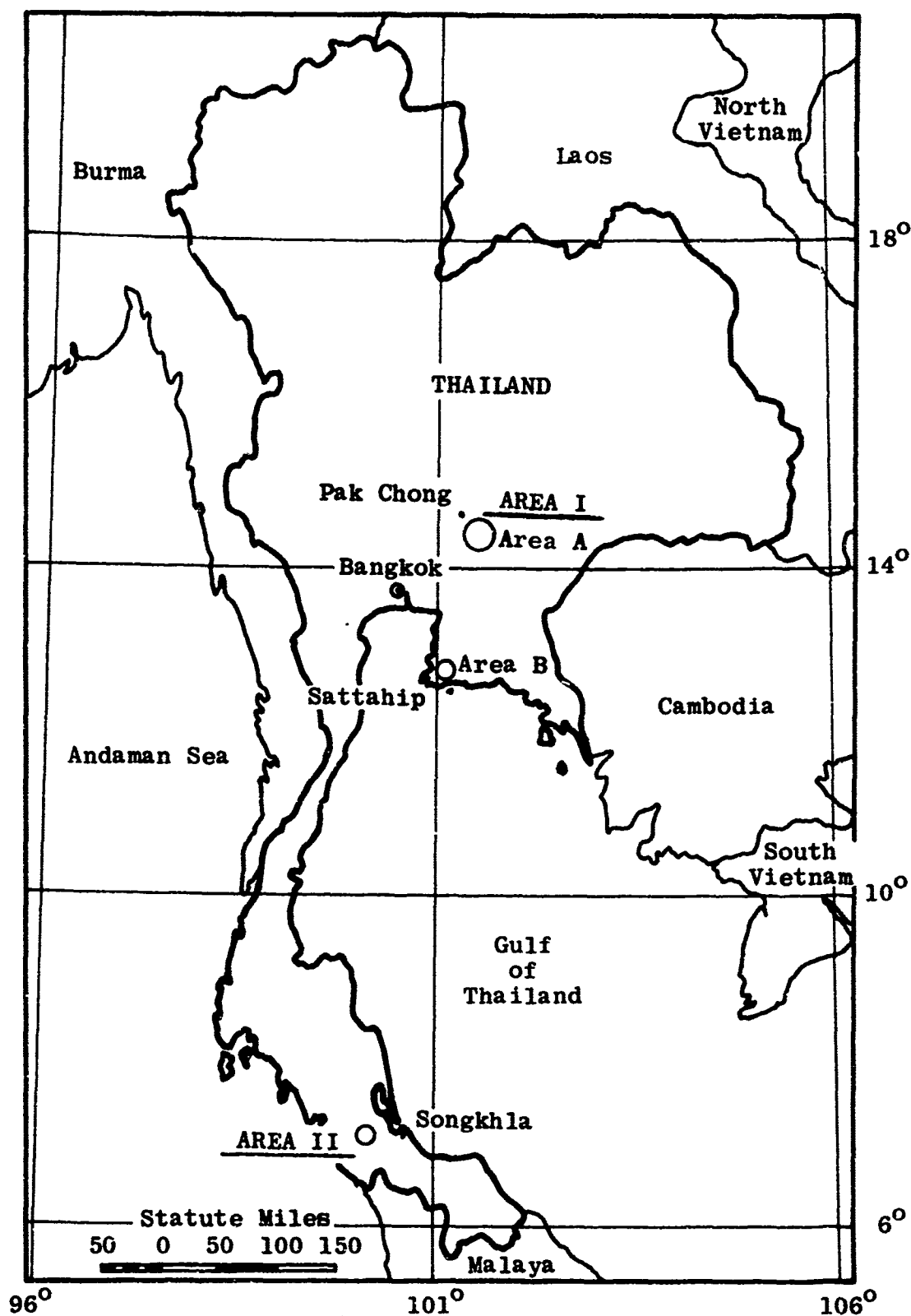


Figure 3.1.1 Locations of Thailand Test Areas

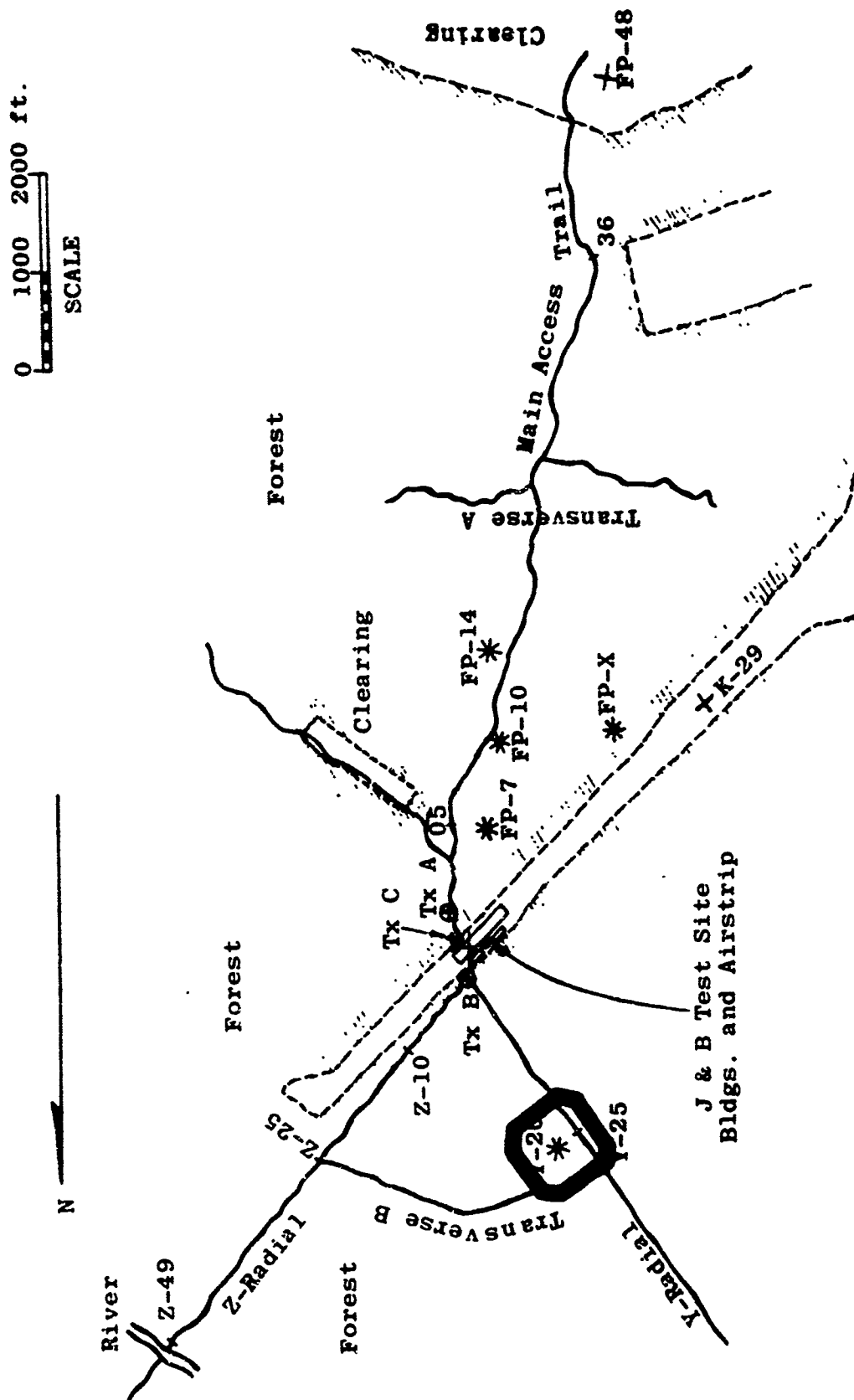


Figure 3.1.2 Sketch of Area II Test Site

the forest along the main access trail increases in density and height until the clearing is reached at 1.6 miles. A profile of the forest canopy along the main access trail is given in Figure 3.1.3.

Descriptions of the foliage and terrain at each of the field points and along the four trails are given in Tables 3.1.2 and 3.1.3.

Table 3.1.1

Measurement Trails for Long Trail Runs

<u>Trail</u>	<u>Direction</u>	<u>Length of Measurement</u>
Main Access Trail	Radial	6200 feet (From sign 05 to 36)
Transverse A	Transverse	3900 feet (Full length of trail)
Z-Radial	Radial	3900 feet (From sign Z-10 to Z-49)
Transverse B	Transverse	3000 feet (From sign Y-25 to Z-25)

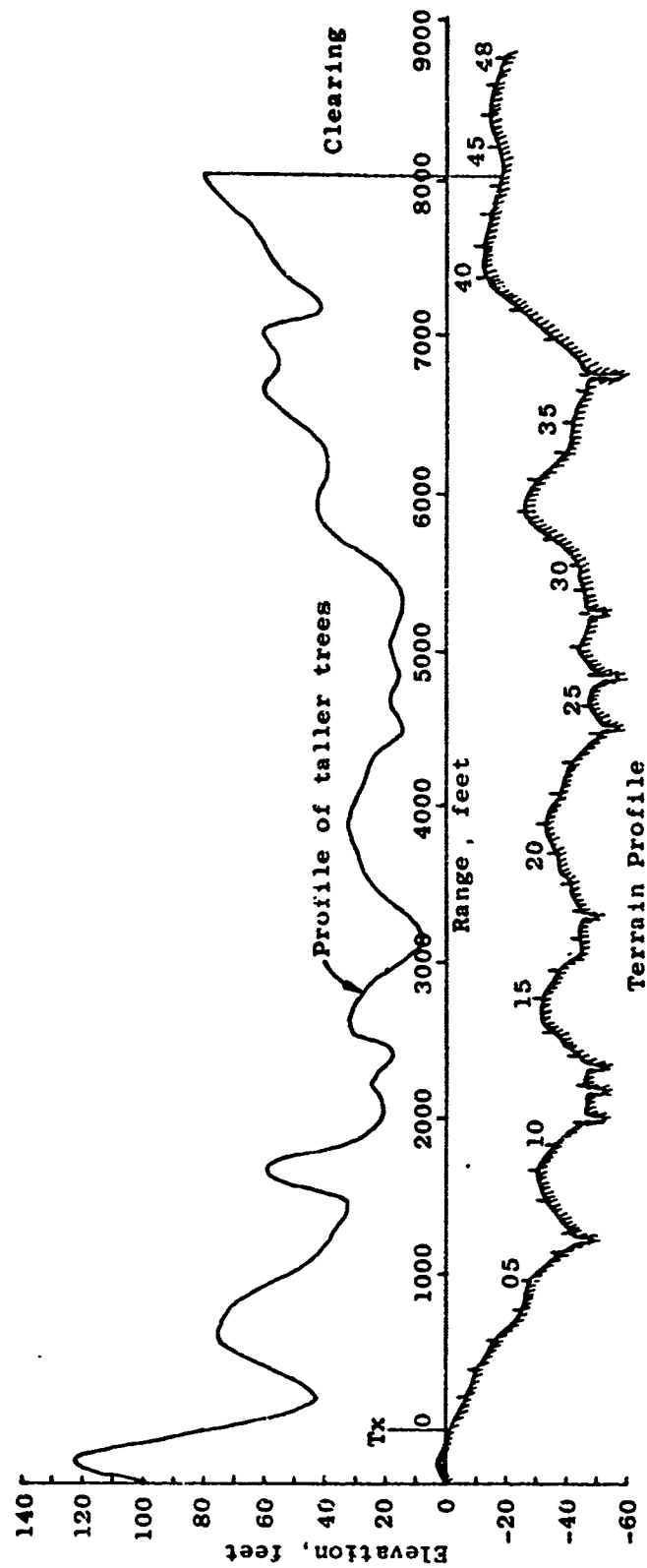


Figure 3.1.3 Terrain and Tree Profiles Along Main Access Trail

Table 3.1.2 Environmental Characteristics of Star Field-Points

Star Field- Point	Biomass Density, Tons/Acre	Average Canopy Ht., Ft.	Height of Tallest Tree, ² Ft.	Largest Tree in F.P., DBH	Number of Trees Counted ³	Remarks
FP-14	88	65	85	16 in.	211	Light forest; field-point located on relatively high, level ground.
FP-10	71 ⁴	75	140-150	18 in.	100	Moderately heavy forest in appearance. Several clumps of bamboo in field-point accompanied by an unusual lack of trees within the field-point circle. Located on sloping ground in a shadow region of a terrain peak.
FP-7	128	80	105-115	25 in	103	Moderately heavy forest. Field point located at a relatively low region of terrain alongside a small creek.
FP-X	116	80	98-118	22 in.	114	Moderately heavy forest. F. P. located on level ground.
Y-20	193	100-120	150-160	38	112	Heavy forest. Located on level ground.

Table 3.1.2 (Continued)

Star Field- Point	Biomass Density ¹ Tons/Acre	Average Canopy Ht., Ft.	Height of Tallest Tree, ² Ft.	Largest Tree in F.P., DBH	Number of Trees Counted ³	Remarks
FP-48	0	---	---	---	0	Located in clearing of grassy meadow. Nearest trees are 20-30 ft. tall located 150-200 ft. distant from center of F.P. in direction of transmitter. Terrain is relatively low and level.
K-29	0	---	---	---	0	Located in clearing cut for airstrip approach. Forest boundary is situated 200 ft. to the NW and about 300 ft. to the SE. Entire clearing area is covered with fallen logs of all sizes; tree stumps rise no more than 5 ft. F.P. located on relatively high terrain on side facing transmitter.

1. Biomass calculations based upon trees within 200-foot circle.
2. Tallest tree in near vicinity of field point.
3. Number of trees counted within 200-foot diameter circle of size 4 inches DBH (diameter at breast height) or greater.
4. Estimated 100-110 for region surrounding field point.

Table 3.1.3
Environmental Description of Long Trails

Main Access Trail. The main access trail passes through two distinct forests on the south side of the J&B site. From the transmitter to approximately FP-10 the forest is moderately heavy with an average canopy height of 80-100 feet. Immediately beyond FP-10 the forest is less heavy, having an average canopy height of 60-70 feet, and is seen for about one-half mile along the trail. Near the end of the measured portion of the trail (sign 36) the heavier forest again appears and the canopy rises to approximately 100 feet.

The predominant variations in the terrain elevation are 20-30 feet; however, in the vicinity of the transmitter the trail has the highest elevation, which is approximately 50 feet above the lowest spot (in a creekbed) of the trail.

Transverse A. The transverse A trail is entirely contained within the lighter forest; hence, the average canopy height is 60-70 feet. In this region some of the tallest trees may reach as high as 85 feet.

Over most of the transverse trail the terrain elevation varies by less than 10 feet; however, the east end of the trail rises approximately 30 feet.

Z-Radial. The forest on the north side of the J&B site is very heavy and is fairly homogeneous. The average canopy height is 100-120 feet, and unusually tall trees may reach to 150 feet.

Variations in the terrain elevation are principally 20-30 feet; however, the highest ground occurring near the half-way region of the trail is approximately 55 feet above the lowest spot of the trail.

Transverse B. The forest is similar to that described for Z-Radial and for field point Y-20.

The terrain elevation varies approximately 20-35 feet over this trail.

3.2 Equipment and Measurement Procedures

All measurements discussed in this report are of field strength as a function of distance with fixed transmitter antenna and moving or "mobile" receiver antenna. All data were taken using the transmitter and receiver system shown in block form in Figure 3.2.1. The transmitted signal was CW, or an unmodulated carrier, at a frequency of 50, 100, or 150 MHz. The receiver was a tunable field-strength meter from which the detected signal envelope was recorded on a Varian strip-chart recorder. The transmitter and receiver antennas were identical half-wave dipoles of either horizontal or vertical polarization. The transmitter antenna was at a fixed location and height for each run. The height was generally one of the following values: 13, 20, 40, 80, 120, 200 feet.

Three locations of the transmitter antenna were used as shown in Figure 3.1.2. For measurements on the south side of the site (i.e., along the main access trail, transverse A, and all field points except Y-20) the transmitter antenna was located at Tx A for transmitter antenna heights up to 120 feet. For measurements on the north side of the site (i.e., radial Z, transverse B, and field point Y-20) the transmitter antenna was located at Tx B for transmitter antenna heights up to 120 feet. For measurements with the transmitting antenna at heights greater than 120 feet, the transmitter antenna was located on a tower on the south side of the site at Tx C.

The mobile receiver antenna, for the low heights (i.e., 20 feet or less), was either hand-carried or mounted on the Rolligon trailer, depending upon the location and/or type of measurement.

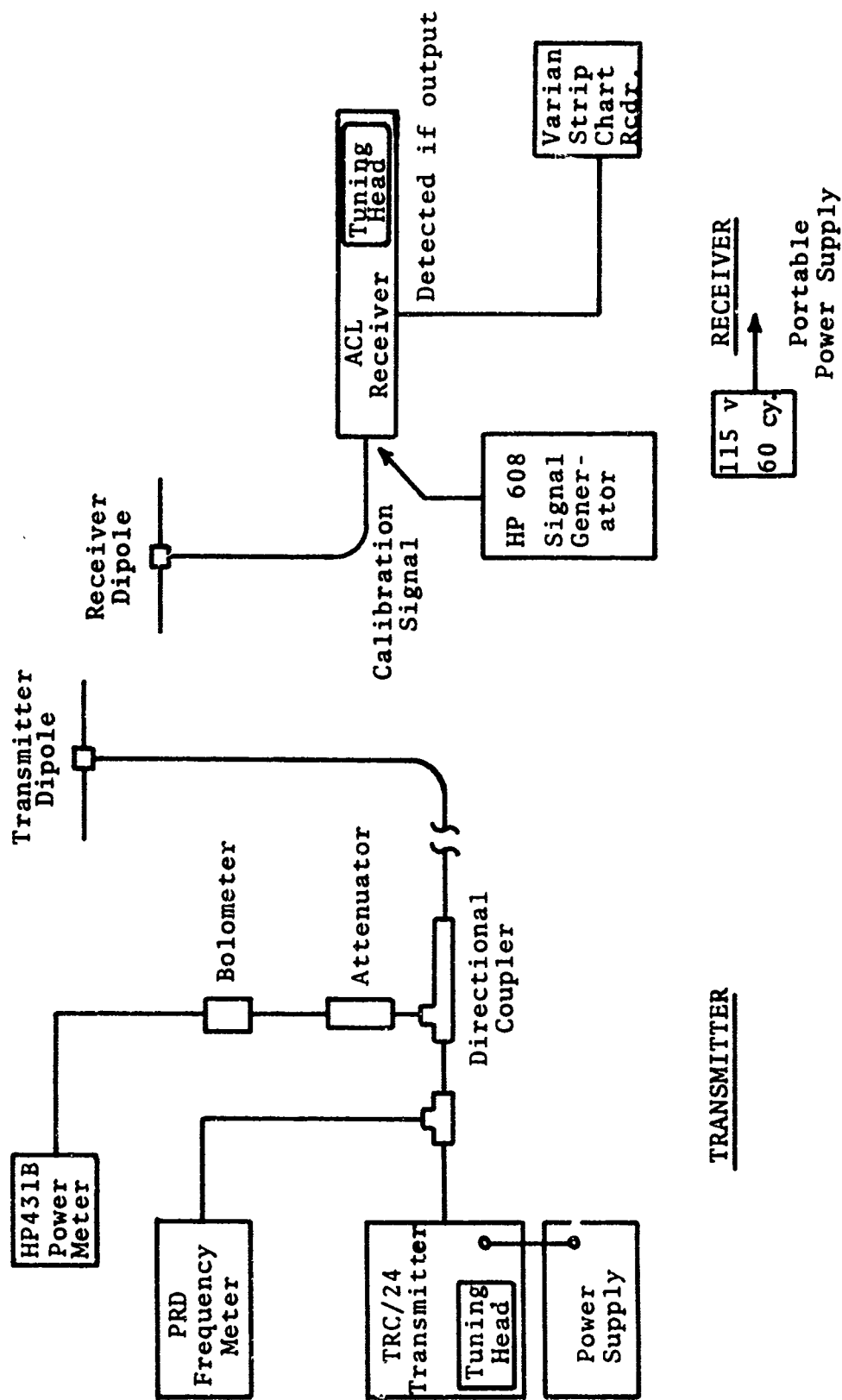


Figure 3.2.1 Block Diagram of Transmitter and Receiver

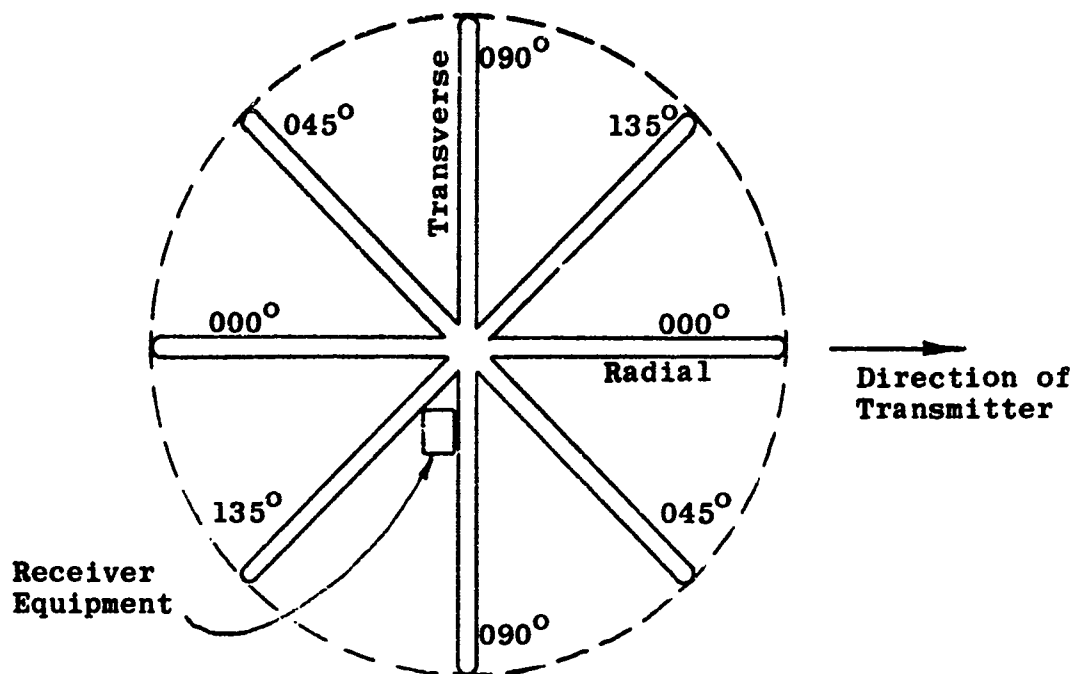
The data presented in this report were obtained from three types of measurements:

- a. Star field-point runs.
- b. High antenna runs.
- c. Long trail runs.

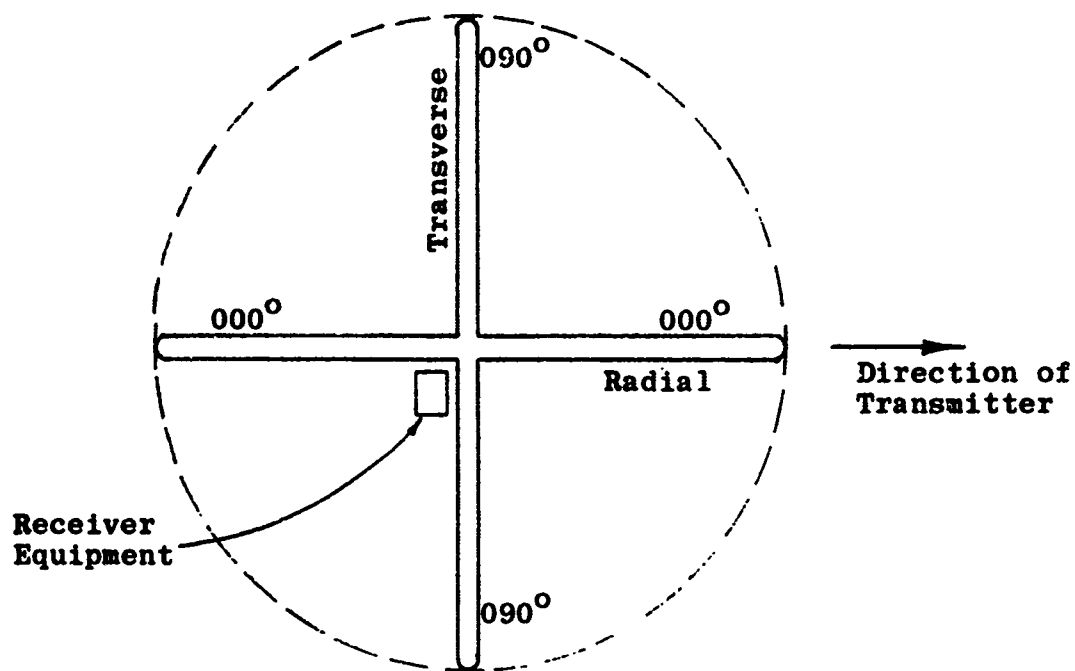
Star Field-Point Runs

The primary purpose of the star field-point measurements was to determine the fundamental statistics of radio field strength variability in foliated environments as a function of both the system parameters and the foliage/terrain characteristics. The star field-point runs obtained a relatively large sample of the radio field strength in the forest environment within a 200-foot diameter circle for various combinations of frequency, polarization, and antenna heights. The size of the sample space was limited to a 200-foot circle in order that the effects on the signal caused by properties of the forest and terrain elevation would remain relatively constant throughout the measurement space. Consequently, the principal variables of the measurements at each field point were the controlled parameters of the measurement system: frequency, polarization, antenna heights.

Five field points were located within the forest, and two were in clearings. Typically, each field point consisted of four 200-foot paths arranged as shown in Figure 3.2.2a. Field point FP-48 in the clearing, however, consisted of two paths as seen in Figure 3.2.2b. These trail patterns suggest the name "star" which is normally used when referring to these runs. A minimum amount of foliage was removed from each field point area. At worst, the individual paths had to allow uninterrupted passage of the 50 MHz horizontal dipole.



a. All Field Points Except FP-48



b. Field Point FP-48 in Clearing

Figure 3.2.2 Star Field Point Measurement Paths Within 200-Foot Diameter Circle

The orientations of the star field-point paths permitted sampling the area in both radial and transverse directions. The paths in the 45-degree directions gave additional sampling space. Marker stakes were placed every 50 feet on all paths to permit distance or location marks to be placed on the recordings.

The receiver antenna was hand-carried at a uniform rate along each of the 200-foot paths of a field point. Since the signal was recorded only while the antenna was being carried along the paths, a star field-point recording consists generally of two or four separate segments of continuous field strength data taken under one set of system parameters: frequency, polarization, and antenna heights (see Figures 3.3.3 and 3.3.5).

For the majority of runs, the receiver antenna was held approximately 6 feet above the ground. In addition, recordings with the receiver at 20 feet were taken with the transmitter antenna at 40 feet only. It should be noted that with horizontal polarization the receiver dipole was always oriented for maximum free-space gain in the direction of the transmitter.

The receiver and recorder equipment were placed on a wooden bench near the center of each field point. Electrical power for this equipment was supplied by one or two portable 1500-watt gasoline driven generators placed about 200 feet from the receiver equipment.

The star field-point data consisted of 239 runs among the seven field points at various combinations of system parameters as diagrammed in Table 3.2.1.

Table 3.2.1
Combinations of Test Parameters for Star Field-Point Measurements

Polar.	Freq.	Tx Ht.	Rx Ht	FP-14	FP-10	FP-7	FP-X	Y-20	FP-48	K-29
HORIZONTAL	50MHz	200ft	6ft	x	x	x		x	x	
		120	6	x	x	x	x	x	x	x
		80	6	x	x	x	x			
		40	6	x	x	x	x		x	x
		40	20	x	x	x	x		x	
		20	6	x	x	x	x			
		13	6	x	x	x	x	x	x	x
	100MHz	200	6	x	x	x		x	x	
		120	6	x	x	x	x	x	x	x
		80	6	x	x	x	x	x		x
		40	6	x	x	x	x	x	x	x
		40	20	x	x	x	x	x	x	x
		20	6	x	x	x	x	x		x
		13	6	x	x	x	x	x	x	x
	150MHz	200	6	x	x	x		x	x	
		120	6	x	x	x	x	x	x	x
		80	6	x	x	x		x		
		40	6	x	x	x	x	x	x	x
		40	20	x	x	x	x	x	x	
		20	6	x	x	x		x		
		13	6	x	x	x	x	x	x	x
VERTICAL	50MHz	200	6	x	x	x		x	x	
		120	6	x	x	x	x	x	x	x
		80	6	x	x					
		40	6	x	x	x	x		x	
		40	20	x	x	x	x		x	
		20	6	x	x					
		13	6	x	x	x	x	x	x	x
	100MHz	200	6	x	x	x		x	x	
		120	6	x	x	x	x	x	x	x
		80	6	x	x	x		x		x
		40	6	x	x	x	x	x	x	x
		40	20	x	x	x	x	x	x	x
		20	6	x	x	x		x		
		13	6	x	x	x		x	x	x
	150MHz	200	6	x	x	x		x	x	
		120	6	x	x	x		x	x	x
		80	6	x	x	x		x		
		40	6	x	x	x	x	x		
		40	20	x	x	x	x	x	x	
		20	6	x	x	x		x		
		13	6	x	x	x	x	x		x

Tx Ht = Transmitter Antenna Height

Rx Ht = Receiver Antenna Height

x denotes combination was used.

High Antenna Runs

Signal strength measurements over a horizontal distance for different receiver antenna heights up to 98 feet were made by a number of special runs in the vicinity of field point Y-20.

Two types of systems were developed which could support the receiver antenna at high heights above the ground and allow the antenna to be moved horizontally at a uniform rate while the signal was being recorded.

One type of system employed a network of ropes and pulleys attached between two tall trees and was set up at three locations. At two of these locations the system was oriented in a radial direction with respect to the transmitter, and the third was in a perpendicular, or transverse, direction. The antenna height could be set to any value up to a maximum height of 58 feet for the transverse and one radial system, and 74 feet for the other radial system. The horizontal translation distance differed for the three locations due to the available tree separations. One radial provided 50 feet of movement, the other radial provided 80 feet, and the transverse gave 100 feet of travel. At each of the three locations the rope and pulley systems were attached to the unobstructed vertical trunks of two large, tall trees beneath their lowest points of branching.

The other method for obtaining mobile measurements at high antenna heights was to mount the receiver antenna on a flexible mast, or tower, and move the top of the mast in a controlled manner by pulling appropriate guy ropes. In this case the antenna path was actually an arc, but the vertical displacement of the receiver antenna during the horizontal

motion was less than two feet for total horizontal displacements of 20 to 30 feet, depending upon the tower height, and is assumed to have negligible effect on the signal.

Typically, these measurements for a particular frequency and polarization began with the antenna raised to the highest position which the antenna supporting system could provide. After the receiver system was calibrated the received signal strength was recorded while the antenna was caused to move at a uniform rate over the full horizontal range of the displacement system. Marks were placed on the recordings at regular intervals of antenna travel. For the pulley and rope systems these marks occurred for every 10 feet of antenna travel, and for the tower sway system the marks occurred about every 2 feet depending upon the height of the measurement. One recording for a particular combination of frequency, polarization, and receiver antenna height constitutes one run. Following this, the antenna was lowered approximately 10 feet, and another recording of the signal strength was made in an identical manner. This measurement process was repeated until the antenna height was, in most cases, about 20 feet above the ground. Many runs, however, were made down to heights of 8 feet to give continuity with the star field-point measurements. A total of 100 of these high antenna runs were made at field point Y-20 and are listed in Table 3.2.2.

Since the tower bending system provided very limited antenna travel, these measurements were performed at only the highest test frequency of 150 MHz in order to maximize the travel distance in terms of number of wavelengths (3 to 4).

The transmitting antenna for all the high antenna runs was located on the 200-foot tower system and was raised to a height of 150 to 165 feet only.

Table 3.2.2
Combinations of Test Parameters for High Antenna Measurements

Polar.	Freq.	Radial 1	Radial 2	Transverse 1	Tower Bending
HORIZONTAL	50MHz	57ft.		57ft.	
		48		48	
		38		38	
		28		28	
		18		18	
		8		8	
	100MHz	53	74 14	58	
		44	64 6	48	
		33	54	38	
		21.5	44	28	
			34	18	
VERTICAL	50MHz	57		58	98
		46		48	88
		38		38	78
		26		28	68
		17.5		18	58
		8.5		8	
	100MHz	58	74 14	57	
		48	64 6	48	
		38	54	38	
		28	44	28	
		18	34	18	
VERTICAL	50MHz	58		57	
		48		48	
		38		38	
		28		28	
		18		18	
		8		8	
	100MHz	50	74 14	58	
		40	64 6	48	
		30	54	38	
		20	44	28	
			34	18	
VERTICAL	150MHz	59		58	98
		49		48	88
		38		38	78
		29		28	68
		19		18	58
		10		8	

Transmitter Antenna Height = 150 - 165 feet.

Numbers in table are receive antenna heights in feet.

Long Trail Runs

The primary purpose of the long trail measurements was to obtain a distribution of signal strength behavior among the different regions of the forest. The measurement trails were located independent of foliage and terrain conditions which provided a representative sampling over the environment. Consequently, the distribution is expected to represent the entire forest over an area in which the same type of forest and terrain prevails. In a sense, the continuous trail runs, by sampling an arbitrary profile or cross-section of the radio field strength, are intended to provide a means of studying the field strength statistics throughout the entire forest.

Continuous recordings of received signal strength were made while the receiver antenna was carried at a uniform rate along each trail for some combinations of frequency, polarization, and transmit antenna height. A mark was placed on the recordings at the moment the antenna passed a trail sign, and the mark was labeled with the corresponding sign number. Motion was continuous from one end of the trail to the other, except for occasional stops necessary to check the tuning and calibration of the receiver. When the end of a trail was reached the receiver operator would radio the transmitter operator and request a change in parameter (e.g., transmitter antenna height). The next run then proceeded in the opposite direction along the trail.

The Rolligon could be used along the main access trail and transverse A trail, hence the continuous recordings of the signal along these trails was accomplished with the receiver system placed aboard a trailer pulled by the Rolligon. This arrangement, described in Semiannual Report #11, placed the receiver antenna at a fixed height of 10 to 13 feet above ground.

The continuous recordings of the signal along radial Z and transverse B were achieved by hand carrying the receiver system along the trails. For these measurements, the receiving antenna was held approximately 6 feet above ground. Equipment power at 115 volts 60 cycles for the portable equipment was derived from a heavy-duty 12-volt truck battery and a Heathkit 400-watt inverter.

A horizontal dipole at the receiver was always oriented for maximum gain in the direction of the transmitter. The antennas mounted on the Rolligon were rigidly attached and therefore turned with the vehicle. Normally the trails did not have bends sharp enough to make it necessary to reorient the horizontal receiver dipole. However, between signs 19 and 21 on the transverse A trail a sharp detour in the trail did make it necessary to manually maintain proper orientation of the horizontal receiver dipole.

A total of 84 long trail runs were made among the four trails. These runs are listed in Table 3.2.3.

3.3 Analysis and Discussion

The VHF signal envelope variations, encountered when the receiving terminal is in motion in a forested jungle environment, can generally be broken into three types:

1. A deterministic mean whose value is governed by the inverse distance squared law of the lateral wave [Sachs and Wyatt, 1966, 1968].
2. Long spatial variations about the mean which are due to terrain and (intuitively) gross foliage features.

Table 3.2.3
Combinations of Test Parameters for Long Trail Measurements

<u>Polar.</u>	<u>Freq.</u>	<u>Tx Ht.</u>	<u>Main Access</u>	<u>Trans-verse A</u>	<u>Z-Radial</u>	<u>Trans-verse B</u>
HORIZONTAL	50MHz	200ft	x			
		120	x		x	x
		80	x	x		
		40	x			
		20	x			
		13	x	x	x	x
	100MHz	200	x	x	x	x
		120	x	x	x	x
		80	x	x		
		40	x	x	x	x
		20	x	x		
		13	x	x	x	x
	150MHz	200	x			
		120	x		x	x
		80	x	x		
		40	x			
		20	x			
		13	x	x	x	x
VERTICAL	50MHz	200	x			
		120	x	x	x	x
		80	x	x		
		40	x	x		
		20	x			
		13	x	x	x	x
	100MHz	200	x	x	x	
		120	x	x		x
		80	x	x		
		40	x	x		
		20	x			
		13	x		x	x
	150MHz	200	x			
		120	x		x	x
		80	x	x		
		40	x			
		20	x			
		13	x	x	x	x

Tx Ht = Transmitter Antenna Height

Receiver Antenna Height = 10-13 ft. for 1. Main Access Trail
2. Transverse A

6 ft. for 1. Z-Radial
2. Transverse B

x denotes combination was used.

3. Short spatial variations which are associated with multipaths due (intuitively) to scattering by the trees.

The deterministic mean is important in any communications application in the environment as it enters directly in establishing the achievable range of communications for a given system. The behavior of the deterministic mean, however, has been discussed in considerable detail elsewhere [Jansky & Bailey, 1966; Sachs and Wyatt, 1966, 1968; Tamir, 1967, Hicks, et al., 1969], and only its inverse distance squared behavior ($40 \log d$ for the signal in decibels where d is distance) is required or utilized here in examining the signal variations about this mean.

The long spatial variations are important in determining adequate power margins, or appropriate adaptable techniques, required to maintain a satisfactory signal level.

The short spatial variations are, among other things, important in determining the error rates for digital transmission for mobile applications in the environment.

In this section, the cumulative probability distribution functions for the long and short spatial signal variations are obtained and discussed in relation to the operational (frequency, polarization, antenna heights) and environmental (foliage, terrain) factors. The probability functions of the short spatial variations obtained by the star field-point runs and the high antenna runs are examined first. These small experimental regions are fairly homogeneous on a local scale, and are expected to provide information on the short spatial variations with minimum effects from long spatial variations.

Also, because the local environments of the star field-points are different for the various locations (i.e., clearing or dense foliage, elevated or depressed terrain, etc.) the effects of gross environmental changes on the probability distributions of the short spatial variations may be examined from these results.

The probability functions of the long and short spatial variations over the long trails are examined next. Because the trails encompass terrain and gross foliage changes, which are fairly representative of the total experimental region of Area II, these results are expected to provide probability functions sufficient for representing Area II. The results are applied to determine error rates in the next section.

It should be noted that other statistical measures of the envelope variability are also important in characterizing propagation effects in the environment, such as the duration and depths of spatial fading and the frequency and time correlation functions. The fading duration and depths have previously been examined in some detail for Area I [Jansky & Bailey, 1966], and the frequency correlations are examined later in this report.

Star Field-Point and High Antenna Runs

All star field-point and high antenna recordings have been analyzed to determine the probability functions of the signal envelope. These statistics were computed by measuring the time that the signal remained above a number of arbitrary levels of amplitude. A clock system was designed for this which consisted of fifteen electric clocks individually controlled from a panel of fifteen switches. Fourteen clocks were available to measure the accumulated times above fourteen

respective levels, and one clock measured the total signal time. For each run the data in the form of a strip-chart recording was reinserted into a Varian recorder, which furnished a convenient means of moving the chart at a uniform, slow speed. A calibrated graticule was placed across the face of the recorder against the recording. While the chart slowly advanced, the amplitude of the moving trace was easily followed by eye as it moved along the calibration scale. Each clock was turned on during the time for which the signal trace exceeded the level represented by the clock. At the end of the run, the accumulated clock times were tabulated. Each clock, or level, time divided by the total run time gives the fraction or percentage of time the signal exceeded the respective levels. Since it is assumed that all the data recordings represent uniform motion of the receiver antenna, the above fractions of time are identically the probabilities that the field strength exceeds the chosen levels. For each run, these values represent a cumulative probability distribution of the signal strength at the particular field point for a known combination of system parameters of frequency, polarization, and antenna heights.

In this analysis, the change in the deterministic mean signal strength over the short paths at each field point has been assumed negligible. In the worst case, this change in signal level is 1 dB for the 200-foot radial path at star field-point 7. In the analysis of each star field-point recording, the clock times at each level for the two or four individual path recordings were added to form an average cumulative probability distribution for the entire run. Equal weighting was assumed for each of the two or four segments. However, the recording times of each path vary somewhat due to different walking rates along each path. The variation among

the clock times for the two or four individual recording segments seldom exceeds 15% of the over-all average time and has been found, in the worst cases, to be insignificant in the determination of the probability distribution parameters.

The cumulative probability distribution of signal amplitude for each run was plotted and the median or 50% probability signal level for each distribution was determined. Next, the signal amplitude values were divided by the corresponding median value. This normalization facilitates plotting the cumulative probability curves on standard probability graphs for identifying the types of distributions (i.e., Gaussian, Rayleigh, Rician, etc.).

The probability distributions of the envelopes were suspected of being Rician because results of pulsed transmission suggested that the total signal is composed of the dominant lateral wave plus lesser multipaths [Hicks and Robertson, 1969; Stein and Jones, 1967].

The Rician probability density function is given by [Stein and Jones, 1967]

$$p(r) = \frac{r}{\sigma^2} I_0 \left[\frac{Ar}{\sigma^2} \right] \exp - \left(\frac{r^2 + A^2}{2\sigma^2} \right). \quad (1)$$

Defining $\gamma_F \equiv \frac{A^2}{2\sigma^2}$ and substituting into Eq. (1) gives

$$p(r) = \frac{2r \gamma_F}{A^2} I_0 \left[\frac{2r \gamma_F}{A} \right] \exp \left[- \gamma_F \left(\frac{r^2}{A^2} + 1 \right) \right]. \quad (2)$$

Normalizing this by the change of variable $R = \frac{r}{A}$ gives

$$p(R) = 2R \gamma_F I_0 [2R \gamma_F] \exp [-\gamma_F(R^2 + 1)]. \quad (3)$$

The cumulative distribution of this density function is

$$P(R > r') = \int_{r'}^{\infty} 2R \gamma_F I_0 [2R \gamma_F] \exp [-\gamma_F(R^2 + 1)] dR. \quad (4)$$

where R is the normalized instantaneous envelope voltage, r' is some arbitrarily selected voltage level, A is the amplitude of the steady component, $2\sigma^2$ is the mean power in the fluctuating signal, and I_0 is the modified Bessel function of the first kind and zeroth order. A convenient way to check the assumption of a Rician distribution and, providing the distribution is Rician, to obtain the power ratio of the steady to fluctuating signal components ($\gamma_F = A^2/2\sigma^2$) is to plot the measured distributions on a family of preplotted Rician distributions, represented by Eq. (4) above, having this ratio as family parameter. Norton et al [1955] have given curves and tables of the Rician cumulative probability distributions, normalized to the steady component, for various values of the parameter $K \equiv 2\sigma^2/A^2$. The values from the tables by Norton et al. [1955] are used here, but normalized to the median rather than the steady component, and with the K parameter inverted and called γ_F . Normalization to the median is done because the median is easily determined directly from a plot of the cumulative probability distribution function. The inversion of their K is for later convenience. A family of curves for the Rician distribution as a function of the

parameter γ_F were plotted and are shown in Figures 3.3.1 and 3.3.2. The Rician distribution curves, as shown, pass through one common point at probability 0.5 and normalized amplitude 1.0. In the present work, γ_F will normally be expressed in decibels defined as $\gamma_F \text{ (dB)} = 10 \log_{10} \gamma_F$. Note that $\gamma_F = -\infty$ dB represents a Rayleigh distribution, and it may be seen from the graph of Figure 3.3.1 that there is very little difference between the curves for $\gamma_F = 0$ dB and $\gamma_F = -\infty$ dB. It is also noted that $\gamma_F = +\infty$, also shown in Figure 3.3.1, corresponds to a Gaussian distribution about a large mean.

The computed (normalized) probability values for each star field-point and high antenna run were plotted on Rician distribution graphs. Two examples of star field-point recordings accompanied by the computed probability values in both tabulated and plotted forms are illustrated. Figure 3.3.3 shows star field-point recording No. 63 taken at field point 14 for 50 MHz, horizontal polarization, transmit antenna height of 80 feet and receive antenna height of 6 feet. The scales shown on the recordings are the calibrated dB levels chosen for the probability computations. The measured clock times of the signal above each level for each of the four recording segments are shown in Table 3.3.1. The values in the right-most column represent the average cumulative probability distribution of the signal strength over the paths for this field point. After the signal level, in linear units, was normalized to the median, the probability values were plotted on the Rician graph shown in Figure 3.3.4. The best fit of these data to the Rician γ_F parameter curves for the 0.10 - 0.90 probability range is $\gamma_F = +10$ dB.

The second example, shown in Figures 3.3.5 and 3.3.6, and Table 3.3.2, illustrates data that are Rayleigh distributed.

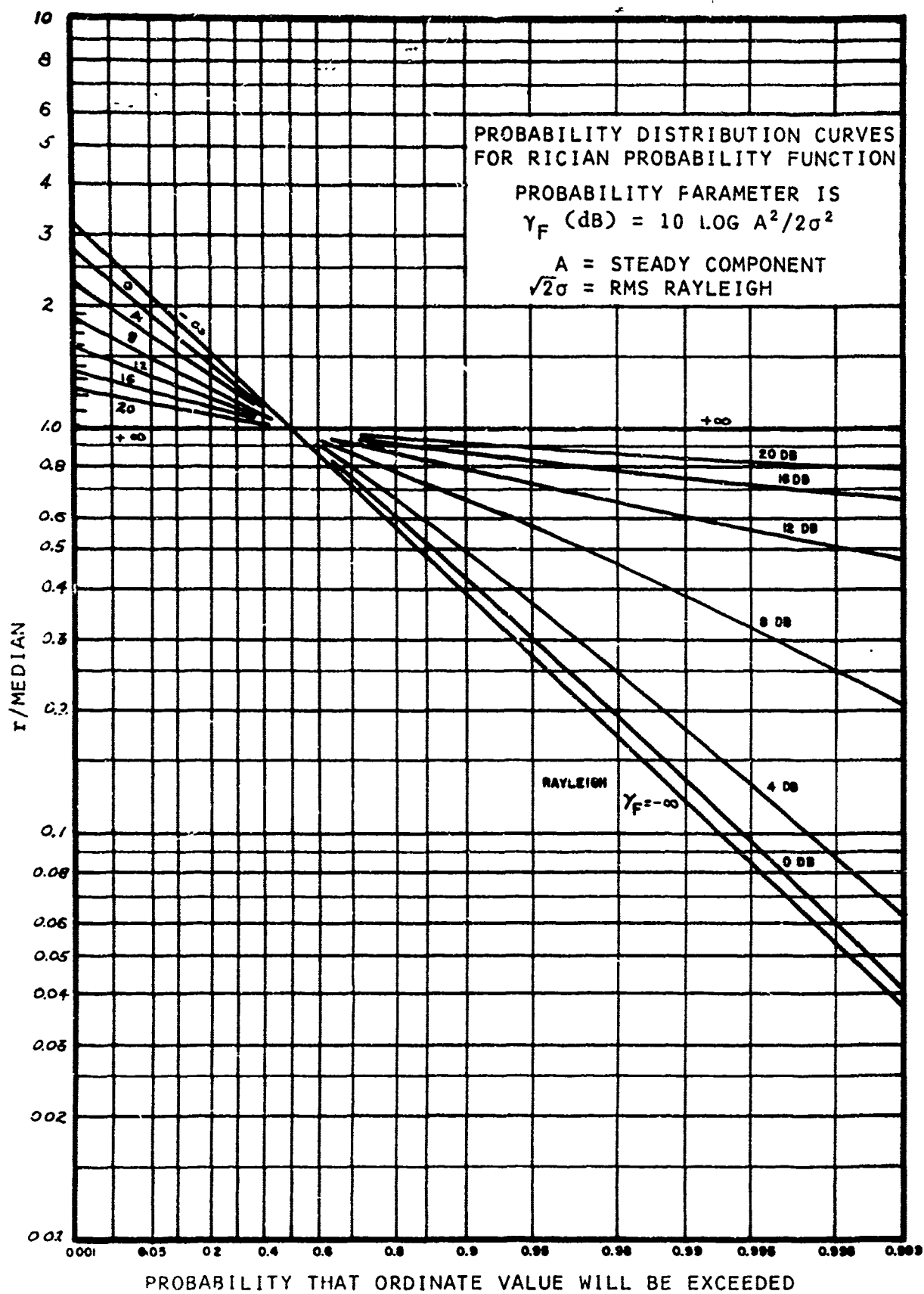


Figure 3.3.1 Probability Distribution Curves

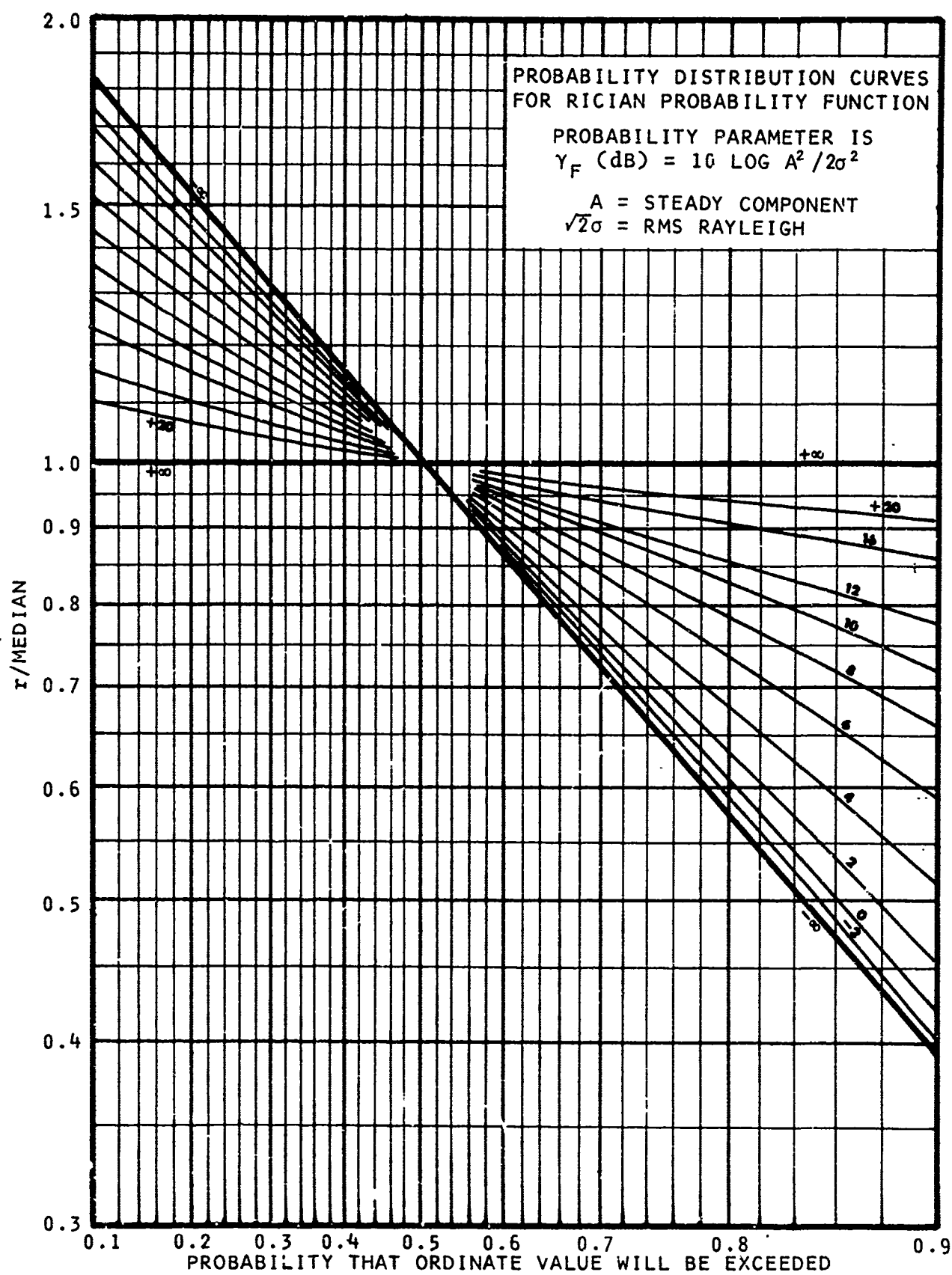


Figure 3.3.2 Probability Distribution Curves

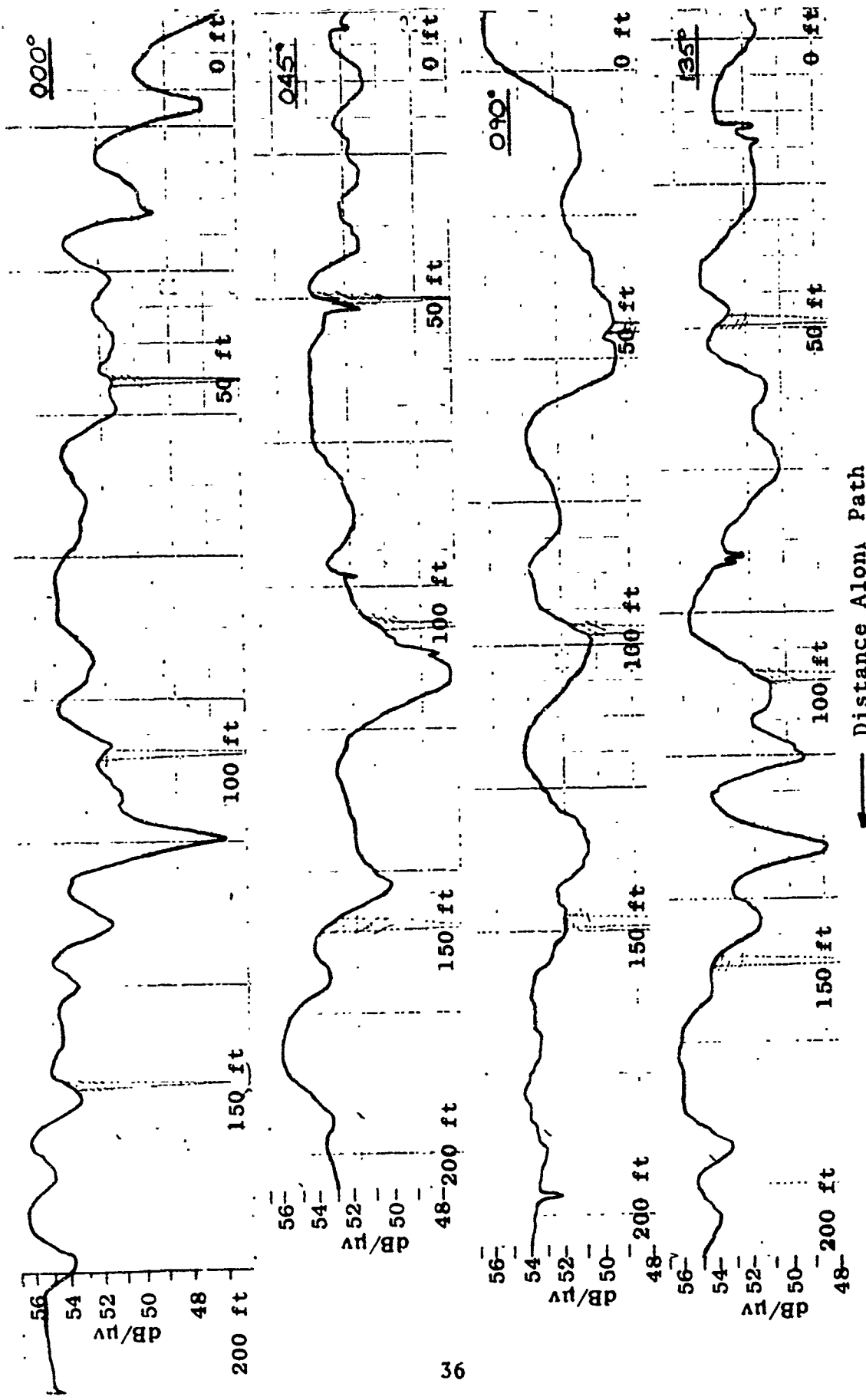


Figure 3.3.3 Signal Recording at Star Field-Point FP-14 (50, 80, H, d, 6)

Table 3.3.1
Time in Seconds That the Signals of Figure 3.3.3
Exceed Given Amplitude Levels *

Signal Level dB	<u>r</u> <u>Median</u>	<u>000°</u>	<u>045°</u>	<u>090°</u>	<u>135°</u>	<u>Total</u>	<u>Probability</u>
+8	1.86	0	0	0	0	0	
+7	1.66	0	0	0	0	0	
+6	1.47	3.5	1.7	0	5.2	10.4	.033
+5	1.31	17.0	5.2	3.0	12.4	37.6	.118
+4	1.16	31.0	8.8	5.1	25.5	70.4	.221
+3	1.04	48.2	29.4	34.5	41.8	153.9	.482
+2	0.93	57.0	40.7	43.0	49.6	190.3	.596
+1	0.83	73.6	64.4	59.0	69.8	266.8	.836
0	0.74	75.1	69.2	70.0	76.7	291.0	.912
-1	0.66	75.8	71.3	77.0	78.9	303.0	.950
-2	0.58	83.4	72.0	78.0	79.9	313.3	.982
-3	0.52	85.9	74.3	78.0	79.9	318.1	.997
-4	0.47	86.9	74.3	78.0	79.9	319.1	1.000
	TOTAL SECONDS	86.9	74.3	78.0	79.9	319.1	

*Ratio of amplitude, r, to median and average fraction of time above level (probability) also shown.

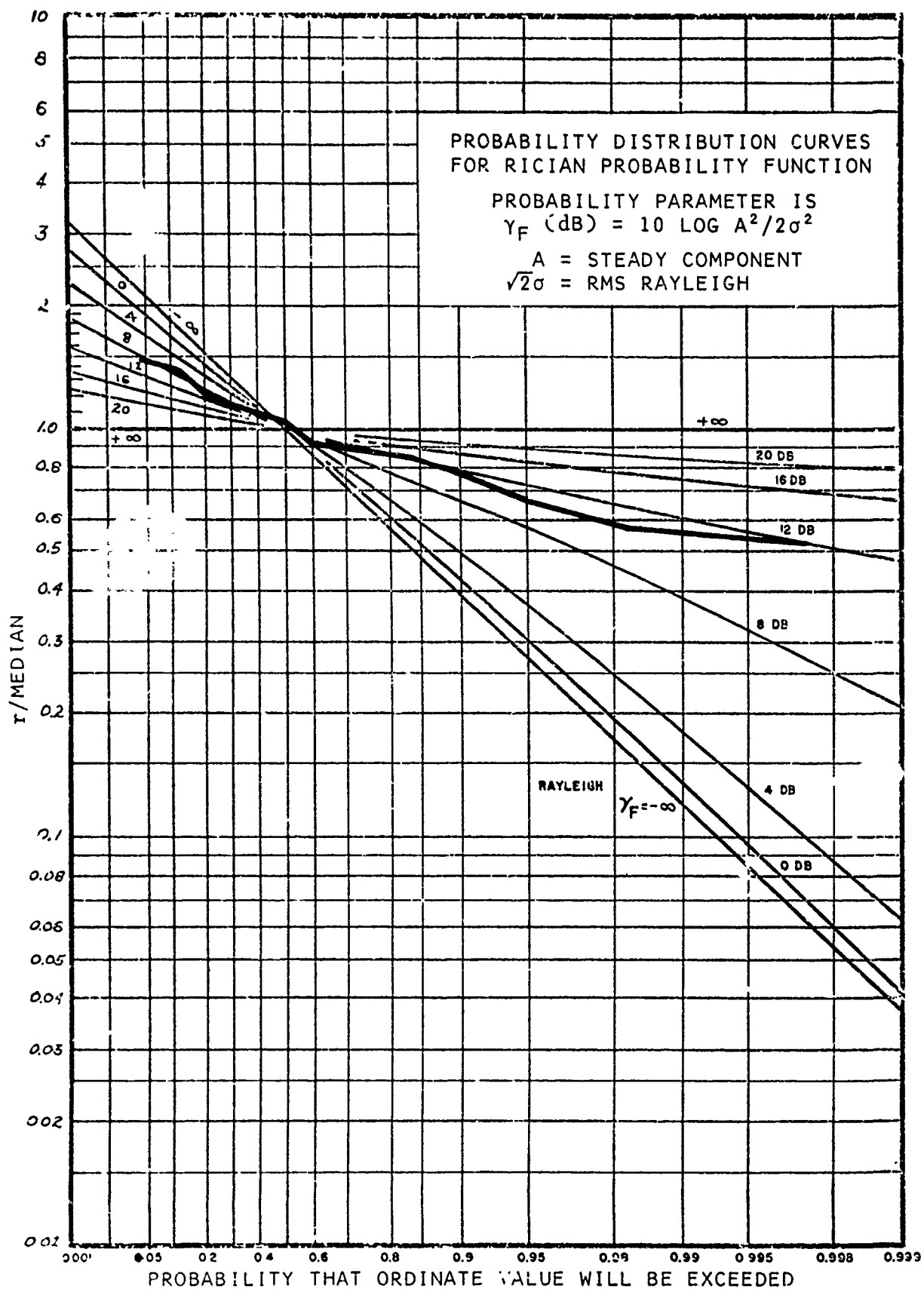
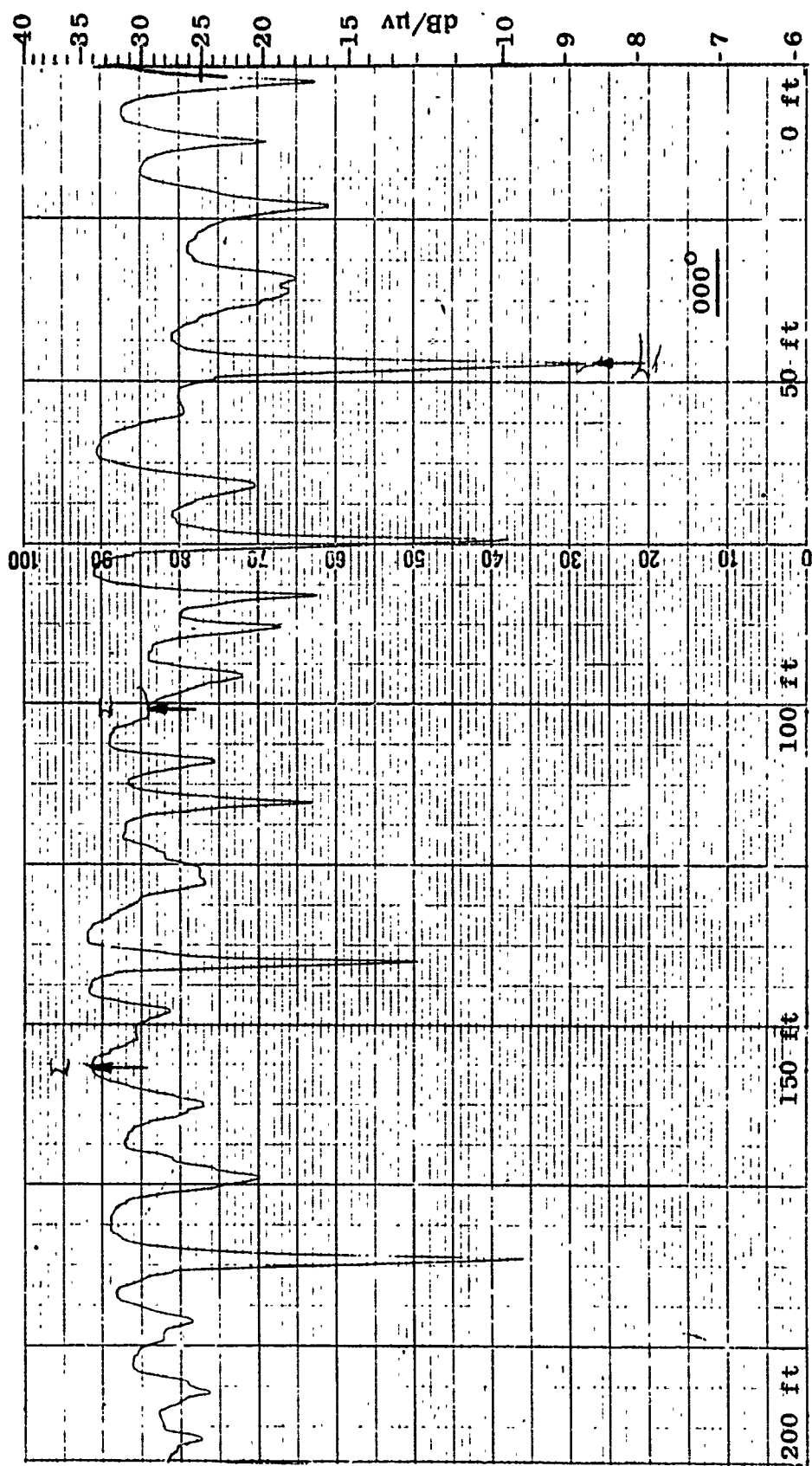


Figure 3.3.4 Plot of Experimental Probability Distribution for Data of Figure 3.3.3



000° Radial Direction

Figure 3.3.5a Signal Recording at Star Field-Point Y-20 (100, 80, V, d, 6)

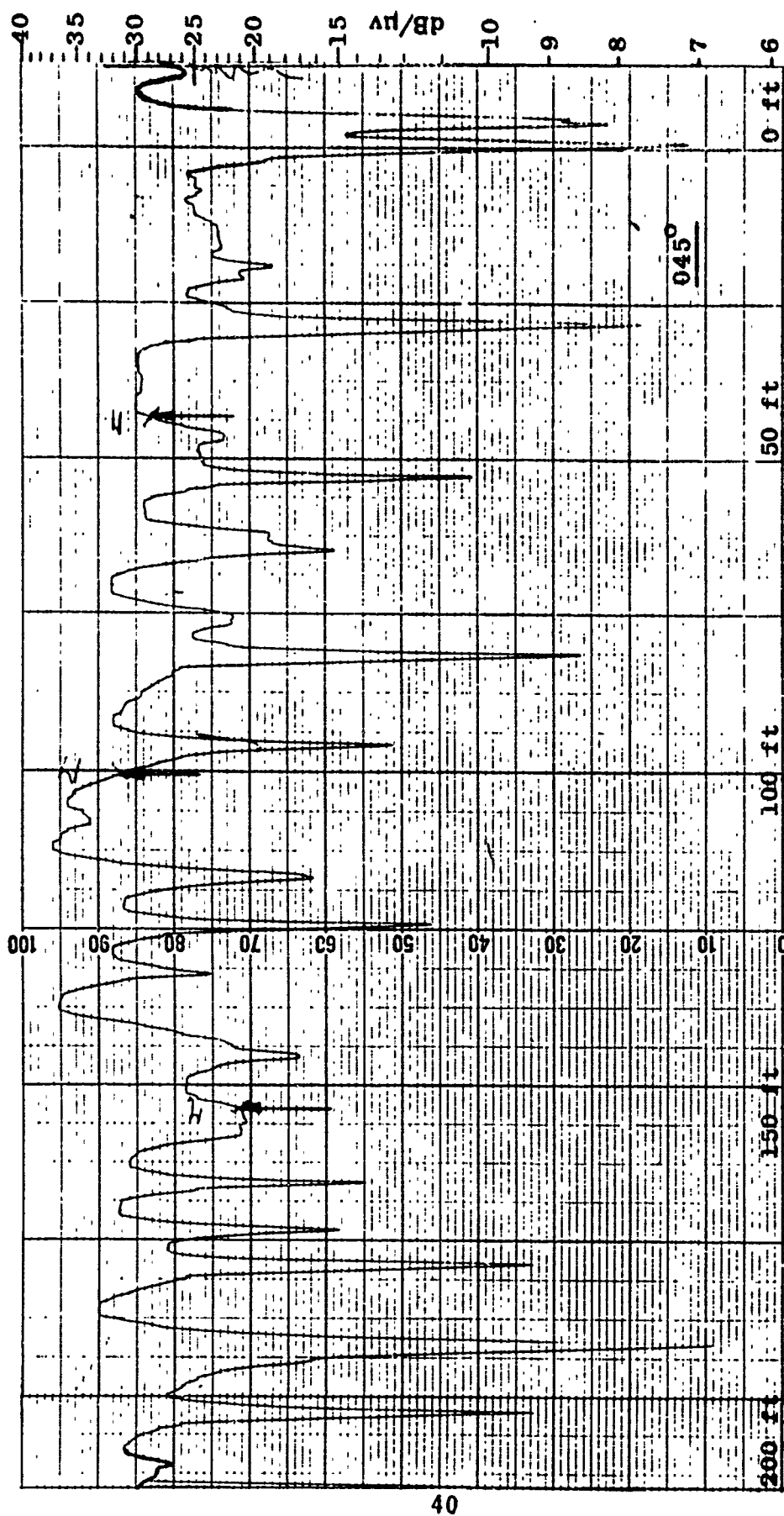


Figure 3.3.5b Signal Recording at 045° Relative to Radial, Y-20 (100, 80, V, d, 6)

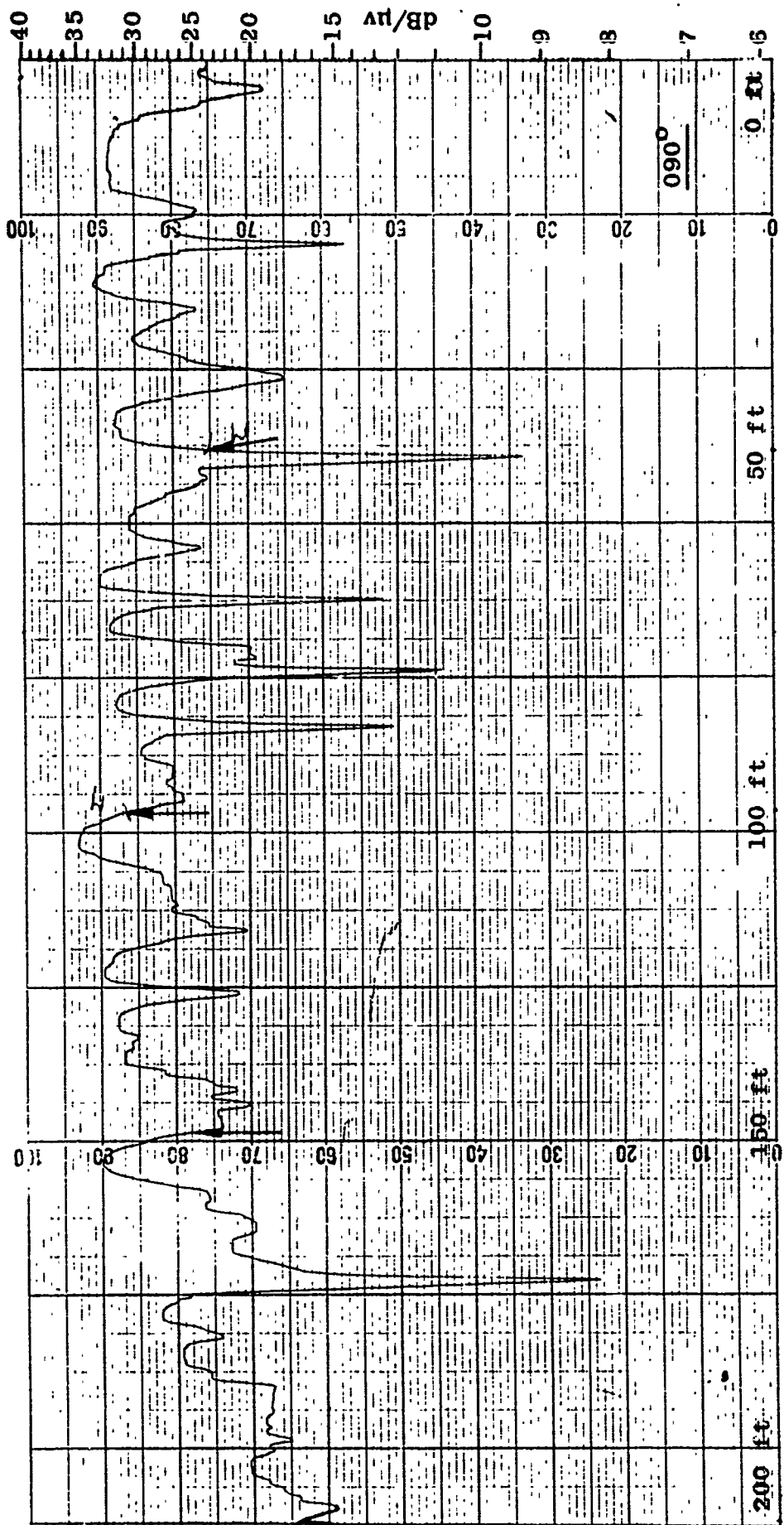


Figure 3.3.5c Signal Recording at 090° (Transverse) (100, 80, V, d, 6)

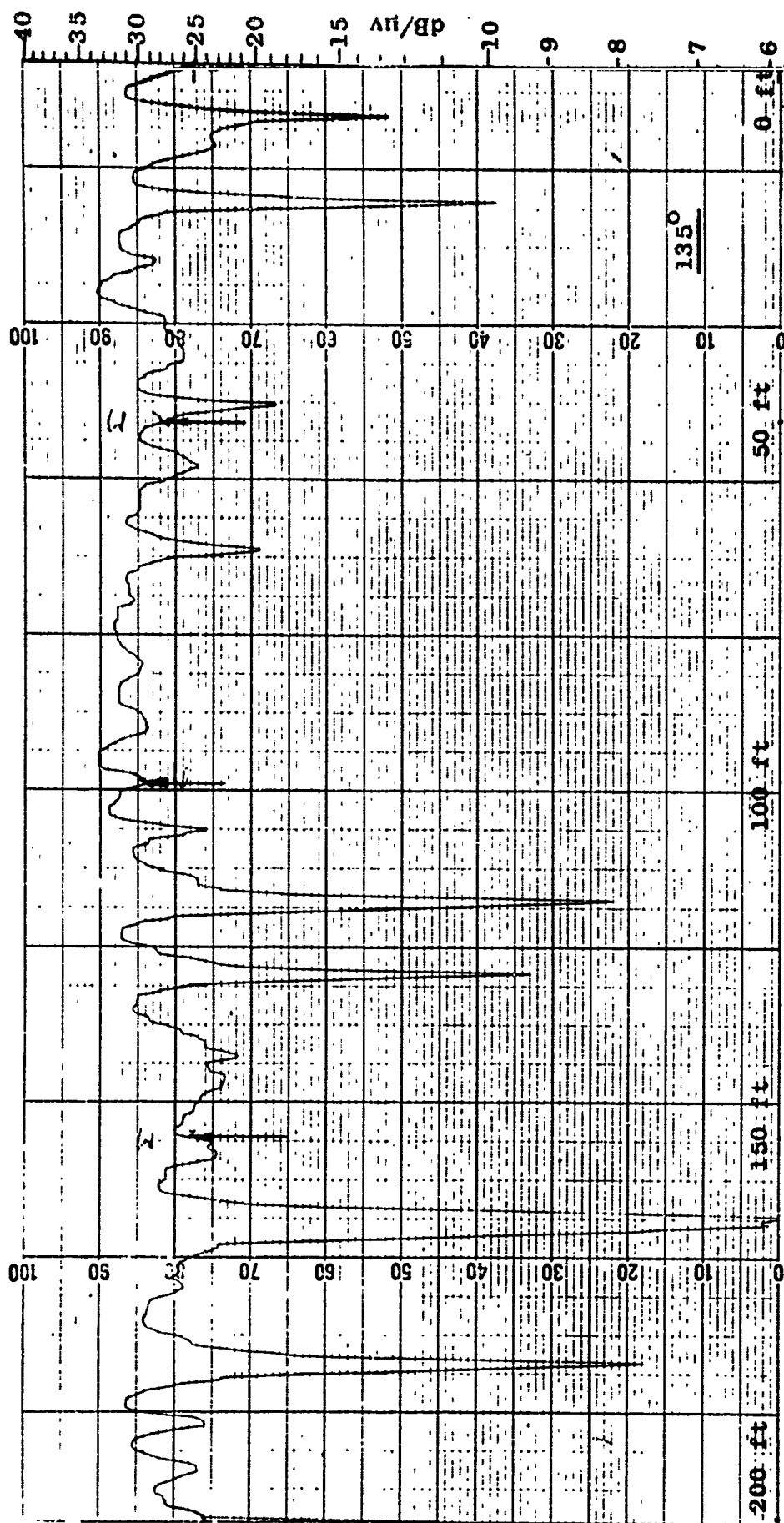


Figure 3.3.5d Signal Recording at 135° Relative to Radial (100, 80, V, d, 6)

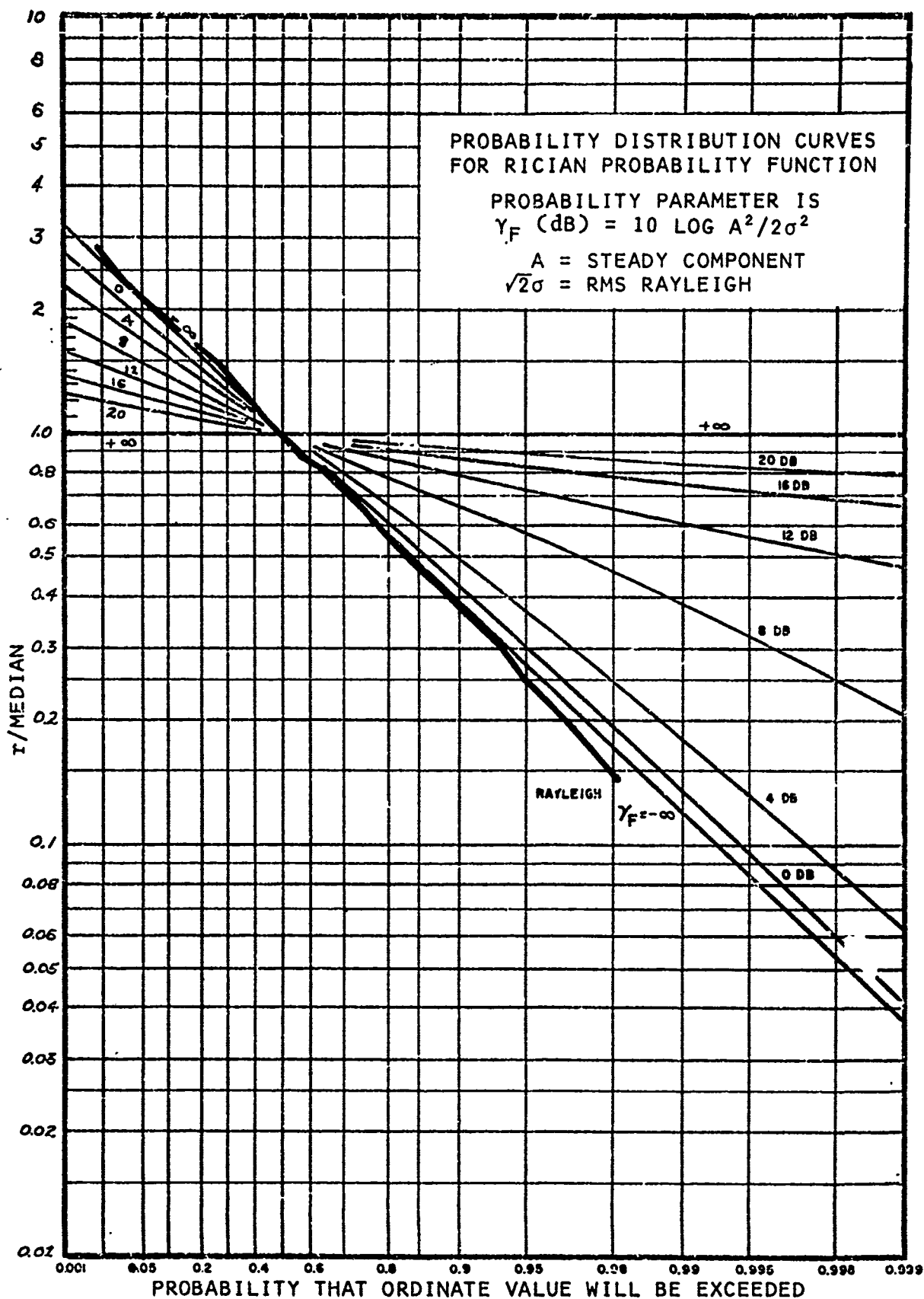


Figure 3.3.6 Plot of Experimental Probability
Distribution for Data of Figure 3.3.5

Table 3.3.2
Time in Seconds That the Signals of Figure 3.3.5
Exceed Given Amplitude Levels *

Signal Level dB	<u>r</u> <u>Median</u>	<u>000°</u>	<u>045°</u>	<u>090°</u>	<u>135°</u>	<u>Total</u>	<u>Probability</u>
+11	2.82	0	0.13	0	0	0.13	.007
+9	2.24	0.17	0.30	0.10	0	0.57	.031
+7	1.78	0.58	0.50	0.64	0.31	2.03	.110
+5	1.41	1.28	1.04	1.38	1.42	5.12	.279
+3	1.12	1.92	1.66	1.87	2.28	7.73	.421
+1	0.89	2.57	2.10	2.55	3.06	10.28	.560
0	0.79	3.20	2.55	2.90	3.47	12.12	.661
-2	0.63	3.57	3.01	3.40	4.02	14.00	.763
-4	0.50	3.80	3.45	3.73	4.19	15.17	.827
-6	0.40	4.02	3.78	4.22	4.28	16.30	.889
-8	0.32	4.17	4.01	4.47	4.33	16.98	.926
-10	0.25	4.23	4.17	4.62	4.41	17.43	.950
-12	0.20	4.28	4.25	4.70	4.45	17.68	.964
-15	0.14	4.32	4.40	4.75	4.53	18.00	.981
TOTAL SECONDS		4.33	4.57	4.77	4.66	18.33	1.000

*Ratio of amplitude, r, to median and average fraction of time above level (probability) also shown.

This example is run No. 249 taken at 100 MHz, vertical polarization, at field point Y-20.

An examination of the plotted distribution curves for all star field-point runs showed that for nearly 80% of the runs the fit of the data to Rician curves, in the 0.10 - 0.90 probability range, was good or very good. For the remaining runs the fit was relatively poor and determination of an average γ_F was, in many of these cases, difficult. In the latter, the experimental distribution often had a slightly greater negative slope than that of the ideal Rayleigh line. Also, it was not uncommon for the experimental distributions to follow a Rician curve at some γ_F below the median, or 0.50 probability level, and to follow another (i.e., a different γ_F) above the median, but the difference between the two values of γ_F rarely exceeded 4 dB. For the runs whose statistics did not closely follow either a Rician or Rayleigh distribution, it was usually evident from an inspection of the signal recording that the measurements were not taken within a sufficiently homogeneous region of the jungle (i.e., the signal was not stationary). In these instances, either an unusually wide and deep null occurred, or the mean signal level shifted appreciably over one or more of the 200-foot paths in the field point.

The values of the parameter γ_F for the star field-point runs are shown in Table 3.3.3 and for the high antenna runs in Table 3.3.4.

Some general characteristics of γ_F as a function of system parameters, i.e., frequency, polarization, antenna heights, and field point locations, as noted from these tabulations are:

Table 3.3.3
The Parameter γ_F for Star Field-Point Measurements

Polar.	Freq.	Tx Ht	Rx Ht	FP-14	FP-10	FP-7	FP-X	Y-20	FP-48	K-29
HORIZONTAL	50MHz	200ft	6ft	+11	R	+9		+1	+18	
		120	6	+11	RR	+8	+9	R	+12	+18
		80	6	+10	0	R	+7			
		40	6	+10	+1	+6	+6		+15	+15
		40	20	+14	-2	+8	+8		+17	
		20	6	+6	0	+2	+3			
		13	6	+5	R	+1	+5	+1	+15	+17
	100MHz	200	6	+5	+4	+5		R	+8	
		120	6	+6	R	+7	+2	R	+9	+12
		80	6	+4	R	+2	+2	0		+12
		40	6	+5	R	R	R	-2	+9	+9
		40	20	+8	+2	+4	+3	+3	+11	+10
		20	6	+5	-2	+1	+3	R		+8
		13	6	+6	0	R	+2	0	+9	+10
	150MHz	200	6	+5	R	-1		R	+9 $\frac{1}{2}$	
		120	6	+2	R	+3	+2	R	+7	+9
		80	6	0	+2	+4		R		
		40	6	+2	R	+3	R	+1	+8	R
		40	20	+1	+4	+1	+3	+2	+15	
		20	6	+4	0	+1		-2		
		13	6	+2	R	R	+4	-2	+3	R
VERTICAL	50MHz	200	6	R	R	0		R	+8	
		120	6	-2	R	R	+1	R	+6	+5
		80	6	R	R					
		40	6	-2	R	0	R		+5	
		40	20	+1	R	R	0		+10	
		20	6	R	R					
		13	6	R	R	R	0	R	+6	R
	100MHz	200	6	R	R	R		R	+4	
		120	6	R	R	R	0	R	+4	+6
		80	6	R	R	R		R		+6
		40	6	R	R	R	+1	R	+5	-2
		40	20	R	-2	R	+3	-2	+4	R
		20	6	-2	+1	R		-2		
		13	6	-2	R	R		-2	R	+1
	150MHz	200	6	R	-2	-2		+2	0	
		120	6	R	R	-2		R	0	+2
		80	6	-2	R	-2		R		
		40	6	R	R	-2	+4	R		
		40	20	R	R	+1	-2	+1	+2	
		20	6	R	R	+2		R		
		13	6	R	R	+2	+2	R		-2

Tx Ht = Transmitter Antenna Height

Rx Ht = Receiver Antenna Height

R denotes Rayleigh distribution.

Table 3.3.4
The Parameter γ_F for High Antenna Measurements

Polar.	Freq.	Radial 1		Radial 2		Transverse 1		Tower Bending	
		Ht	γ_F	Ht	γ_F	Ht	γ_F	Ht	γ_F
HORIZONTAL	50MHz	57	+16			57	+10		
		48	+22			48	+4		
		38	+18			38	+4		
	100MHz	28	+20			28	+6		
		18	+12			18	+4		
		8	+8			8	R		
	150MHz	53	+8	74	+12	58	+4		
		44	+9	64	+8	48	+3		
		33	0	54	+6	38	R		
VERTICAL	50MHz	21½	0	44	R	28	+4		
				34	+6	18	+4		
				24	+7	8	+4		
	100MHz			14	+4				
				6	R				
	150MHz	57	+9			58	R	98	+22
		46	R			48	R	88	+15
		38	R			38	R	78	+18
VERTICAL	50MHz	26	0			28	-2	68	+18
		17½	-2			18	+2	58	0
		8½	0			8	0		
	100MHz	58	+7			57	R		
		48	+3			48	R		
		38	+4			38	-2		
	150MHz	28	+4			28	+3		
		18	R			18	R		
		8	+5			8	+4		
VERTICAL	50MHz	50	0	74	R	58	+4		
		40	R	64	R	48	+6		
		30	R	54	-2	38	+2		
	100MHz	20	R	44	R	28	R		
				34	R	18	0		
				24	+3	8	+5		
	150MHz			14	R				
				6	-2				
VERTICAL	50MHz	59	R			58	R	98	+6
		49	0			48	R	88	0
		38	0			38	R	78	R
	100MHz	29	0			28	R	68	R
		19	R			18	0	58	R
		10	0			8	0		
	150MHz								

R denotes Rayleigh distribution.

Ht = antenna height in feet.

Transmitter antenna height = 150 - 165 feet.

1. At field points within the foliage, the distribution is predominantly Rician for horizontal polarization and is essentially Rayleigh for vertical polarization.
2. The values of γ_F are larger for field points in clearings than for field points within the forest. Also, γ_F is larger in the relatively light forest than in the heavier forests characterized by taller trees.
3. γ_F generally decreases with increasing frequency.
4. For increasing transmitter antenna heights (other things held constant), γ_F generally increases, but in some cases γ_F appears to vary independently of transmitter antenna height.
5. In most cases an increase in the receiver antenna height from 6 to 20 feet caused a significant increase in γ_F ; however, in a few cases γ_F decreased slightly.

Results of the high antenna runs are:

1. The values of γ_F do not increase uniformly with increasing antenna height. There is, however, a tendency for the smallest values of γ_F to occur at the lowest heights and the largest values to occur at the highest heights.
2. In 6 out of 8 cases, with vertical polarization, the distribution was Rayleigh or near-Rayleigh

for receiver antenna heights up to approximately 60 feet above the ground. The canopy height in the vicinity of these measurements was 100 to 120 feet.

3. Although all height-variability runs were taken in the vicinity of Y-20, there does not appear to be much correlation between values of γ_F corresponding to similar antenna heights at two or three different locations. This is attributed to two factors: limited sampling and local non-homogeneities in the forest.

These results, which show the distributions to be Rician or Rayleigh, support the scatter model proposed by Hicks and Robertson [1969]. The results also show that the system parameter having the greatest over-all effect on γ_F , or the signal variability, is polarization. The effects of frequency and antenna heights on γ_F are, apparently, less significant and less predictable than the effect of polarization.

Although the highest values of γ_F were observed with signals measured in clearings (FP-48 and K-29), there were a few runs in which the received signals in the clearing were Rayleigh distributed. For the field points located within the forest, it is evident that, other things being equal, a considerable variation in the values of γ_F exists among the different field points. The highest values of γ_F from the field points in the forest were measured at FP-14, where the forest is relatively light and has a low canopy height (see Table 3.1.2). The lowest values of γ_F were measured at FP-10 and Y-20. Field point Y-20 is located in the heaviest forest measured in Area II and FP-10, as shown in Table 3.1.2, is

located in a somewhat light or moderately heavy forest. The signal statistics for field points FP-7 are very similar to those of FP-X and are intermediate between those for FP-14 and Y-20. The environmental characteristics of FP-7 are very similar to those of FP-X and are intermediate between those for FP-14 and Y-20. The environmental characteristics of FP-7 and FP-X also appear to be very similar and numerically lie between those of FP-14 and Y-20. Hence, with the exception of FP-10, the results show that γ_F decreases as the forest biomass and tree height increase. The results at FP-10 are, however, probably influenced by terrain, as FP-10 was shadowed from the transmitter to some degree by high ground and, as shown in the next section, γ_F generally decreases in the shadow zones. The results of FP-7 are somewhat in question because it may be located sufficiently near the transmitter to permit reception of a direct signal through the foliage. Nevertheless, there appears to be a definite (though inverse) correlation between γ_F and the biomass and/or tree height. However, since tree height (and diameter) and density are directly related to the biomass, the more significant vegetation factor cannot be deduced here.

It is clear that these results are in qualitative agreement with the physical concepts of a scatter model [Hicks and Robertson, 1969]. For example, as the biomass increases (assuming tree height constant) the propagation loss is intuitively expected to increase, thereby decreasing the dominant lateral wave component of the signal by a greater amount than the scattered components because the lateral wave passes through a larger portion of the vegetation. Thus, γ_F may be expected to decrease with increasing biomass. Also, if there are a very few tall trees emerging from the forest in the vicinity of the receiver (which allows the assumption that

biomass and canopy height remain about the same) then the lateral wave, or dominant component, may remain about the same while the scattered signal (scattered by the few larger trees) increases. This also decreases γ_F . Thus, in the more likely case where greater emergent tree heights also correspond to larger biomass, these two effects will act together to reduce $\gamma_F = A^2/2\sigma^2$ by increasing the scatter (i.e., increasing $2\sigma^2$) and by decreasing the specular component, A . Clearly, further work is required to quantitatively relate the vegetation characteristics to the signal characteristics, and an analytical scatter model appears to provide a very direct avenue for this.

Several aspects of the star field-point data require further consideration and analysis. For example, the spatial separation between deep signal fades is a function not only of signal wavelength [Jansky & Bailey, 1966; 1968] but also of the direction of antenna travel through the forest with respect to the direction of the transmitter. This property, which is more evident with horizontal polarization than with vertical, can be seen from the sample recording presented in Figure 3.3.3. This shows that the separation between deep fades for the signal measured on the radial, or 100° path, is approximately one-half wavelength (10 feet at 50 MHz), whereas the separations between nulls for the 090° path are approximately one wavelength and those for the 045° and 135° paths are somewhere between. This implies that the fading rate and other signal statistics for a mobile receiver, for example, will vary with the direction of travel relative to the transmitter, and should be investigated.

Long Trail Runs

A number of long trail recordings have been analyzed to determine the statistical behavior of both the long spatial

variations and the short spatial variations. As a part of this analysis it was necessary to remove the deterministic mean signal level. For the main access trail and Z-radial recordings the deterministic mean levels were drawn at a slope of $40 \log d$, whereas those for the transverse trail recordings were drawn at constant levels or zero slope. In the case of transverse A, however, the two halves of the trail were displaced by an amount requiring the deterministic mean level for the more distant half to be drawn 2 dB below the level for the less distant half. Note that it is not necessary that the deterministic mean curve be drawn at the true mean level of the signal (the slope of the mean curve is important), because the offset of the true mean level is determined from the analysis.

The distributions of the long spatial signal variations were studied first. Eight continuous trail recordings, taken along the main access trail, were analyzed in the following manner. The average of the short spatial variations, which constitutes the long spatial variations, was drawn by hand on each recording. With a straight edge, the distance-above-level technique was used to determine the cumulative probability distribution of the long spatial variations with respect to the deterministic mean line. Each amplitude level, although not actually drawn on the recordings, was a line parallel to the deterministic mean line and separated from it by some fixed number of decibels. In general, these levels were taken at each dB above and below the deterministic mean line, and a sufficient number of levels were used to span the variations of the long-term mean. The distributions were plotted on Gaussian probability graph paper using both linear and logarithmic scales. An example of the probability distribution of the long spatial variations for a long-trail recording along the main access trail is shown in Figure 3.3.7. Many of

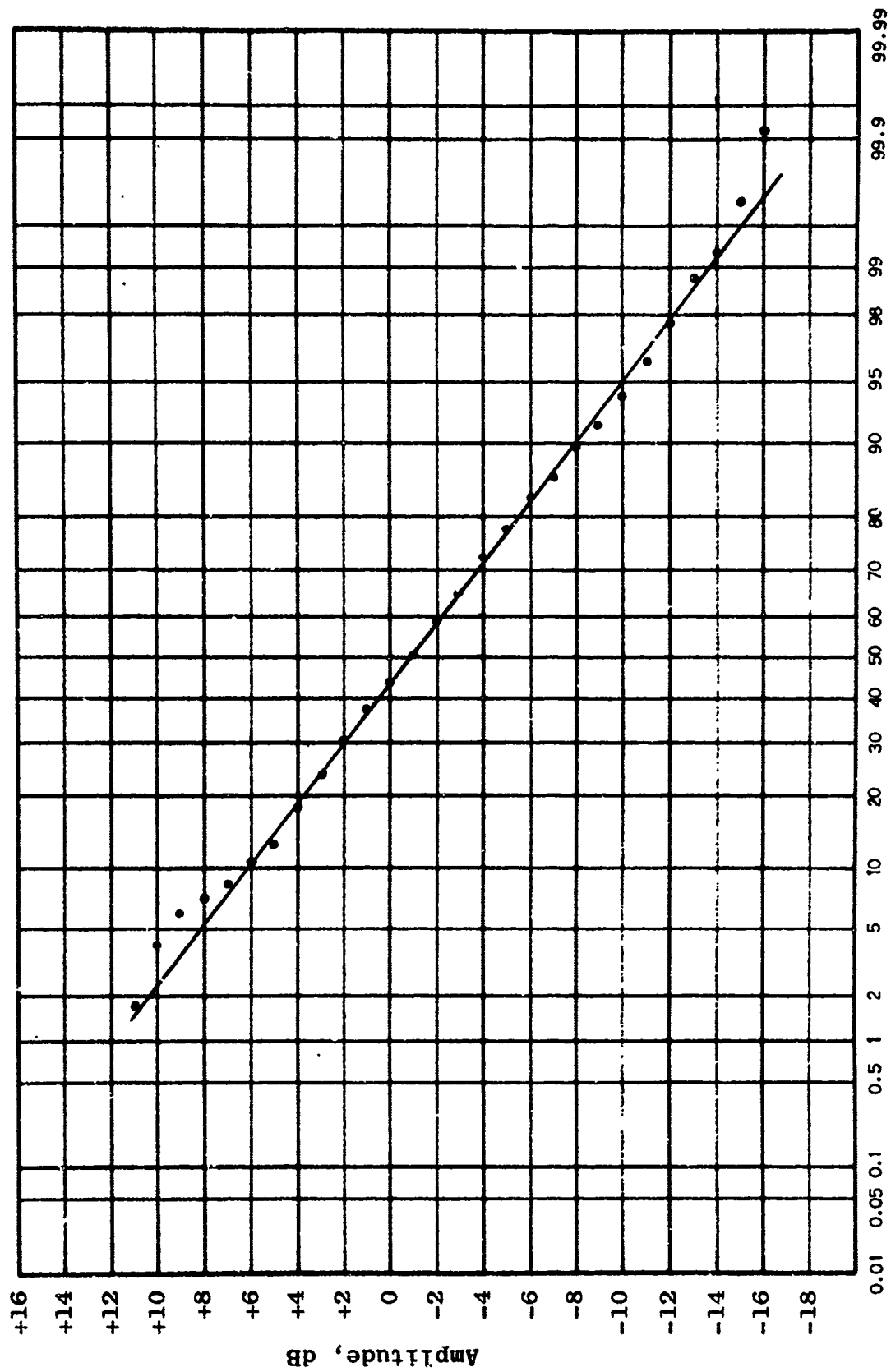


Figure 3.3.7 Cumulative Probability Distribution of Long Spatial Variations About Deterministic Mean

the curves were fairly linear for the signal levels plotted on a linear scale, but the log-normal distribution appeared to provide the best over-all fit to the data. Thus, plotting each on log-normal paper, the standard deviation for each was determined and is tabulated below.

STANDARD DEVIATION OF LOG-NORMAL DISTRIBUTIONS
OF LONG-TERM SIGNAL MEAN FROM RUNS TAKEN ALONG
THE MAIN ACCESS TRAIL

<u>Frequency</u>	<u>Polarization</u>	<u>Transmitting Antenna Height</u>	<u>Standard Deviation</u>
50	H	13	4.5 dB
50	H	20	6.2
50	H	40	4.8
50	H	80	6.4
50	H	120	5.0
50	H	200	4.8
100	H	40	6.0
150	H	40	4.9
Average			5.3 dB

No trend is evident in the above values of standard deviation over the range of parameters shown. The spread of the standard deviation is less than 2 dB. The results of the analysis of these eight runs on the main access trail indicate that the long-term signal variations are log-normally distributed about the deterministic mean level with a standard deviation of approximately 5.3 dB, for the receiver antenna height at 10 feet. The values of the standard deviation appear to be independent of the transmitter antenna height.

The log-normal distribution is in agreement with the distribution of signal variations over rough earth in the

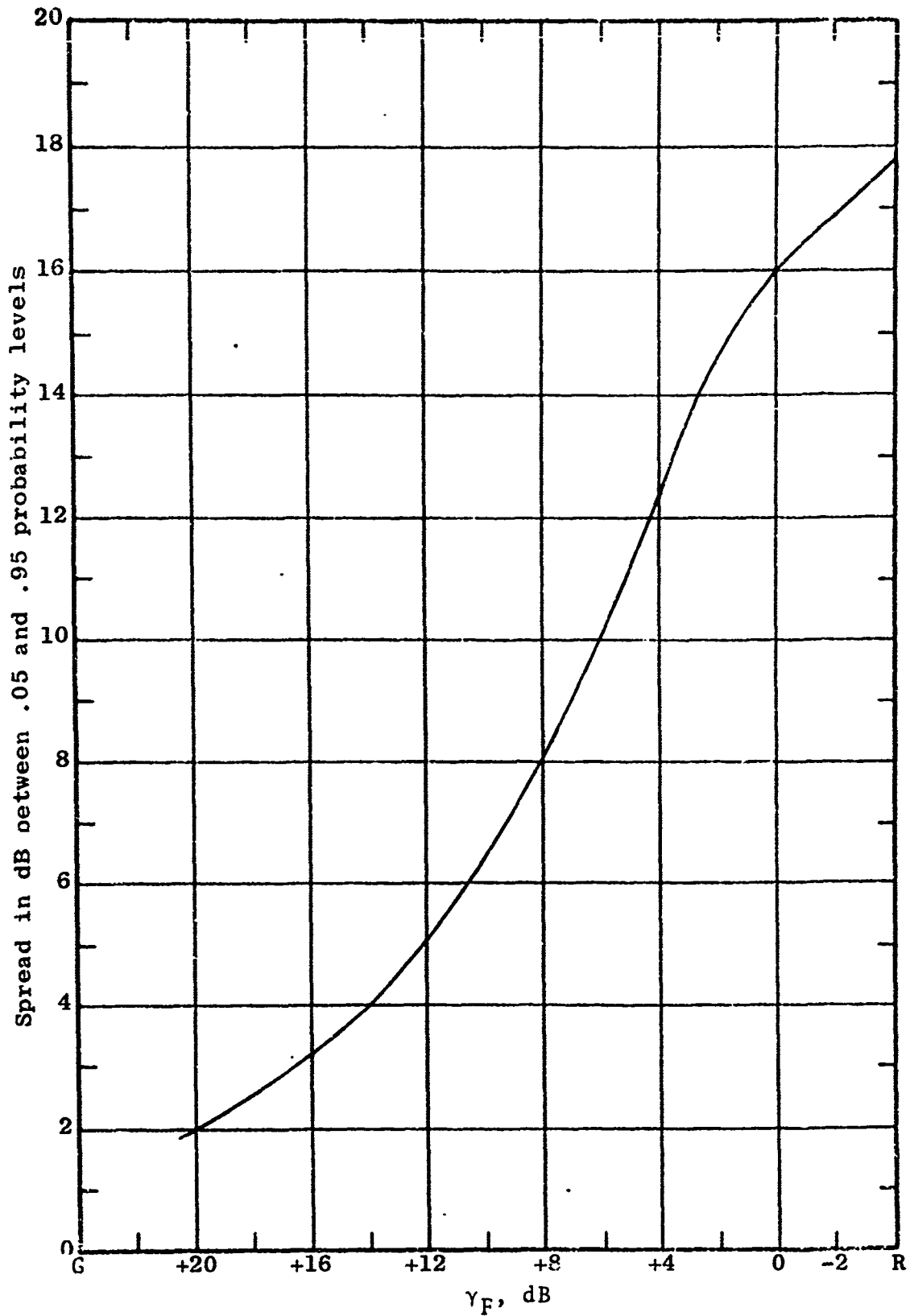
absence of foliage [Egli, 1957], and also with the distribution of the long-term mean for signals transmitted via the ionosphere and troposphere [Schwartz, Bennett and Stein, 1966]. Hence, it is reasonable to associate the long spatial variations with terrain and gross vegetation factors.

The second type of analysis of the continuous trail recordings involved characterizing statistically the total received signal behavior normalized to a constant transmission range. The statistics of the total signal for continuous trail recordings has been reported earlier for Area I [Jansky & Bailey, 1965]; however, in that work the analysis involved measuring the statistics of signal variations over distance samples of 0.2 miles and 0.5 miles. Since the long-term mean would be expected to vary considerably over these distances, it is not surprising that the results showed a log-normal distribution in all cases. In the present study the total signal statistics of long trail recordings have been determined in much finer detail.

The analysis of the short spatial variations of the long trail recordings was done next and has been based upon the major finding of the star field-point analysis; that is, the statistics of short-term signal variations over a sample in which the average signal level (average of the short spatial variations) remains nearly constant can be adequately characterized by a Rician distribution. As shown previously, the γ_F parameter alone is sufficient to describe the particular Rician statistics except for a scaling factor which can be determined from some absolute measure of the statistics; e.g., mean, median, etc. Now, for a given Rician distribution, a distinct relationship exists between the γ_F of this distribution and the spread in dB over which the signal varies between

some upper and lower percentile levels. Referring to the Rician probability graph of Figure 3.3.1, for example, it can be seen that for a distribution having $\gamma_F = + 4$ dB the upper 10% (probability 0.1) of the signal occurs at 3.5 dB above the median, and the lower 10% (probability 0.9) level occurs 5.6 dB below the median. Thus, $\gamma_F = + 4$ dB corresponds to a 9.1 dB spread between the 10 - 90 percentile levels. Conversely, a 9.1 dB spread between the 10 - 90 percentile levels of a Rician distribution implies that $\gamma_F = + 4$ dB for the distribution.

Use was made of this one-to-one relationship in the analysis of the short spatial variations for the long trail runs. Percentile levels of 5% - 95% (probability range 0.05 - 0.95) were chosen, and the corresponding relationship between γ_F and the level spread v is shown in Figure 3.3.8. Note from this curve that the maximum spread, representing a Rayleigh distribution, is approximately 18 dB. Assuming the short spatial variations to be Rician distributed and breaking the data into segments, the technique for determining the γ_F of the distributions was accomplished as follows. A straightedge was placed on the signal trace, aligned parallel to the deterministic mean line, and for the upper percentile level the straightedge was shifted up and down without changing its slope until it was visually estimated that the signal exceeded the straightedge position or level for 5% of the time. The position of this level was marked. The process was repeated at the lower percentile level, except the straightedge was shifted up or down until the level was found where the signal fell below the level 5% of the time, and this level was marked. The difference in dB between these two levels gave, through use of the curve in Figure 3.3.8, an estimate of the γ_F parameter for the given segment of signal data.



G denotes Gaussian distribution
R denotes Rayleigh distribution

Figure 3.3.8 Amplitude Spread Between Probability Limits Versus γ_F for Rician Distribution

The analysis of the long trail runs involved breaking up the total trail distance for each recording into a number of small segments such that for each segment the following conditions were satisfied as closely as possible.

- a. The mean level of the short spatial variations is reasonably constant with respect to the deterministic mean line over the segment.
- b. The variability of the short spatial variations appears to be about the same throughout the segment.
- c. The length of the segment is as long as possible.

Conditions b and c were well satisfied in most cases. Condition a, however, could not always be fulfilled, and it was occasionally necessary to include the effect of a varying mean within a segment. In a few cases, the segments were as short as 20 feet, but in most they were considerably larger. Three measurements were taken on each segment :

- a. The length, x_i , of the segment (trail distance in appropriate units).
- b. The mean level, m_i , in dB with respect to the deterministic mean level line.
- c. The spread, v_i , in dB between the 0.05 - 0.95 probability levels of the signal.

Each segment is thus represented in the functional form of (x_i, v_i, m_i) which becomes, through the use of the curve of

Figure 3.3.8, (x_i, γ_{Fi}, m_i) , $i = 1, 2, \dots, n$ where

$$\sum_{i=1}^n x_i = \text{total trail length of a long trail recording.}$$

A typical example of the results of this analysis is given in Table 3.3.5 for a continuous trail recording along the main access trail at 50 MHz, horizontal polarization, transmitter antenna height of 20 feet, and receiver height of 10 feet.

The short spatial variations over twenty continuous trail recordings have been analyzed in this manner, and the signal behavior of each run has been characterized in tabulated form (not shown) by the quantities (x_i, γ_{Fi}, m_i) . These results provide a considerable amount of detailed information concerning the nature of the distribution of signal strengths within the forest environment and are considered to be representative of the general forest region of Area II.

The analyses indicate that, in general, the values of γ_F vary over a wide range for each trail recording and are independent of transmission range. The cumulative probability distribution of γ_F with distance (or with time, assuming that antenna travel is at constant velocity) has been calculated for each run. For illustrative purposes, the cumulative probability distribution of γ_F in dB for the data presented in Table 3.3.5 is shown plotted in Figure 3.3.9. The cumulative probability distribution of the mean levels m_i in dB of these data is also shown in Figure 3.3.9.

A possible correlation between the mean m_i and γ_{Fi} of each segment of the continuous trail data in Table 3.3.5 was examined by plotting m_i versus γ_{Fi} and is shown in Figure 3.3.10. All the points are contained within the shaded area

Table 3.3.5
 Characteristics of Signal Along Main Access Trail
 (50, 20, H, d, 10)

<u>Segment No.</u>	<u>Segment Length x</u>	<u>γ_F, dB</u>	<u>Segment Mean m</u>
1	0.4	+7.0	+5 dB
2	0.9	+10.5	+7
3	0.4	+3.5	-4
4	0.6	+20.0	+4
5	1.2	+7.0	-3
6	0.6	R	-9
7	1.2	+4.3	+1
8	1.7	+4.3	-5
9	1.5	+2.6	-3
10	2.5	+11.8	+3
11	1.0	+0.2	-4
12	1.0	+10.5	+3
13	1.2	+6.1	+3
14	1.5	+10.5	+4
15	1.9	+10.5	-1
16	1.4	+2.6	-6
17	2.8	+16.4	+2
18	1.9	+9.2	0
19	1.9	+13.8	+6
20	2.1	+9.2	+2
21	1.3	R	-8
22	0.9	+6.1	-4
23	0.5	+13.8	+1
24	0.6	R	-7
25	1.0	+8.0	-1

Note: Segment length is 200x feet.
 R denotes Rayleigh distribution.

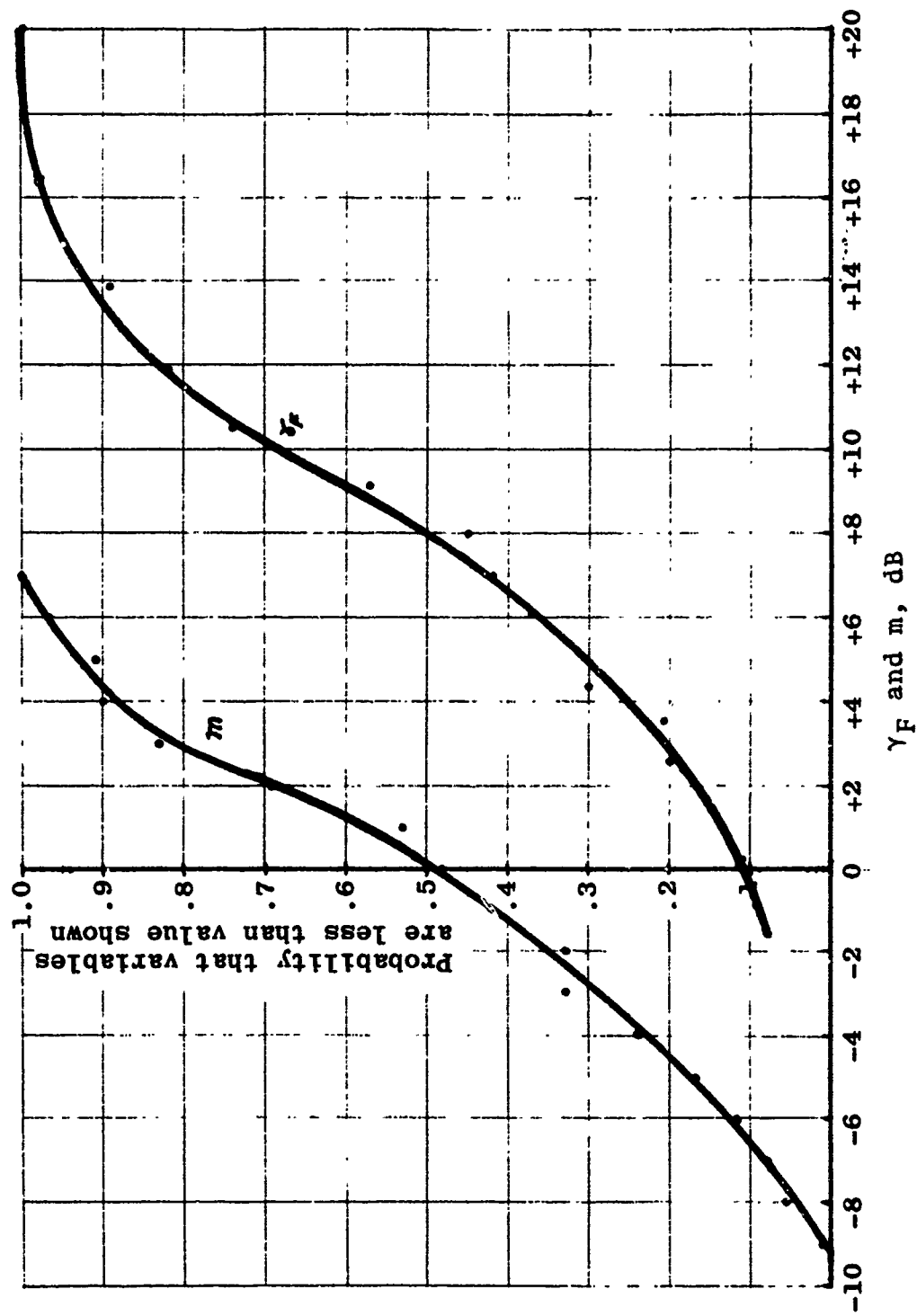


Figure 3.3.9 Cumulative Distribution of γ_F and m for Data in Table 3.3.5

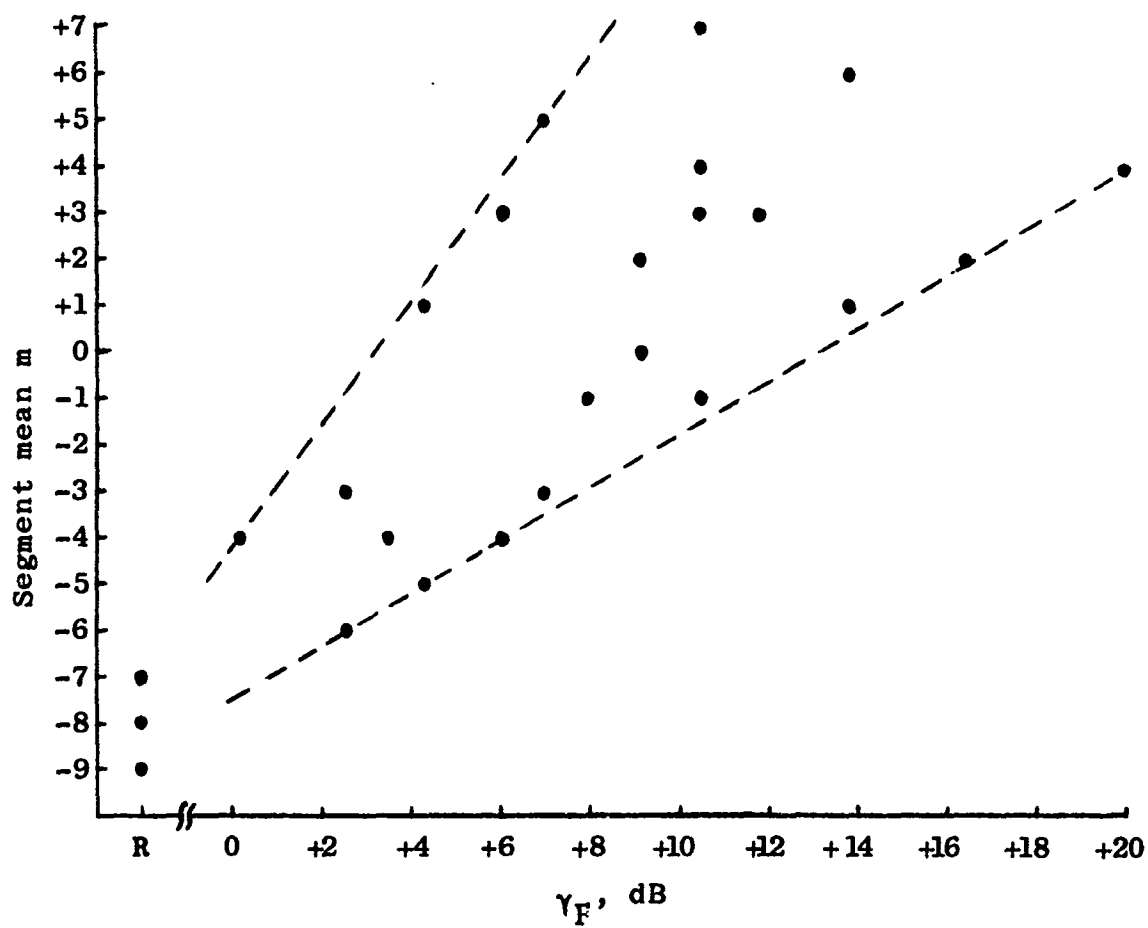


Figure 3.3.10 Plot of m_1 Versus γ_F for Data from Table 3.3.5 (R denotes Rayleigh distribution).

and indicate that a positive correlation exists between the two variables. All runs for which the data have been plotted in this manner show similar correlation. The average straight-line slope through the plotted points (m_i, γ_{Fi}) ranges from 0.75 to 3. It should be recalled that the changes in mean signal level discussed here are those caused by terrain or gross vegetation factors in the local environment of the receiver (such as depicted by the environmental differences between star field points) and are not the result of changes in the over-all signal strength level due, for instance, to varying transmission range or adjustments in the transmitter power level which are unrelated to the statistics of signal fading. Thus, the positive correlation obtained here between γ_F and m_i is consistent with the negative correlation of γ_F with biomass (and other related factors) obtained from the analysis of star field-point data discussed in the previous section, and provides further support for the concepts of the qualitative scatter model. However, unlike the case of the star field point-data, some insight may be gained here as to whether either the steady signal A^2 , or the scattered components of the signal, $2\sigma^2$, is being influenced the most heavily by the environmental factors. This can be investigated as follows.

The mean of a Rician distributed variable r given by Eq.(1) is

$$m = \int_0^{\infty} r p(r) dr = \sigma \sqrt{\frac{\pi}{2}} e^{-\frac{\gamma_F}{2}} \left[(1 + \gamma_F) I_0 \left(\frac{\gamma_F}{2} \right) + \gamma_F I_1 \left(\frac{\gamma_F}{2} \right) \right] \quad (5)$$

where $\gamma_F = A^2/2\sigma^2$ as defined previously, and I_0 and I_1 are modified Bessel functions of the first kind, zero and first

order respectively. Dividing both sides of Eq.(5) by $\sqrt{2}\sigma$ gives

$$\frac{m_1}{\sqrt{2}\sigma} = \frac{\sqrt{\pi}}{2} e^{-\frac{\gamma_F}{2}} \left[(1 + \gamma_F) I_0 \left(\frac{\gamma_F}{2} \right) + \gamma_F I_1 \left(\frac{\gamma_F}{2} \right) \right].$$

A plot of $m_1/\sqrt{2}\sigma$ as a function of γ_F is shown on dB scales in Figure 3.3.11 where $(m/\sqrt{2}\sigma)_{dB} = 20 \log_{10}(m/\sqrt{2}\sigma)_{lin}$ and $(\gamma_F)_{dB} = 10 \log_{10}(\gamma_F)_{lin}$. This curve gives the theoretical relationship between the quantities shown for any Rician process. One interpretation, which is of interest here, is the following. If the magnitude of the Rayleigh component σ remains constant, and only the specular component A is varied in a Rician process, then the relationship between the mean and $\gamma_F = A^2/2\sigma^2$ of the process is given by the curve of Figure 3.3.11. A comparison of this theoretical curve with the trend of data seen in Figure 3.3.10, then, suggests that the scattered signal component σ remained relatively constant or steady throughout the continuous trail run.

The constant σ process may be further examined and some insight gained into the relationship between the signal statistics and the terrain and vegetation over the trail. This aspect of the long trail data has not yet been fully analyzed, but some results of the initial attempt along these lines are discussed next.

As mentioned above, the quantities γ_F and m are sufficient to define a Rician distribution. Clearly, the same distribution may also be expressed by the quantities A and $\sqrt{2}\sigma$. The tabulated data in the form of (x_i, γ_{Fi}, m_i) (see Table 3.3.5) for thirteen long trail runs have been transformed into the quantities $(x_i, A_i, \sqrt{2}\sigma_i)$ for the purpose of examining

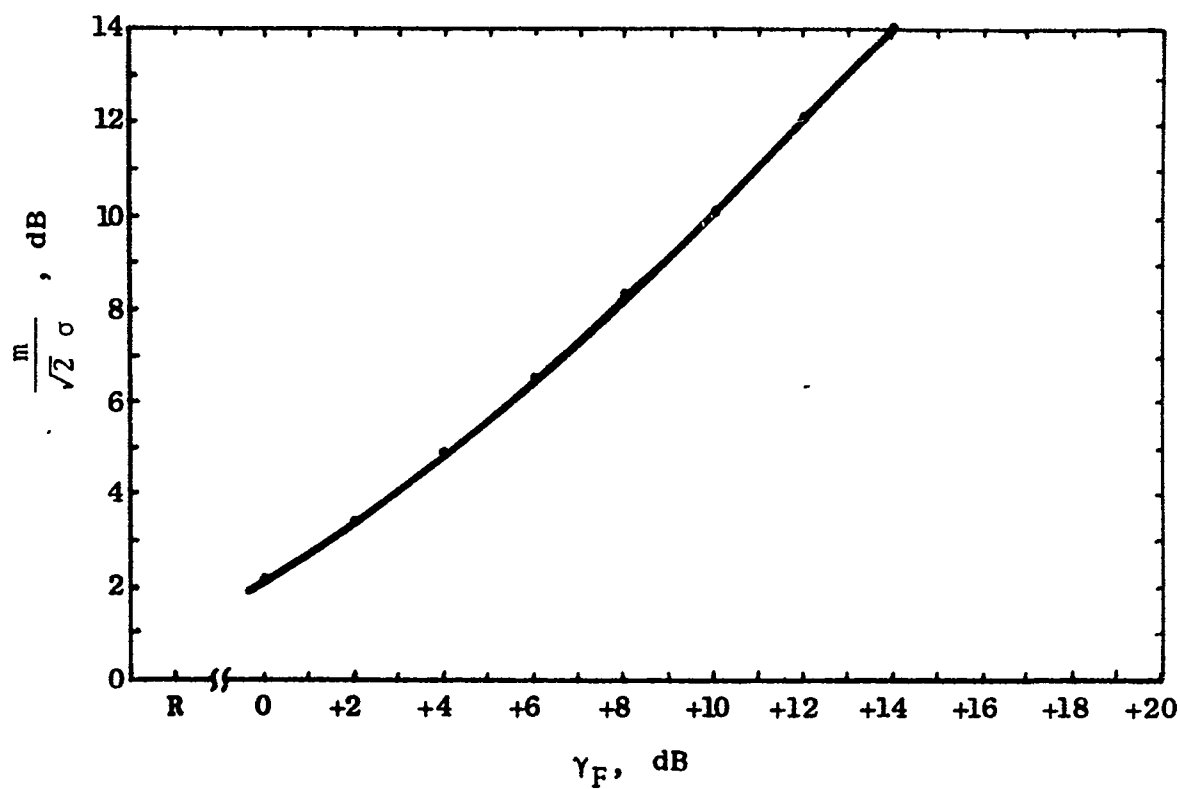


Figure 3.3.11 Plot of $m/\sqrt{2}\sigma$ Versus γ_F for a Rician Distribution

the variations of A and $\sqrt{2}\sigma$ with trail distance. The transformation of the quantities (γ_F, m) into $(A, \sqrt{2}\sigma)$ was accomplished by first computing the value of $\sqrt{2}\sigma$, using the curve of $m/\sqrt{2}\sigma$ versus γ_F shown plotted in Figure 3.3.11, and then computing A from $\gamma_F = A^2/2\sigma^2$. It is noted that A could have been equated to m , with little error for $\gamma_F > 2$ dB, but the method employed here does not so restrict γ_F . The magnitudes of A and $\sqrt{2}\sigma$ were plotted for each run; an example of which is illustrated in Figure 3.3.12. The two quantities were plotted on identical linear vertical scales to permit direct comparison. The average value of A is approximately 1.0 because the values of the segment means m_i in each tabulation were adjusted to give an over-all mean level of zero dB for each run. The elevation profile of the trail (main access trail) for this example is included in Figure 3.3.12.

An examination of these results shows several general characteristics of both the scattered components $\sqrt{2}\sigma$ and the steady component A for each run. Of the thirteen runs studied, twelve were made with horizontal polarization at the three test frequencies, and one was with vertical polarization at 50 MHz along the main access trail.

The following characteristics were noted.

1. The mean value of $\sqrt{2}\sigma$ over a run is smaller than that of A . For runs made along the main access trail, the mean of $\sqrt{2}\sigma$ is 25% - 50% of the mean of A . For runs made in the heavier forest (Z-radial and transverse B) the mean of $\sqrt{2}\sigma$ is 50% - 70% of the mean of A .

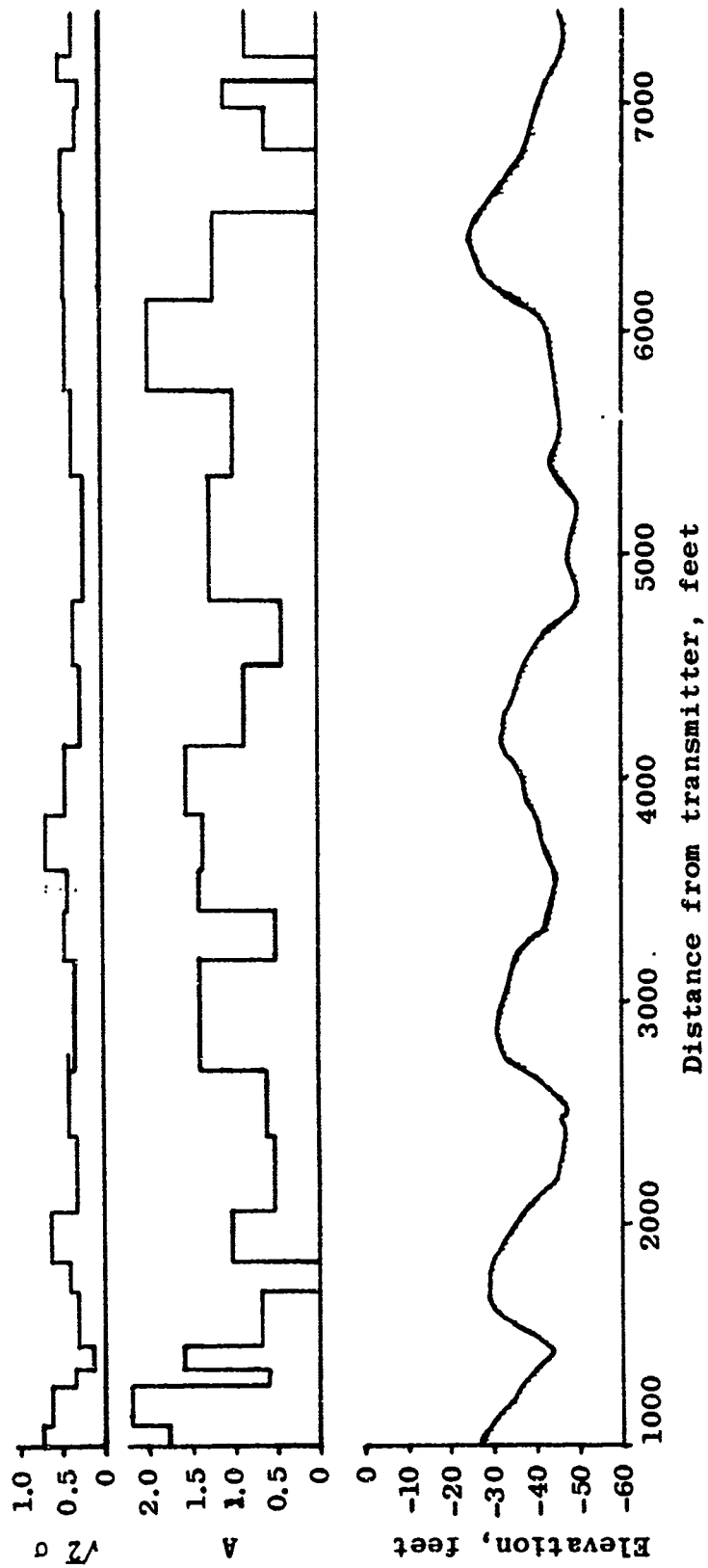


Figure 3.3.12 Plot of $\sqrt{Z} \sigma$, A , and Terrain Elevation Over Main Access Trail

2. The $\sqrt{Z}\sigma$ values exhibit less variation than does A. All runs made in the heavier jungle produced greater variations in $\sqrt{Z}\sigma$ than did the runs made along the main access trail.
3. The distributions of $\sqrt{Z}\sigma$ (not shown) were found to fit either a normal or log-normal distribution. The ratio of the standard deviation to the mean ranged from .27 - .64 for runs made along the main access trail and from .50 - .84 for runs made in the heavier forest.
4. There appears to be little or no short-term correlation between $\sqrt{Z}\sigma$ and A. For runs made in the heavier forest (Z-radial and transverse B) some correlation is evident between $\sqrt{Z}\sigma$ and A and the terrain elevation.
5. The distribution of the steady component A (not shown) was approximately Rayleigh.
6. There appears to be a moderate degree of correlation between A and the terrain elevation. That is, the magnitude of A tends to increase in regions of relatively high terrain.

Thus, in general, the terrain appears to affect the dominant or steady signal component to a greater extent than it does the scattered components. In the case of vertical polarization, however, it appears that there is, effectively, no dominant component because the distribution is generally Rayleigh. For horizontal polarization the distribution is usually Rician, indicating the presence of a dominant

component. Again, these are in qualitative agreement with the scatter model concepts, but it is reiterated that further analysis is required to ascertain quantitative relationships between the environmental factors and the signal characteristics.

3.4 Probability of Error For Digital Transmission

An important application of the statistics derived from CW signal envelope data measured in the forest is the determination of the probability of error in digital transmission systems operating in the environment. The probability of error is a number representing the fraction of transmitted pulses (marks and spaces) which on the average are expected to be received erroneously, i.e., a transmitted mark (or space) is interpreted as a space (or mark) by the decision circuit in the receiver. The error probability provides a measure of performance of a pulse code modulation (PCM) system operating through a given environment and is, in general, a function of the type of modulation, the receiver signal-to-noise ratio (SNR), and appropriate signal statistics of the transmission medium or channel [Stein and Jones, 1967]. Of the various kinds of pulse modulation techniques available, only noncoherent frequency-shift keying (FSK) is treated here.* The condition of frequency-flat reception is realized in practice by limiting the signal bandwidth to a sufficiently small fraction of the channel coherent bandwidth. The frequency selective properties of a forested radio channel are discussed later in this report.

* The error probability curves for FSK shown in this report, when reduced by 3 dB in SNR, are identical to those of differentially coherent phase-shift keying (DPSK).

The probability of error curves for a noncoherent FSK (binary system) for additive Gaussian noise only (nonfading) and for Rayleigh fading are shown in Figure 3.4.1. The steep curve on the left represents the probability of error as a function of SNR due to additive Gaussian noise only without channel fading. In the presence of channel fading for which the received signal envelope is Rayleigh distributed about some mean SNR, γ_0 , the probability of error increases considerably, as is shown by the second curve of Figure 3.4.1. The probability of error due to channel fading is easily derived from the nonfading curve as follows [Stein and Jones, 1967].

The SNR variable γ of the nonfading curve $P_1(\gamma)$ is treated as a random variable having a probability density function $p(\gamma)$ representing the statistics of the fading. At an average SNR γ_0 where

$$\gamma_0 = \bar{\gamma} = \int_{-\infty}^{+\infty} \gamma p(\gamma) d\gamma \quad (6)$$

the error rate shown by each point on the fading curve $P_2(\gamma_0)$ is the average of a distribution of error rates given by the nonfading curve $P_1(\gamma)$ when the signal-to-noise ratio γ is varying over its distribution $p(\gamma)$; that is,

$$P_2(\gamma_0) = \int_{-\infty}^{+\infty} P_1(\gamma) p(\gamma) d\gamma \quad (7)$$

In the case of noncoherent FSK, the nonfading curve is

$$P_1(\gamma) = \frac{1}{2} e^{-\frac{\gamma}{2}} \quad (8)$$

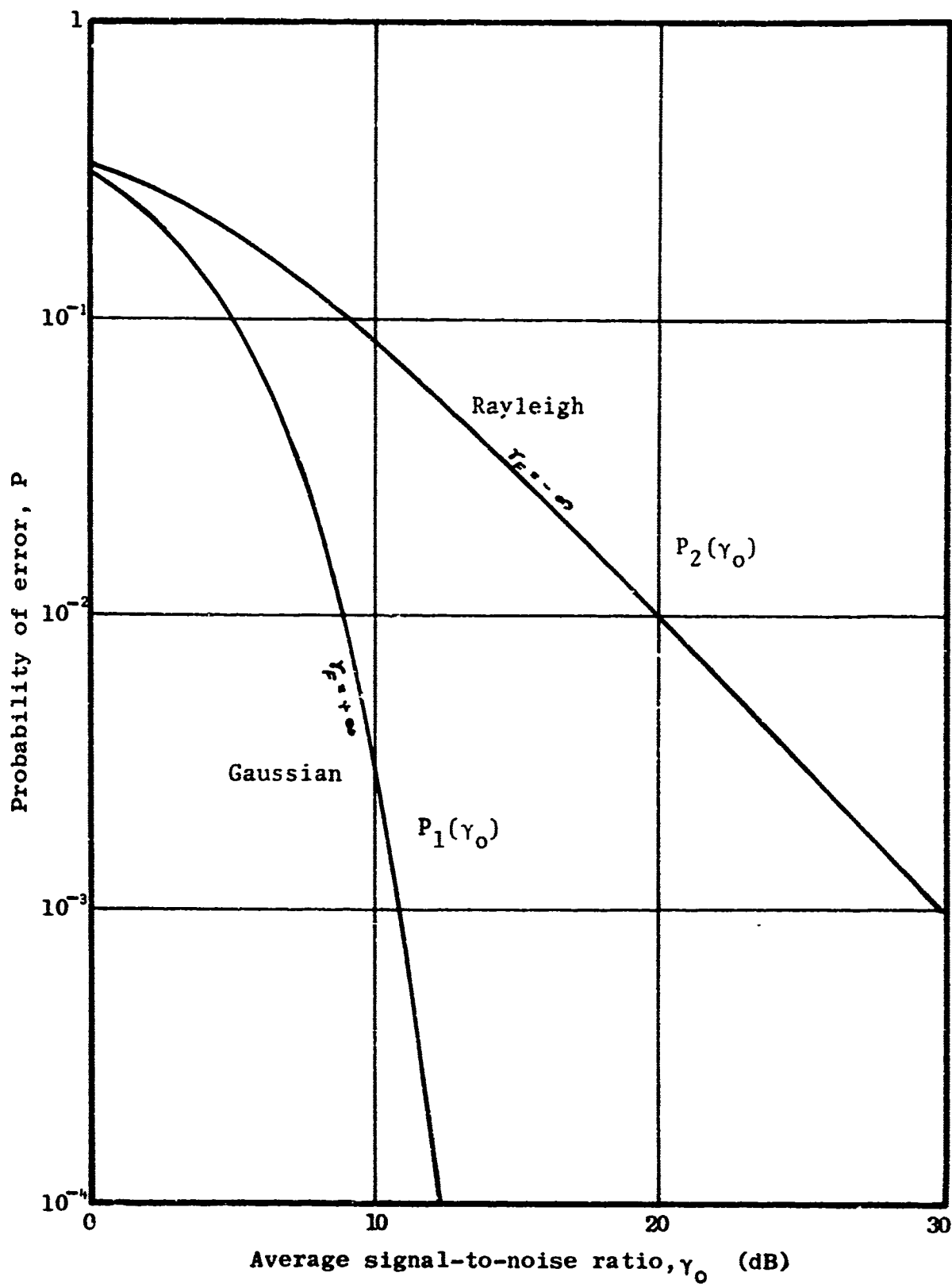


Figure 3.4.1 Probability of Error for Noncoherent, Binary, FSK System

where γ is the signal-to-noise power ratio. The probability density function of a Rayleigh fading channel is

$$p(r) = \frac{2r}{r_0^2} e^{-\frac{r^2}{r_0^2}} \quad (9)$$

where r is the magnitude of signal envelope or signal intensity, and r_0 is the rms of the distribution. The signal-to-noise power ratio is defined by

$$\gamma = \frac{r^2}{2N^2} \quad (10)$$

where N is the noise intensity at the receiver filter output. With the change in variable given by Eq.(10) the probability density function of a Rayleigh fading channel becomes

$$p(\gamma) = \frac{1}{\gamma_0} e^{-\frac{\gamma}{\gamma_0}} \quad (11)$$

where γ_0 is defined by Eq.(6). From Eq.(7) the probability of error for noncoherent FSK in the presence of Rayleigh fading is

$$P_2(\gamma_0) = \frac{1}{2 + \gamma_0} \quad (12)$$

For a Rician channel in which the probability density function of the fading signal envelope is given by Eq.(1), the probability of error for noncoherent FSK derived in the

same manner as shown for Rayleigh fading becomes [Nesenbergs, 1964]

$$P(\gamma_o, \gamma_F) = \frac{1 + \gamma_F}{2 + 2\gamma_F + \gamma_o} e^{-\frac{\gamma_F \gamma_o}{2 + 2\gamma_F + \gamma_o}} \quad (13)$$

Curves of this function are shown plotted in Figure 3.4.2 for several values of the Rician parameter γ_F .

It is noted that when both terminals are stationary there is no fading of the signal except for that due to the disturbance of wind in the vicinity of either terminal [Hicks and Robertson, 1969]. Unless an antenna is placed at the location of a deep signal interference minima, however, the variation of received signal strength with wind appears to be relatively minor, particularly at lower VHF frequencies. In the absence of fading, as with fixed antennas, the Rician curves do not apply, and the error rate is determined from the additive Gaussian-noise curve $P_1(\gamma)$, and γ (receiver SNR) is the only quantity that needs to be ascertained. Obviously, the error rate will be a minimum when either one or both antennas are located at an interference peak.

If one terminal is moving in a forest the fading statistics can, from the previous section, be assumed to be Rician. The error rate curves for a Rician fading channel, Figure 3.4.2, can then be applied directly to a communications link in a forested environment if both the average receiver signal-to-noise ratio and the parameter γ_F , as one moves from region to region, can be determined. If the receiver has a field-strength meter or a calibrated S-meter it may be possible to estimate the average receiver signal-to-noise ratio.

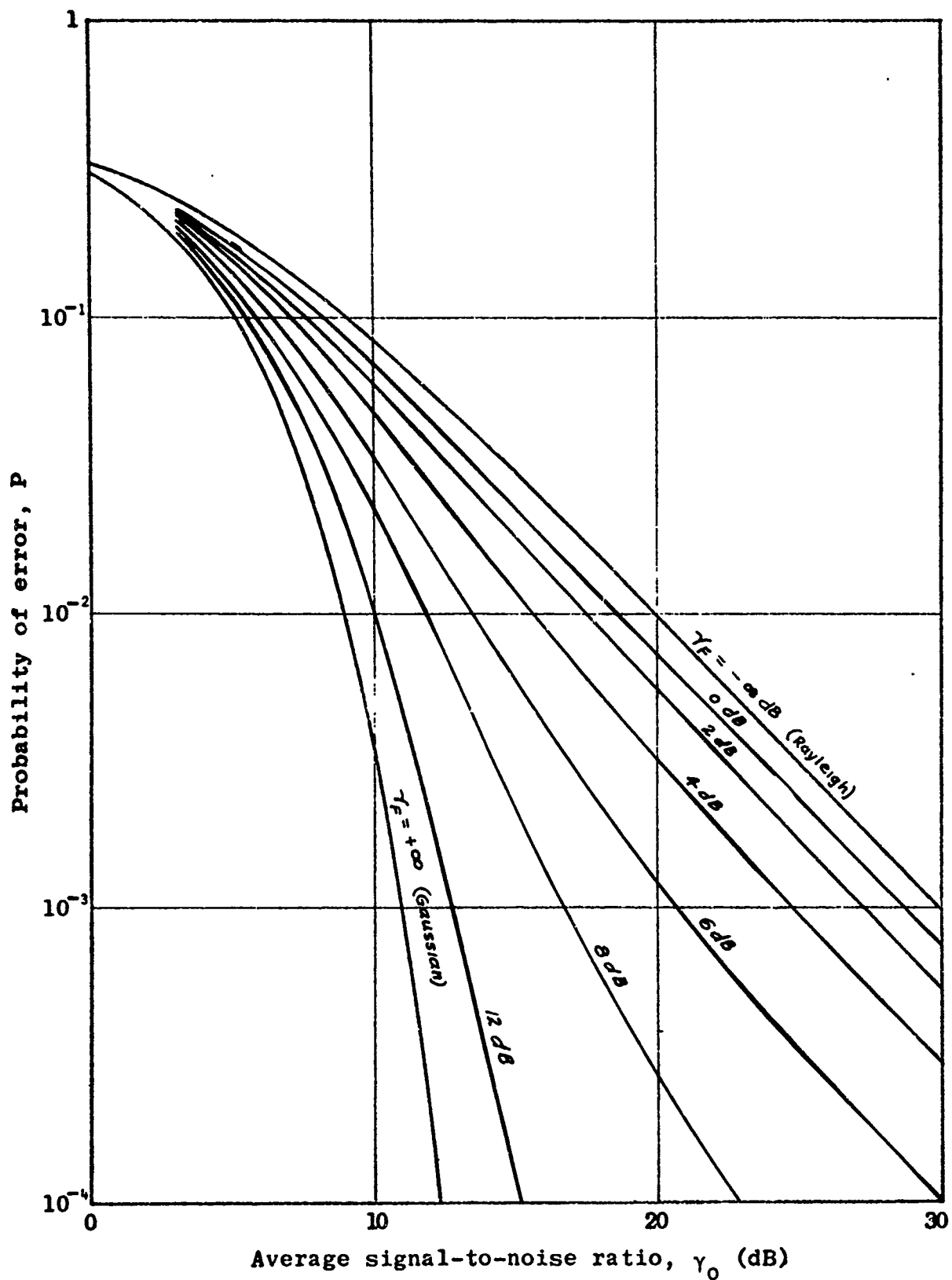


Figure 3.4.2 Probability of Error for a Noncoherent FSK System in a Rician Fading Channel

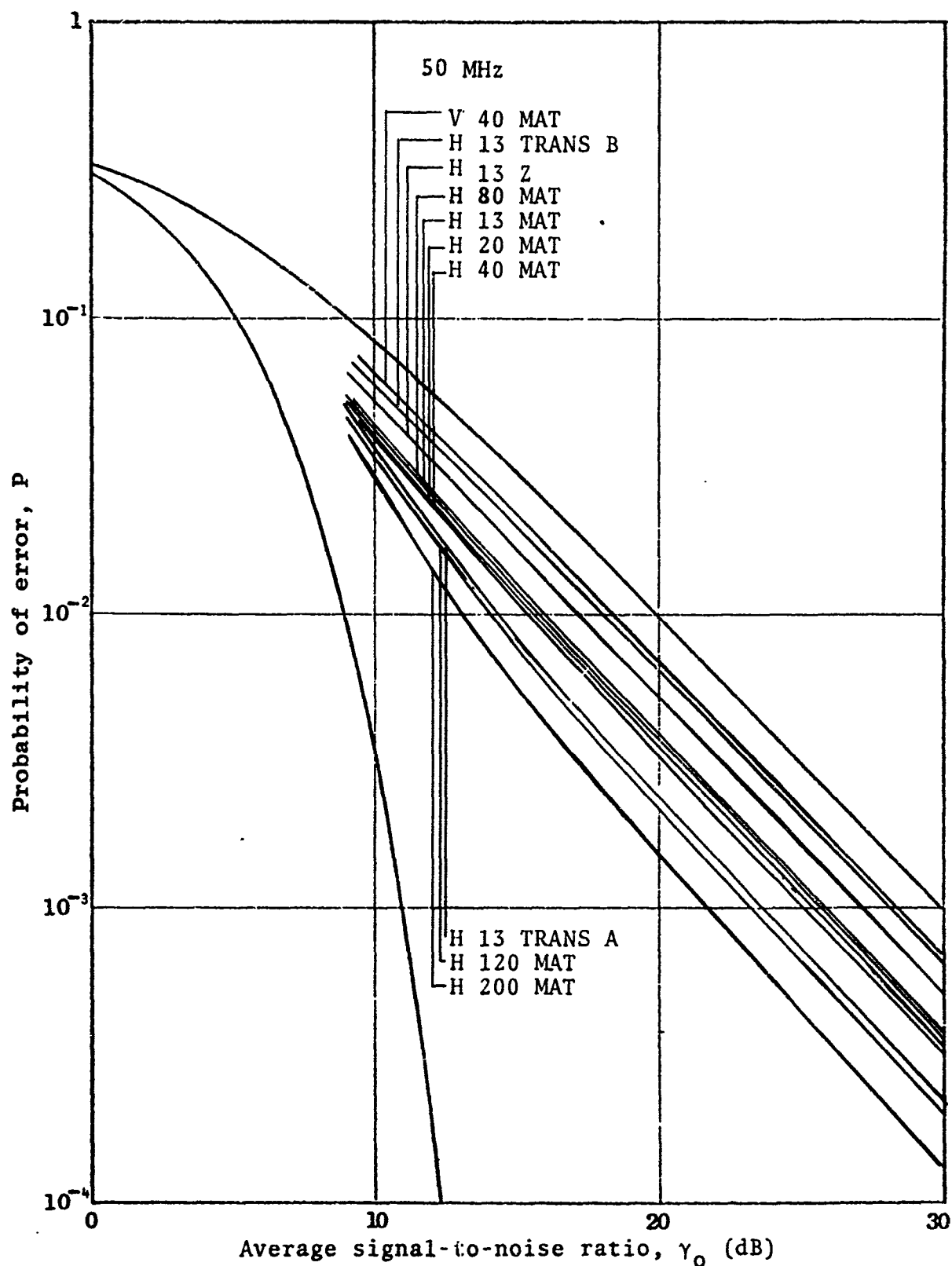
An estimate of γ_F in the region may be obtained by observing the range in dB over which 90% of the signal varied (within the 5% - 95% levels) and applying the curve shown in Figure 3.3.8. This technique is approximate, but it permits one to quickly estimate, for instance, whether or not a region is causing Rayleigh or near-Rayleigh fading.

An alternative, somewhat general, approach is to determine the average probability of error that would be expected when the receiver (or transmitter) is traveling over large areas of a forest. The analyses of star field-point and long trail runs have shown that the Rician distribution, at a particular γ_F , represents the fading statistics within a very limited region only; and, in general, both γ_F and the mean signal level vary considerably from region to region. Distributions of γ_F for the forest have been determined from the long trail data, but, due to long spatial variations or changes in the mean, the probability of error is clearly not a function of γ_F alone. In fact, it can be seen from the curves of Figure 3.4.2 that a 1 dB change in mean signal level about an average SNR can be as significant upon error rate as a 1 dB change in γ_F . Consequently, a mathematical expression for the statistics of long trail data must necessarily include the variations of both γ_F and m in order that the average probability of error can be accurately calculated. The most direct approach, and that which has been followed here, is to apply the actual data to the probability of error curves for Rician fading. At some fixed average SNR, γ_0 , the values of γ_{Fi} and m_i for each i -th segment of a run were used to calculate the probability of error $P_{ei}(m_i + \gamma_0, \gamma_{Fi})$ for the segment, where the computation was done according to Eq.(13) with m , γ_0 , and γ_F expressed in linear units. The average probability $P_e(\gamma_0)$ for the run is the weighted average of the probabilities of the segments, computed as follows:

$$P_e(\gamma_0) = \frac{\sum_i x_i P_{ei}(m_i + \gamma_0, \gamma_{Fi})}{\sum_i x_i}$$

where x_i is the length of the i -th segment and $\sum_i x_i$ is the total trail length measured. For each run, $P_e(\gamma_0)$ was computed for three values of γ_0 : 10 dB, 20 dB, 30 dB. Composite probability of error curves for twenty long trail runs were computed in this manner and are shown plotted in Figures 3.4.3, 3.4.4 and 3.4.5 for the three test frequencies of 50, 100 and 150 MHz, respectively. The curves show that the probability of error generally associated with the lighter forest (main access trail and transverse A) is generally smaller than with the heavier forest (Z-radial and transverse B), as expected, since γ_F is inversely correlated with the forest density and error probability. This difference may also be due in part to the fact that the receive antenna height for the north side measurements (trails Z and transverse B) was 6 feet above ground, and for the south side (main access trail and transverse A) the height was 10 to 13 feet, since the probability of error can be seen to decrease with increasing antenna heights. Also, horizontal polarization yields a smaller probability of error than vertical polarization. The 50 MHz measurements on the main access trail (Figure 3.4.3) indicate that a marked decrease in error probability occurs when the transmit antenna is raised to and above the forest canopy (i.e., for 50 H 120 and 50 H 200, MAT).

A comparison has been made between the probability of error curves derived from the data and the theoretical Rician probability of error curves of Figure 3.4.2, and it is evident that the empirical curves can be approximated by Rician curves at appropriate values of γ_F . Accordingly, the empirical probability of error curves, as shown at each test



H and V are for Horizontal and Vertical Polarization, the numbers represent transmit antenna height in feet, and the letters denote the long trails (i.e., MAT = Main Access Trail).

Figure 3.4.3 Average Probability of Error for Noncoherent FSK System Operating at 50 MHz in Area II

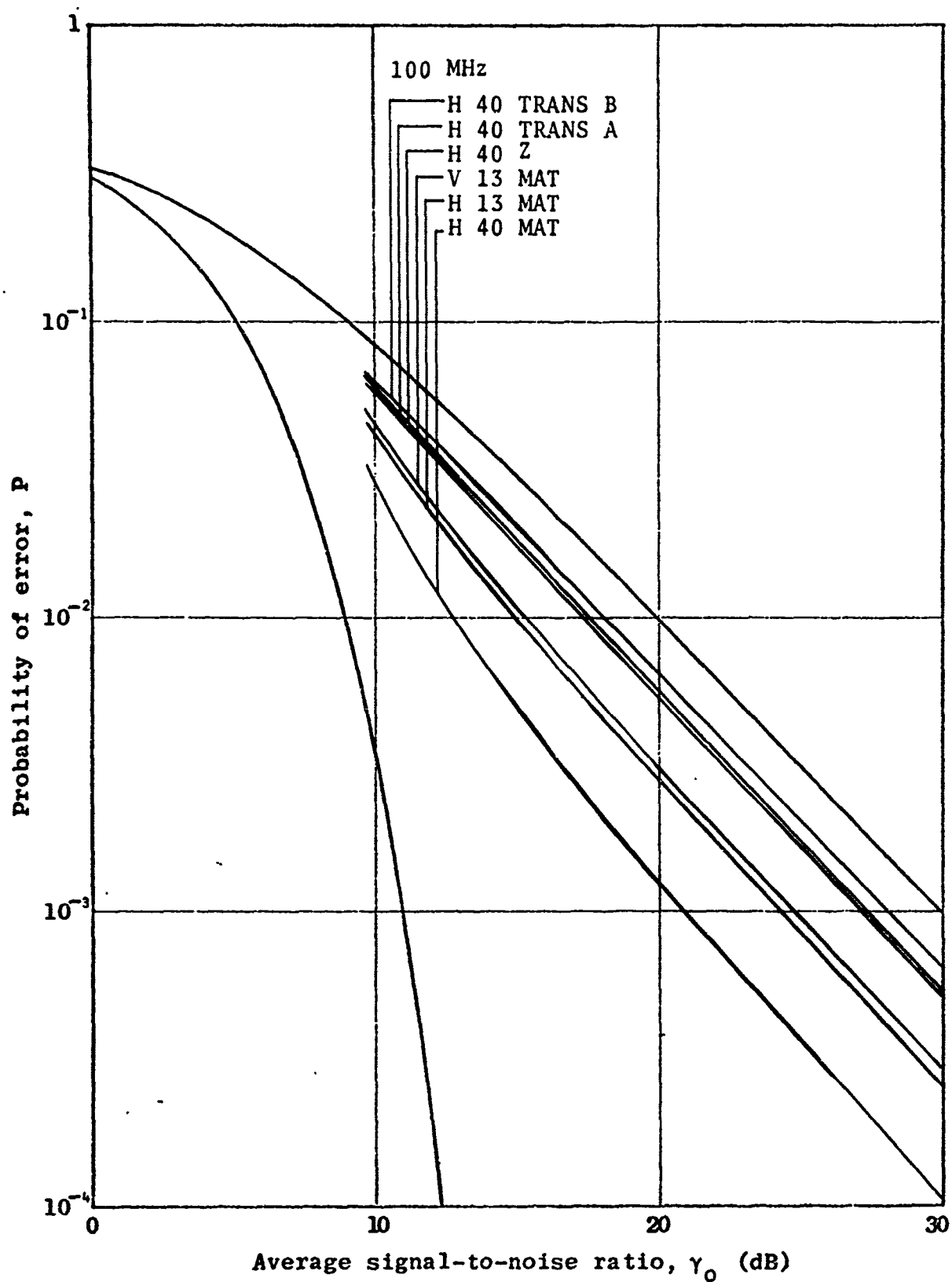


Figure 3.4.4 Average Probability of Error at 100 MHz.
Nomenclature same as in Figure 3.4.3.

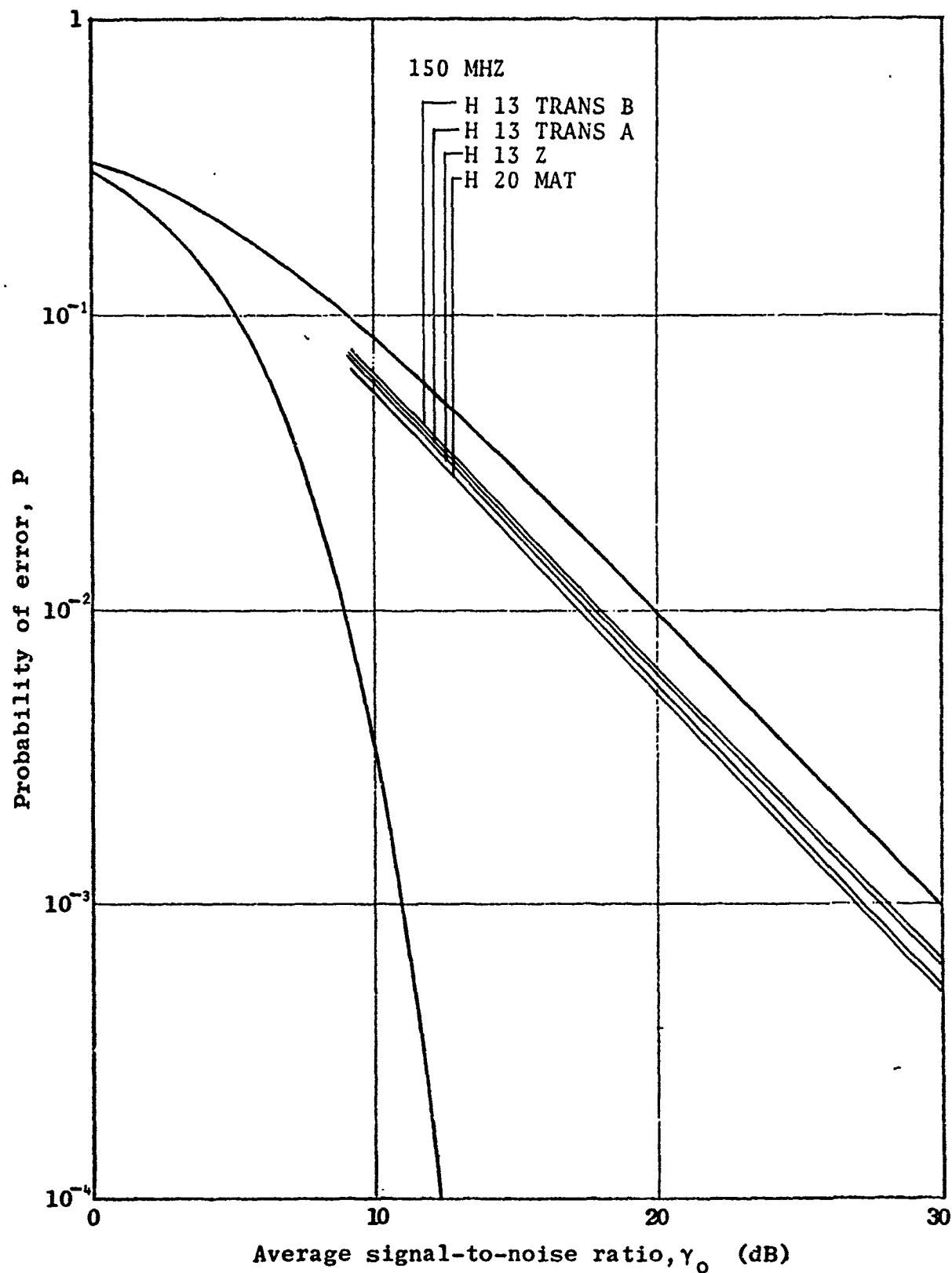


Figure 3.4.5 Average Probability of Error at 150 MHz.
Nomenclature Same as in Figure 3.4.3.

frequency, are represented in the table below by a range of Rician curves between two values of γ_F . For example, the long trail data have shown that for horizontal polarization the probability of error expected in a heavy tropical rain forest (Z-radial and transverse B) for a transmit height of 40 feet and receiver height of 6 feet is equivalent to that for Rician fading having values of γ_F between +1 dB and +2 dB.

Table of Ranges of Rician Parameter γ_F ,
Giving Probability of Error Curves
Equivalent to the Composite Probability of Error
Curves of Figures 3.4.3, 3.4.4 and 3.4.5

<u>Test Frequency</u>	<u>Main Access Trail and Transverse A</u>	<u>Z-Radial and Transverse B</u>
50 H*	+3 dB to +5 dB	0 dB to +2 dB
100 H	+4 dB to +6 dB	+1 dB to +2 dB
150 H	+1 dB to +2 dB	+1 dB to +2 dB

Only two runs of vertical polarization were analyzed. At 50 MHz the calculated curves for vertical polarization gave larger probability of error values than did the curves for horizontal polarization. However, this was not the case for the vertical polarization run at 100 MHz (see Figure 3.4.4).

Further analyses of the long trail runs are required to verify the apparent trends in the relationships among the empirical probability of error curves as a function of system parameters and the characteristics of the forest.

* Runs for transmit heights of 120 and 200 feet are excluded.

4. DATA COLLECTION AND ANALYSIS - SWEPT FREQUENCY

Intelligent design and operation of digital or pulse code modulated systems, which are generally wideband, require considerably more knowledge about the effects of the transmission channel than do narrowband systems. Both require knowledge about the median signal strength and, by differing degrees, the first order probability of the spatial variations of the envelope. Frequency- and time-selective fading of the channel are of greatest importance, however, to wideband systems.

The behavior of the median, or average, signal in tropical forested environments has been investigated extensively during the past six years [Jansky & Bailey Semiannual Reports 1 - 10 and Final Volumes I and II] and the first order probabilities of the spatial variations are discussed in the preceding sections. This section discusses frequency-selective properties of the tropical forested channel at 50, 100 and 150 MHz, for horizontal and vertical polarization. The primary purpose is to determine the coherent bandwidth of this channel at these frequencies.

4.1 Experimental Equipment and Procedures

In general, two slightly different types of measurements were made in this part of the program. The majority were of amplitude as a function of frequency while the remainder were of both amplitude and phase as a function of frequency. In order to obtain these data a constant amplitude, or flat, frequency spectrum was transmitted by sweeping the frequency

over the desired bandwidth. Measurements of swept frequency amplitude response only were termed SF runs while those yielding both amplitude and phase information were labeled PA runs. The transmitting instrumentation was identical for both SF and PA measurements, but the receiving system for the latter was necessarily more complex since it required measurements of relative phase.

A block diagram of the instrumentation for the transmitting terminal is shown in Figure 4.1.1. Block diagrams of the receiving terminal instrumentation for SF and PA measurements are shown in Figures 4.1.2 and 4.1.3, respectively.

The transmitter for both SF and PA measurements was a standard TRC-24 which was modified to accept an amplified sweep generator input and transmit a constant amplitude, linear frequency sweep over a 4 MHz bandwidth. Since the bandpass characteristics in the transmitter at the test frequencies (50, 100 and 150 MHz) were not flat over the 4 MHz bandwidth, a directional coupler and detector were employed at the transmitter output to provide automatic leveling (ALC) for the sweep generator. This leveling reduced the average transmitter output power from a nominal 90 watts to approximately 30 watts and resulted in an output with less than one dB ripple. A second directional coupler was used at the transmitter output to provide an undetected output for monitoring output power and observing the transmitted sweep on a spectrum analyzer. A frequency meter and line probe were also connected to the output in order to set the center frequency and end points of the sweep. In order to prevent the resultant transmitter output from appearing as an FM pulse, care was taken that the sweep width did not exceed the transmitter bandwidth, and retrace blanking of the sweep was not used.

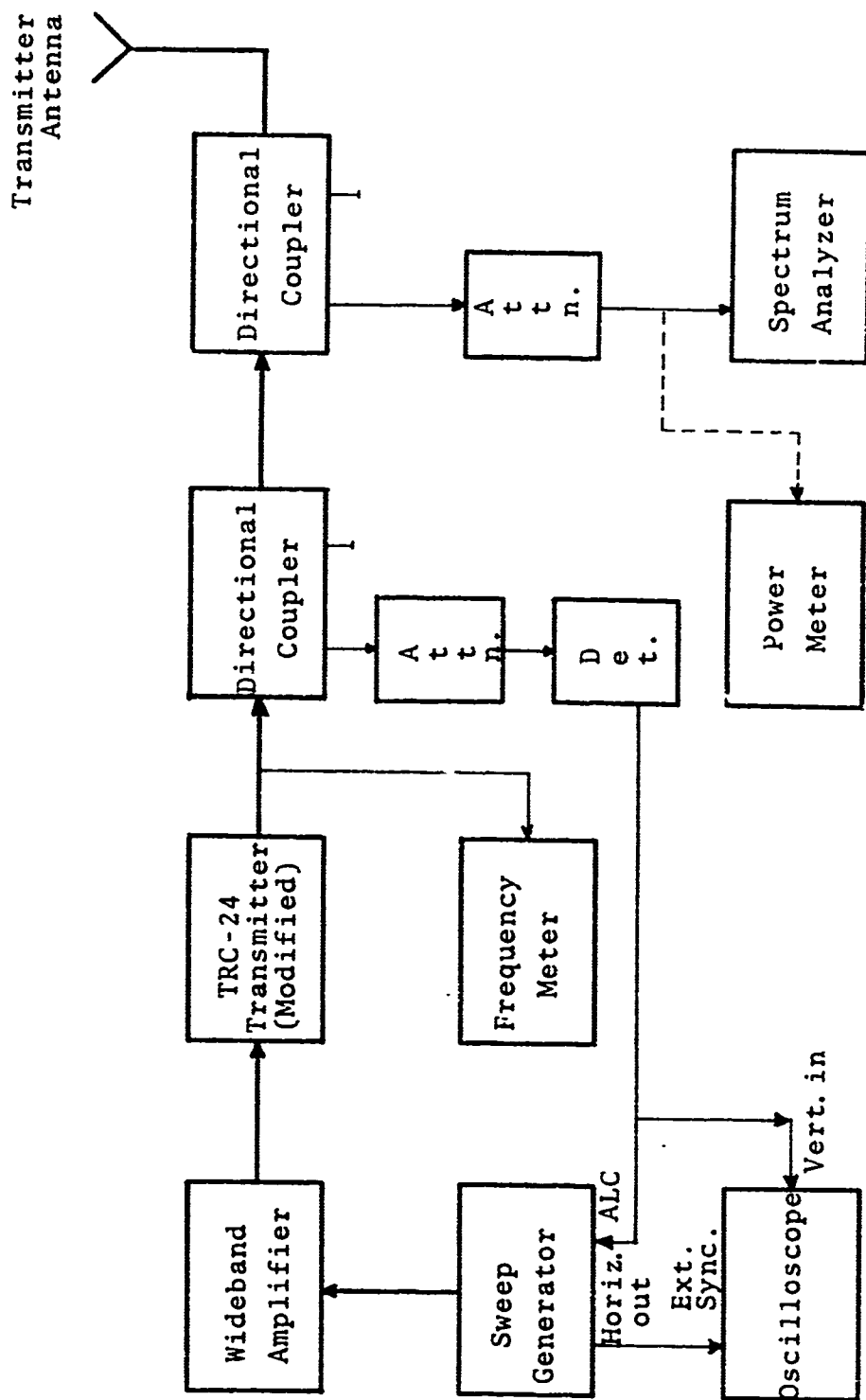


Figure 4.1.1.1 Transmitter Instrumentation Block Diagram for Amplitude and Phase vs. Swept-Frequency Measurements

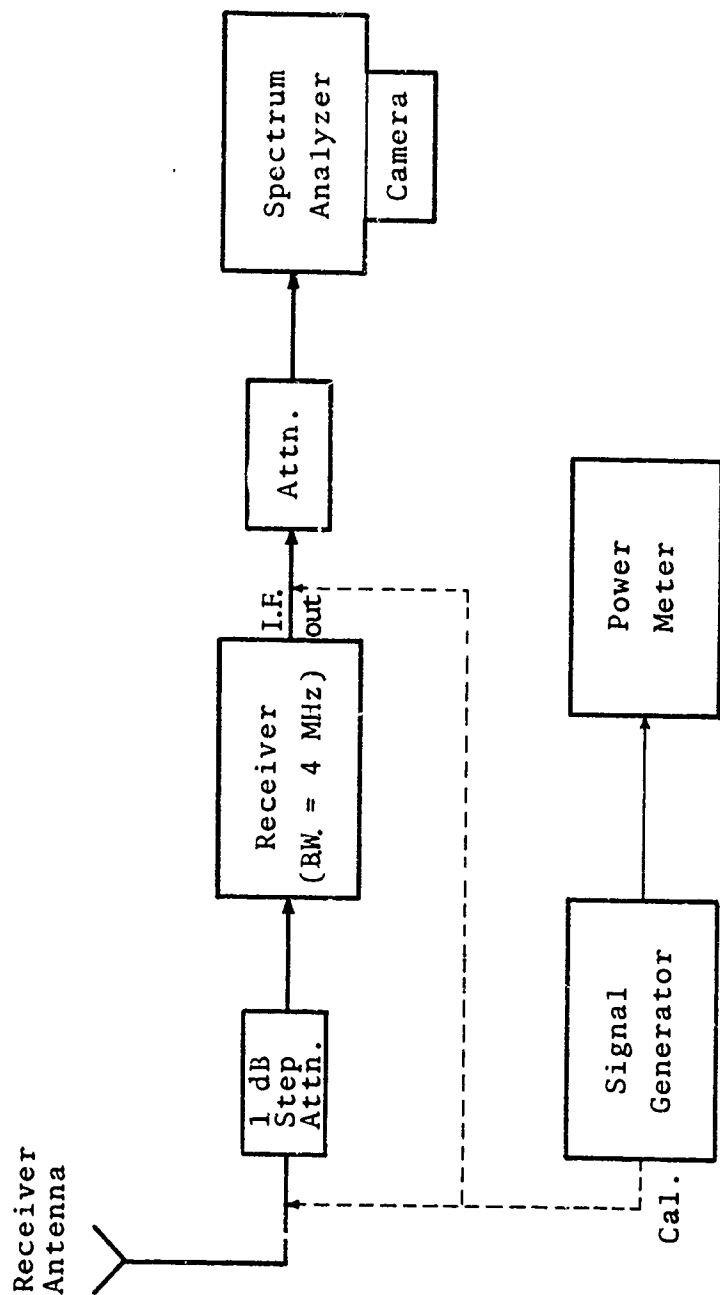


Figure 4.1.1.2 Receiver Instrumentation Block Diagram for Amplitude vs. Swept-Frequency Measurements

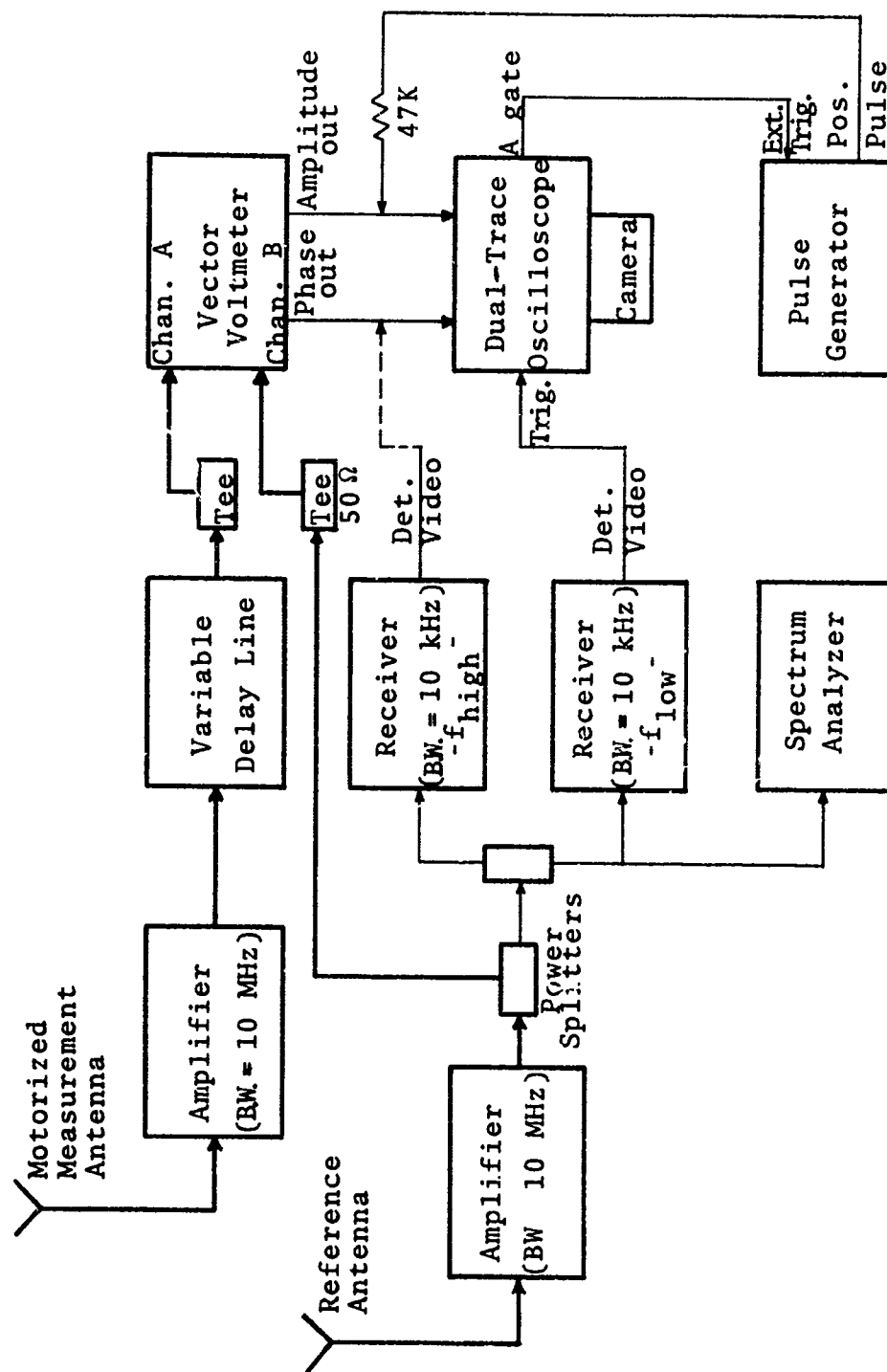


Figure 4.1.3 Receiver Instrumentation Block Diagram for Amplitude and Phase vs. Swept-Frequency Measurements

Standard $\lambda/2$ dipoles for each frequency were employed for transmitting. These antennas were matched to 50 ohms at the center frequencies and had sufficient bandwidth for the transmitted sweep.

In general, the receiving system for the SF measurements employed an ACL receiver with continuously tunable plug-in heads and a bandwidth of at least 4 MHz. The IF output of the receiver (21.4 MHz) was displayed on the spectrum analyzer and provided the data which were recorded on single frame 35 mm film. At those receiver locations near the transmitter where the received signal was stronger than -50 dBm, the spectrum analyzer was tuned to the transmitted frequency and used without the accompanying ACL receiver. The receiving antennas were standard $\lambda/2$ dipoles identical to those used at the transmitting terminal.

Amplitude and frequency calibration of the receiving system was achieved by use of the HP-608 signal generator and HP-431B power meter. For measurements utilizing the ACL receiver the system was calibrated in frequency by inserting a -90 dBm reference signal, at the center frequency of the sweep, into the receiver in its 10 kHz bandwidth position and tuning to the reference signal. The receiver was then returned to the 4 MHz bandwidth position and the IF gain adjusted to a full scale display on the spectrum analyzer. For measurements involving the spectrum analyzer only, a -50 dBm reference signal was fed directly into the analyzer and its gain was adjusted for full graticule display.

The PA measurements utilized an HP-8405 vector voltmeter to obtain amplitude and phase information. This instrument is a two-channel tuned volt/phasemeter of one kHz

bandwidth which has the capability of measuring the absolute signal amplitude on either channel and the phase difference between them. With its automatic phase locked tuning, the reference channel will follow slowly drifting or swept frequency signals, thus making it a suitable instrument for the PA measurements.

The signal for the reference channel was obtained from a directional beam antenna in a fixed location near tree-top level while the signal for the measurement channel was obtained from a movable standard $\lambda/2$ dipole immersed in the foliage. An amplifier of known gain and 10 MHz bandwidth was used in each channel to provide adequate signal levels for the vector voltmeter. A variable delay line was inserted in the measurement channel to balance the propagation time, since, in general, the phase delays for the two channels were different.

The recorder outputs from the vector voltmeter, which are proportional to phase and amplitude, were simultaneously displayed on a dual-trace oscilloscope and provided the PA data which were recorded on single frame 35 mm film. In order to synchronize the oscilloscope to the received sweep, two narrowband (10 kHz) receivers were connected to the reference antenna. One was tuned to the lowest end of the sweep frequency and provided a trigger output for the scope while the second was tuned to the highest frequency of the sweep to allow synchronization between the transmitted and oscilloscope sweeps. A pulse generator was also triggered from the first receiver and provided identification of the amplitude trace.

Two locations of the transmitting antenna along with field point locations are shown in Figure 3.1.2. In order to maintain a continuous foliated propagation path for

all measurements, the transmitting antenna was located on the same side of the site clearing as the particular field point being used. Thus, transmitter location $T_x A$ was used for field points 7 and 10 while $T_x B$ applied to field points Y-20, Y-25, and Z-29.

As previously discussed, two slightly different types of swept frequency data were acquired in this part of the measurement program. In addition to the different measurement instrumentation, the test procedures also varied slightly. The swept frequency amplitude or SF data were acquired with the receiver located at the star field points. Only the radial and transverse paths at each field point were used for SF measurements and marker ropes, 10λ in length, were placed along the paths with incremental location marks every $\lambda/10$. The receiving antenna for the SF measurements was six feet above ground and hand carried along the paths over a total distance of 10λ at each path, with momentary stops at each $\lambda/10$ incremental marker to permit photographing the received spectrum at a fixed antenna position. In general, transmitting heights of 40 feet were used for the SF measurements; however, at location Z-29 where the signal was weak it was necessary to raise the antenna height to 80 feet to provide an adequate signal-to-noise ratio. For all measurements using horizontal polarization, the antennas were oriented for maximum gain along the transmitter/receiver direction.

Data for the swept frequency amplitude/phase, or PA runs, were obtained at the same locations and paths used for the SF runs, but due to equipment limitations, the measurement procedures were necessarily changed. Since the automatic phase locking capability of the vector voltmeter was limited to sweep rates of less than 15 MHz/sec., it was necessary to reduce the

transmitted sweep rate to approximately 0.25 sweeps per second, including retrace time. As a result, a hand-carried antenna could not easily be held stationary throughout a sweep, so the receiving antenna, 6 feet above ground, was affixed to a rigid motor-driven bench to provide the necessary stability. The bench, which was made portable for transporting to the different field points and re-orienting for radial and transverse runs, was 40 feet long and thus restricted the total length of each run to this distance. For data acquisition, the motorized receiver antenna was stopped momentarily at 1-foot distance increments for 50 MHz runs, and 6-inch increments for 100 and 150 MHz runs, while the receiver phase and amplitude display were photographed. Most of the measurements were conducted at night when the winds were calm, relative to those during the daylight hours, to minimize possible time variations due to wind-driven tree motion.

The reference beam antenna was located approximately 250 feet in the transverse direction, from the motor-driven bench and elevated to near treetop level on an aluminum tower. As the reference tower was raised, the received amplitude sweep was observed on the measurement antenna to ensure that the aluminum mast did not influence the measurements. In general the transmitting antenna was elevated to 80 feet for the measurements; however, in one instance it was necessary to alter this height in order to obtain a flat response on the reference antenna. When using horizontal polarization all three antennas were aligned for maximum gain along the transmitter/receiver azimuth.

4.2 Data Analysis and Discussion

The measurements were of signal amplitude and phase as a function of frequency as the frequency was swept over a 4 MHz band about the center frequencies of 30, 100 or 150 MHz. These measurements were made with the receiver in different locations, for horizontal and vertical polarization and for different transmit antenna heights. The set of data pertaining to each combination of these operational and environmental parameters consisted of about one hundred photographs of the scope face of a spectrum analyzer displaying the response as a function of swept frequency, taken over a distance of about 10 wavelengths with the distance between photographs being (equally) spaced at $1/10$ wavelength. Some 120 sets of such data were taken, constituting about 12,000 photographs. Figure 4.2.1 is an example of a set of such data. (See Figure 4.2.8 for data nomenclature.)

To facilitate the required statistical analysis, it is most convenient to convert the analogue data of each photograph to digital form. This and the subsequent analysis is somewhat lengthy, and only about 2600 photographs have been digitized thus far. Of those digitized, about 1900, representing 19 different combinations of operational parameters, have been selected for analysis. Figure 4.2.2 is a diagram showing those combinations of operational and environmental parameters for the measurements being analyzed. These were selected because they represent the major operational and environmental parameters employed.

The primary analysis goal is determination of the coherent bandwidth of the tropical forested environment. The coherent bandwidth is essentially the maximum bandwidth over

NOT REPRODUCIBLE

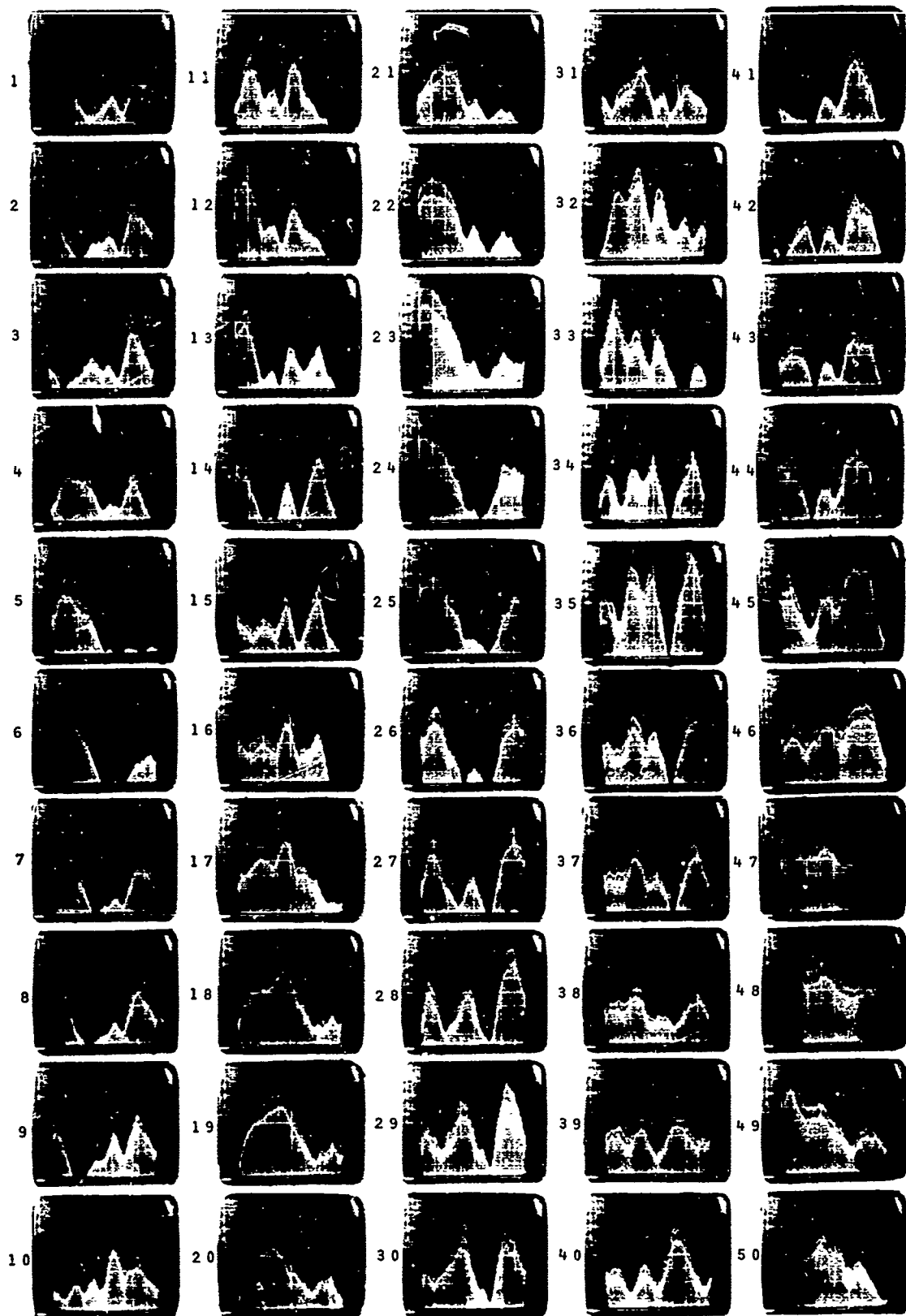


Figure 4.2.1 Signal Amplitude as a Function of Distance and Frequency



Figure 4.2.1 (continued)

NOT REPRODUCIBLE

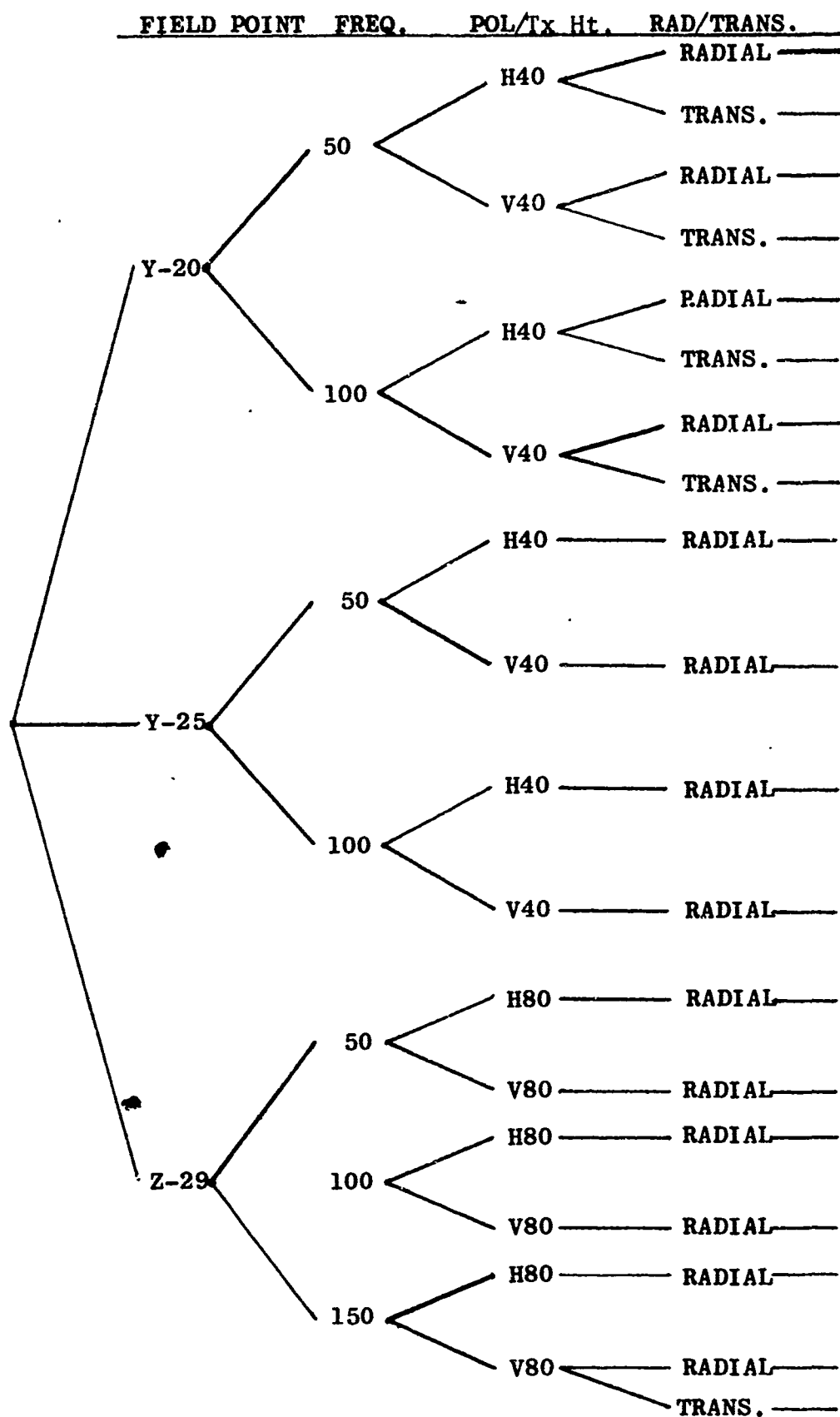


Figure 4.2.2 Diagram of Configurations of Swept-Frequency Runs Analyzed

which all frequencies in the band are affected by the environment in a like manner from instant to instant. This means that the fading which may occur at one frequency in the band also occurs at the same instant at all other frequencies within the band; or, simply stated, the fading is flat rather than being frequency selective over the coherent bandwidth. In fact, the coherent bandwidth is sometimes called the "flat-fading" bandwidth [Stein and Jones, 1967].

The mathematical measure of the coherent bandwidth is the maximum frequency separation Δf between two tones for which the normalized correlation coefficient of the two tones remains near unity. This is imprecise, and for definiteness the coherent bandwidth is generally taken as the frequency separation at which the frequency correlation function falls to some convenient value, such as $1/e$ or 0.5. This provides a quantitative measure or definition of the coherent bandwidth; but it is accepted as giving only the order of magnitude of the actual bandwidth over which frequency-selective fading may be assumed negligible. Practically, this means that the system bandwidth should be somewhat less than the measured coherent bandwidth if frequency-selective fading is to be avoided. The grossness of this measure is partly due to the fact that the tolerable frequency selectivity may differ for different systems and for different performance requirements, and partly because the frequency correlation function, from which the coherent bandwidth is obtained, does not adequately account for the presence of unusually deep, selective fades that may be particularly detrimental to communications [Schwartz, et al., 1966]. That such deep fades occur in the tropical forest environment may be seen in Figure 4.2.1 which shows several cases of deep nulls in the amplitude. These nulls occur within a narrow band, which, as shown later, is within the nominal

coherent bandwidth. Further aspects of the forested environment are mentioned later in relation to the frequency selectivity; but attention is directed now to obtaining the frequency correlation functions.

The amplitude trace on each photograph of the swept-frequency data being examined (Figure 4.2.2) was sampled at each 0.25 MHz. These equally spaced samples, 17 for each photograph, are the digital values representing the analogue data of the photograph. The spacing between samples of 0.25 MHz was based on the Nyquist criterion, which requires a sampling rate of at least two samples per wavelength for the highest frequency of interest in the random signal. A perusal of the photographs indicated that the major amplitude variations, as a function of swept frequency, were generally on the order of one cycle or less per one megahertz or so spacing; hence, a spacing between samples of 0.25 MHz was deemed sufficient.

With the conversion of the data to digital form, there are ≈ 1700 data samples, plus the digitized samples of a calibration photograph in most cases, for each test configuration shown in Figure 4.2.2. In principle, a single swept-frequency trace is sufficient for obtaining the frequency correlation function, providing the frequency sweep is wide enough to yield an adequate number of samples to compute a statistically reliable correlation function. In our case the sweep is too narrow to provide enough random samples, and successive sweeps are made to obtain the required samples. The tropical forest transmission channel, because measurements were taken only when the winds were very calm, was nearly static; thus, time variations due to wind-driven tree motion were generally very small at the VHF frequencies. Hence, repeated frequency sweeps at a fixed position in the tropical

forest environment would produce (virtually) identical traces and offer no useful data beyond that contained in a single sweep. Thus, to obtain a sufficiently large set of random samples, the successive sweeps were performed with the receiver antenna moved a short distance between each recorded sweep. As mentioned above, ≈ 100 such sweeps were performed for each operational configuration, with the antenna moved a distance of $\lambda/10$ between sweeps. The total distance moved per configuration was thus 10 wavelengths, and was so limited in order that the set of data would be from a reasonably homogeneous region of the environment. Stated differently, the total length was limited in an attempt to obtain a statistically stationary set of random samples, which was not always successful, as is mentioned later. The equal spacing of $\lambda/10$ between sweeps was done primarily for the purpose of obtaining reliable spatial correlations, which will be discussed further in a forthcoming report. For present purposes, it suffices to say that the $\lambda/10$ spacing was large enough to yield different, random samples of amplitude versus swept frequency.

Now, let each amplitude sample of the data be denoted by $e_j(f_i)$, where f_i is the frequency at which the i^{th} sample within each photograph was made ($i = 1, 2, 3, \dots, 17$), and j represents the j^{th} sweep, or photograph ($j = 1, 2, 3, \dots, 101$) within each data set. Because the transmitted sweep was not perfectly flat in amplitude, the sampled data are corrected, where possible, to account for this. This is done by dividing the $e_j(f_i)$ by $C(f_i)$, where $C(f_i)$ are the amplitude values of the calibration sweep, where calibration sweeps were available. In those cases where no calibration sweep was available,* the

* Obtaining a calibration sweep for the data discussed here involved physically transporting the complete set of receiving equipment from the receiving point in the jungle back to the transmitting location. This often involved transporting the receive equipment a mile or more through the somewhat rugged environment; hence only periodic calibrations were made.

transmitted sweep was assumed to be flat. That this assumption is a reasonable one may be seen from Figure 4.2.3, which illustrates the sampled values of a calibration sweep. In most cases, the calibration sweeps were reasonably flat, with the greatest departure being at the leading and trailing edges of the sweep. Because of this rounding of the edges, the first and last samples are not utilized in the analysis. This effectively reduces the width of the sweep to 3.5 MHz.

In computing correlations it is customary to remove the mean of the data. The mean of each sweep is

$$m_j = \frac{1}{15} \sum_{i=1}^{15} e_j(f_i)/C(f_i)$$

where $C(f_i)$ are the calibration values, where available, and unity otherwise. The zero-mean random variables are in units proportional to voltage, and given by

$$a_j(f_i) = m_j - e_j(f_i)/C(f_i)$$

The variance of the amplitude fluctuations with frequency, used to normalize the frequency correlation function, is given by

$$\sigma_j^2 = \frac{1}{15} \sum_{i=1}^{15} a_j^2(f_i) \quad (1)$$

The variances were computed for the data of the operating configurations given in Figure 4.2.2. It should be pointed out

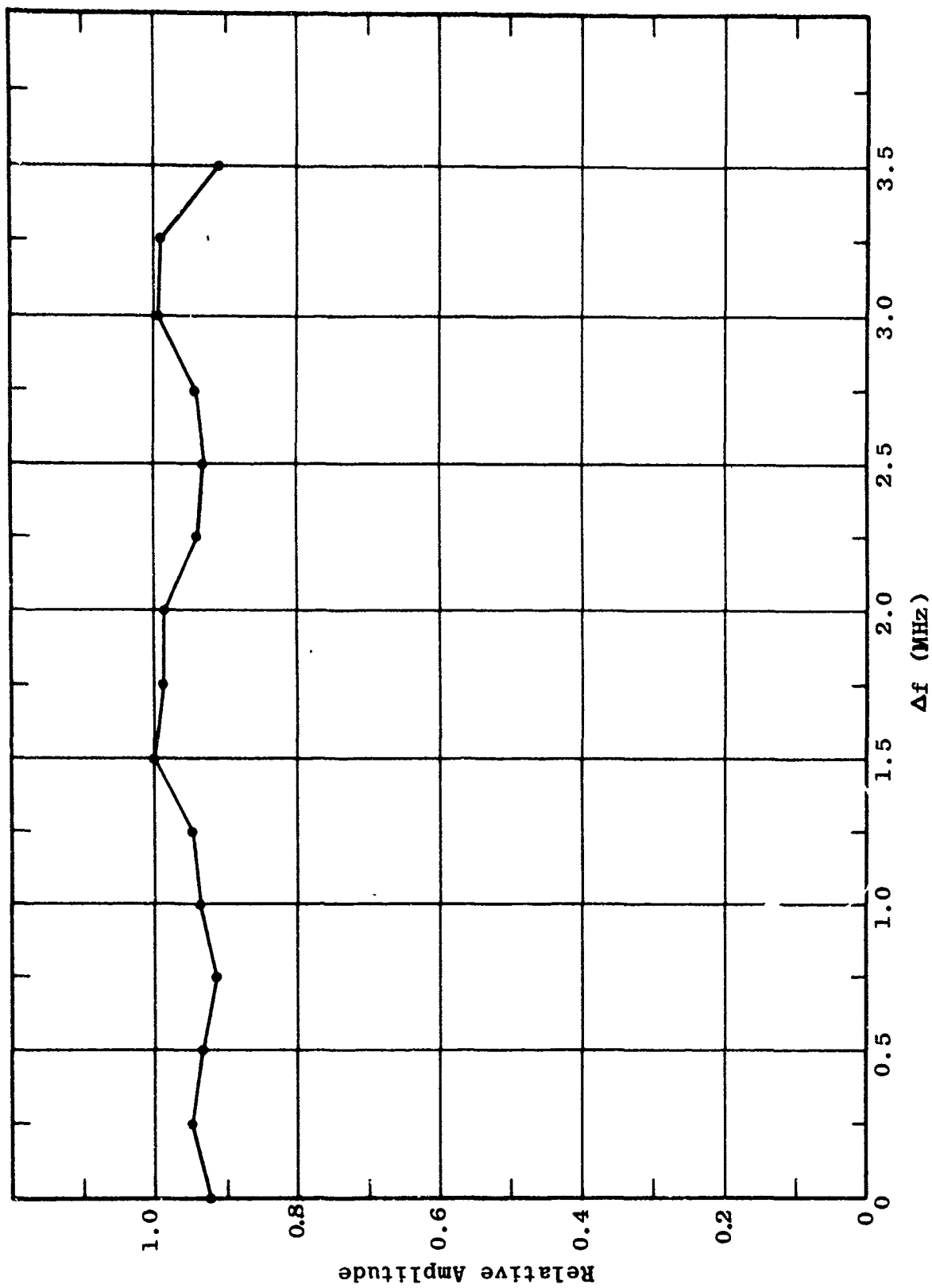


Figure 4.2.3 Illustration of Transmitted Amplitude Versus Frequency

that the mean m_j and the variances σ_j^2 varied considerably from sweep to sweep (i.e., for different values of j). Also, a mean which changed linearly with frequency would have been more representative in several cases. The linear changing mean and the different variances are indicative of a nonstationary random process. The effect of the linear changing mean and different variances can, at least in some cases, be removed but this has not been done here and stationarity is assumed.

The normalized frequency autocorrelation function for one sweep is given by

$$\rho_j(\Delta f) = \frac{\sum_{i=1}^{15 - \Delta f / .25 \text{ MHz}} a_j(f_i) a_j(f_i + \Delta f)}{(15 - \Delta f / .25 \text{ MHz}) \sigma_j^2}; \quad (2)$$

$$\Delta f = q \cdot .25 \text{ MHz},$$

$$q = 0, 1, 2, \dots, 14.$$

Assuming the signal statistics are stationary throughout the environmental region sampled, the values of $\rho_j(\Delta f)$ are averaged over j to obtain more reliable values of $\rho(\Delta f)$. This gives

$$\rho(\Delta f) = \frac{1}{101} \sum_{j=1}^{101} \rho_j(\Delta f) \quad (3)$$

The frequency correlation functions for the 19 combinations of operational parameters are shown in Figures 4.2.4 to 4.2.22. The operational configuration, including location in the environment, is identified with the appropriate correlation function.

In some cases, the measurements were made with the receiver moved transverse to the transmit-receive direction, but in most cases the receiver was positioned along the transmit-receive direction. The $1/e$ point, or coherent bandwidth, is identified on each correlation curve.

The coherent bandwidths, or the frequency spread at the $1/e$ point of the correlations, are summarized in Table 4.2.1. No trend in the coherent bandwidth is apparent from these results. The maximum coherent bandwidth is 0.59 MHz, the minimum is 0.31 MHz, and the average is 0.46 MHz. These are, as mentioned earlier, an order of magnitude estimate of the maximum allowable operating bandwidth (i.e., an operational bandwidth of perhaps $1/10$ the coherent bandwidth would be used) if frequency-selective fading is to be avoided; and even then there is some uncertainty that this will be achieved due to deep fades such as those evident in Figure 4.2.1.

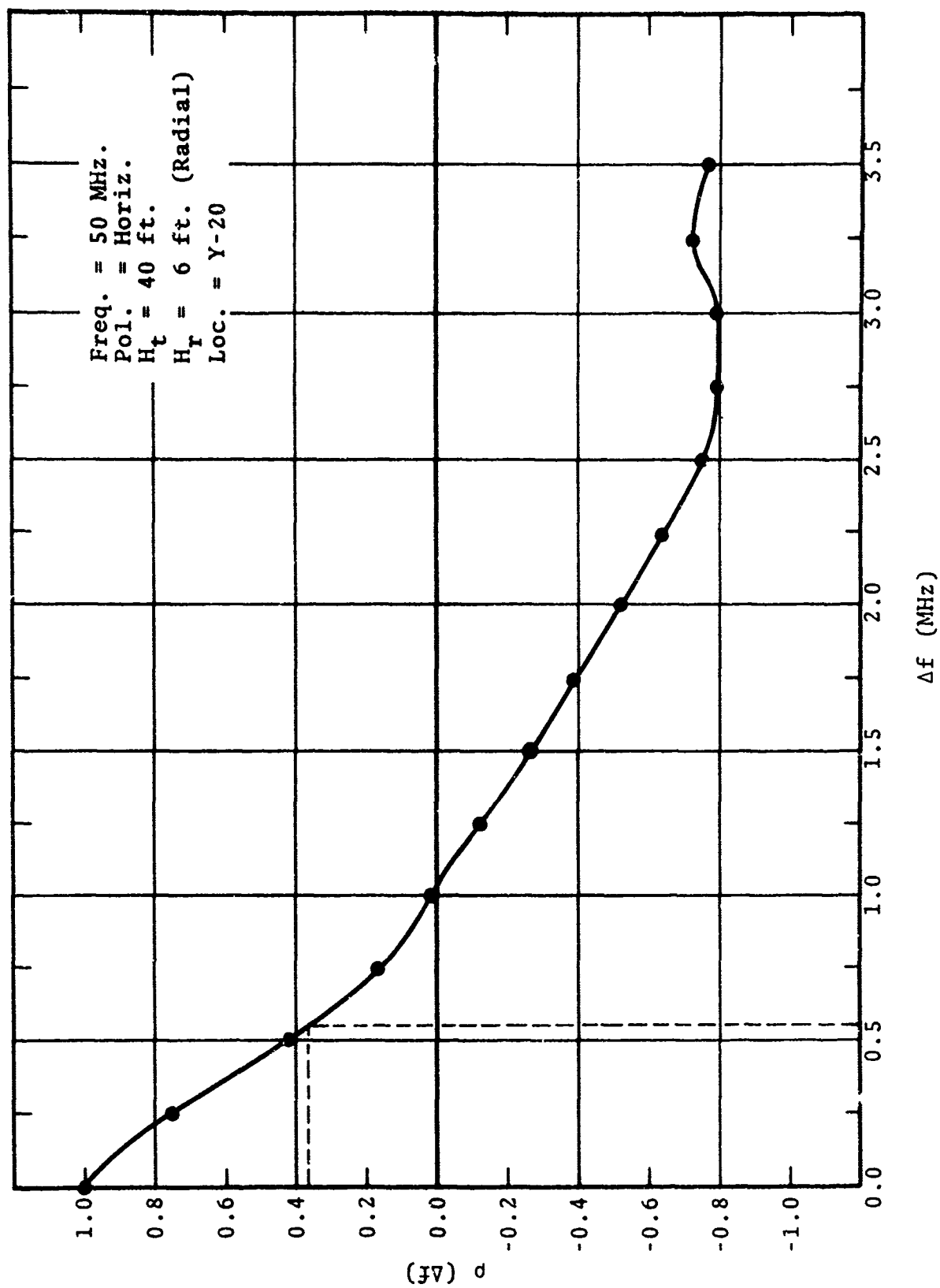


Figure 4.2.4 Normalized Frequency Correlation Coefficient

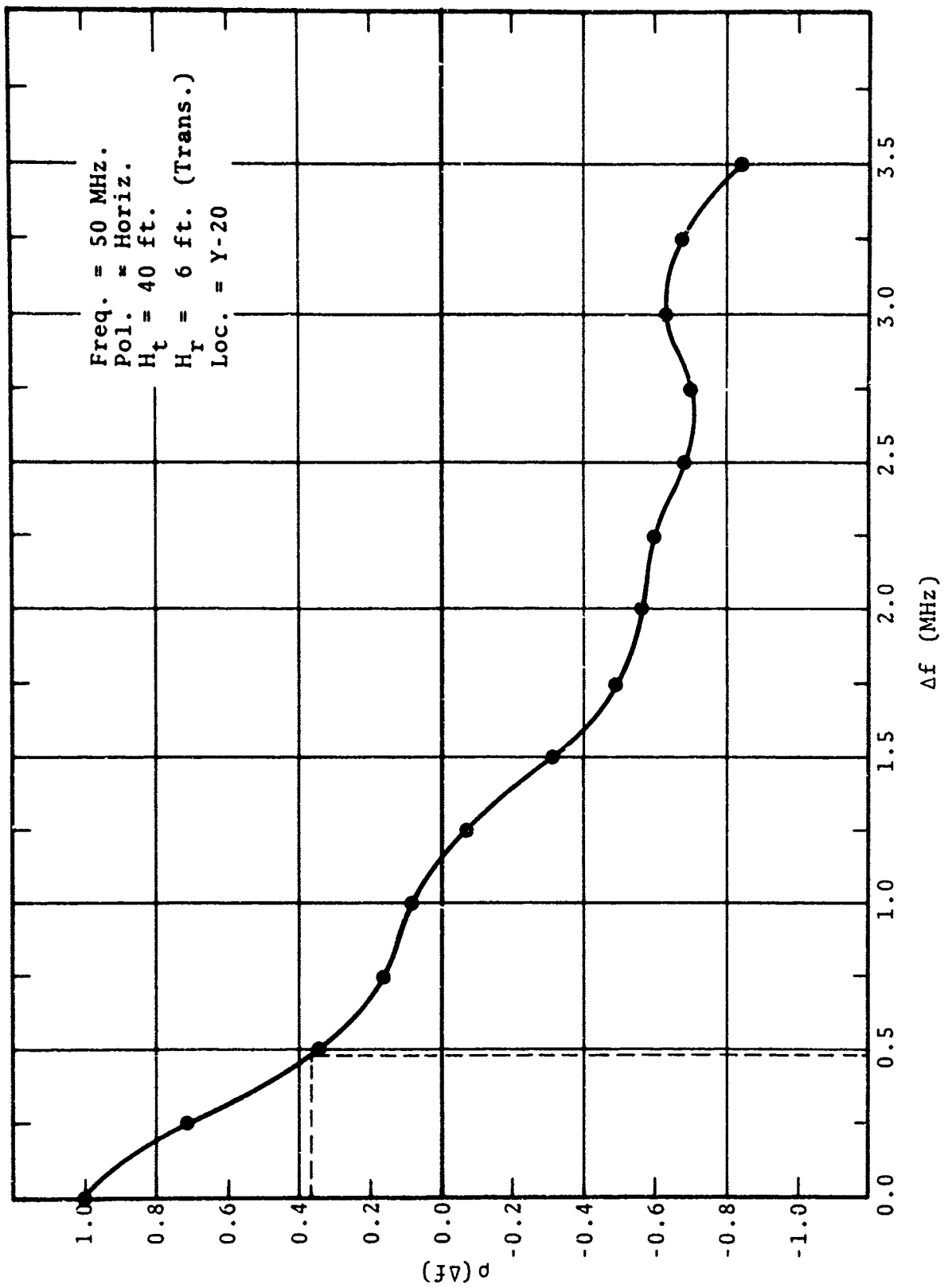


Figure 4.2.5 Normalized Frequency Correlation Coefficient

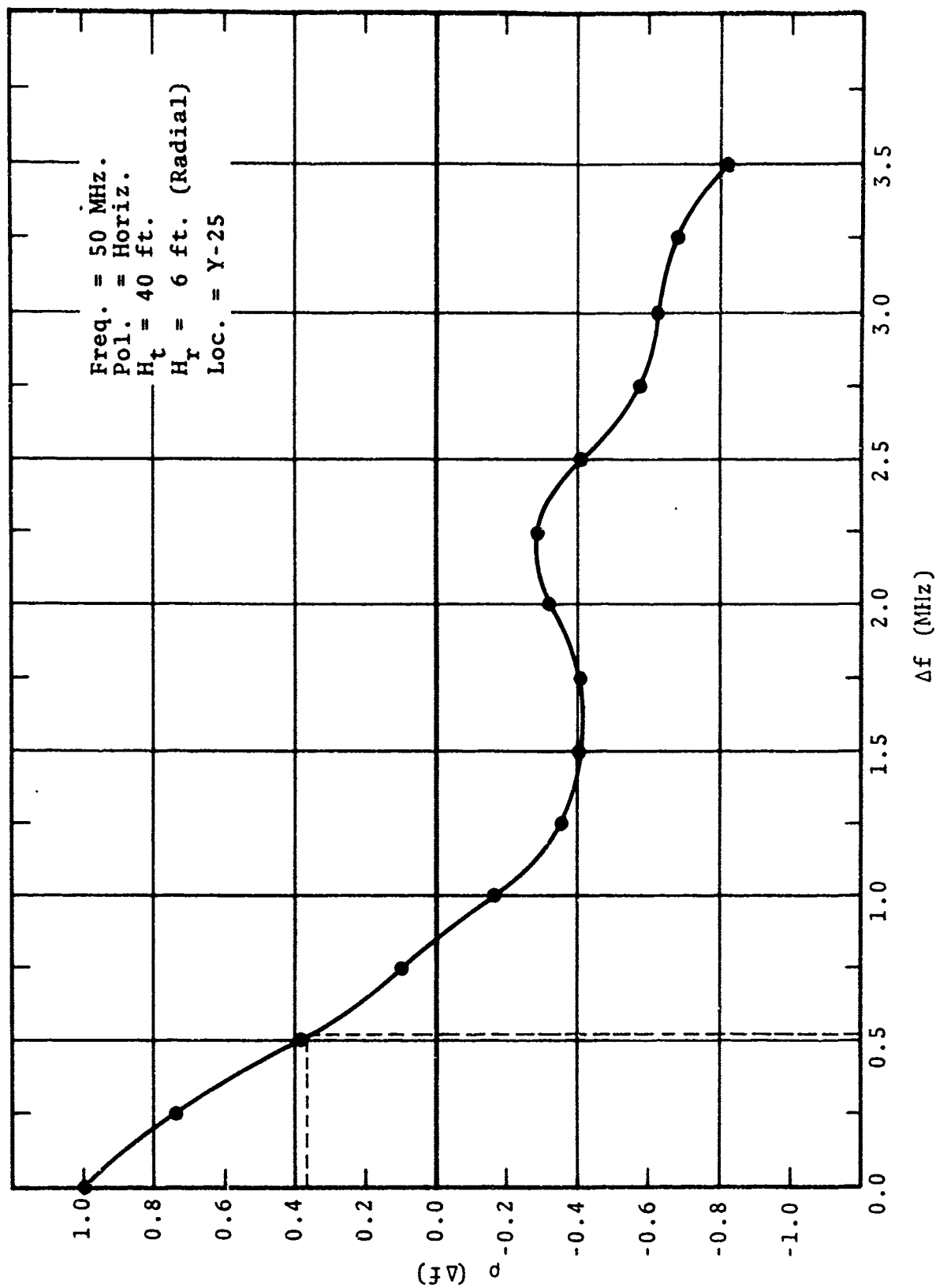


Figure 4.2.6 Normalized Frequency Correlation Coefficient

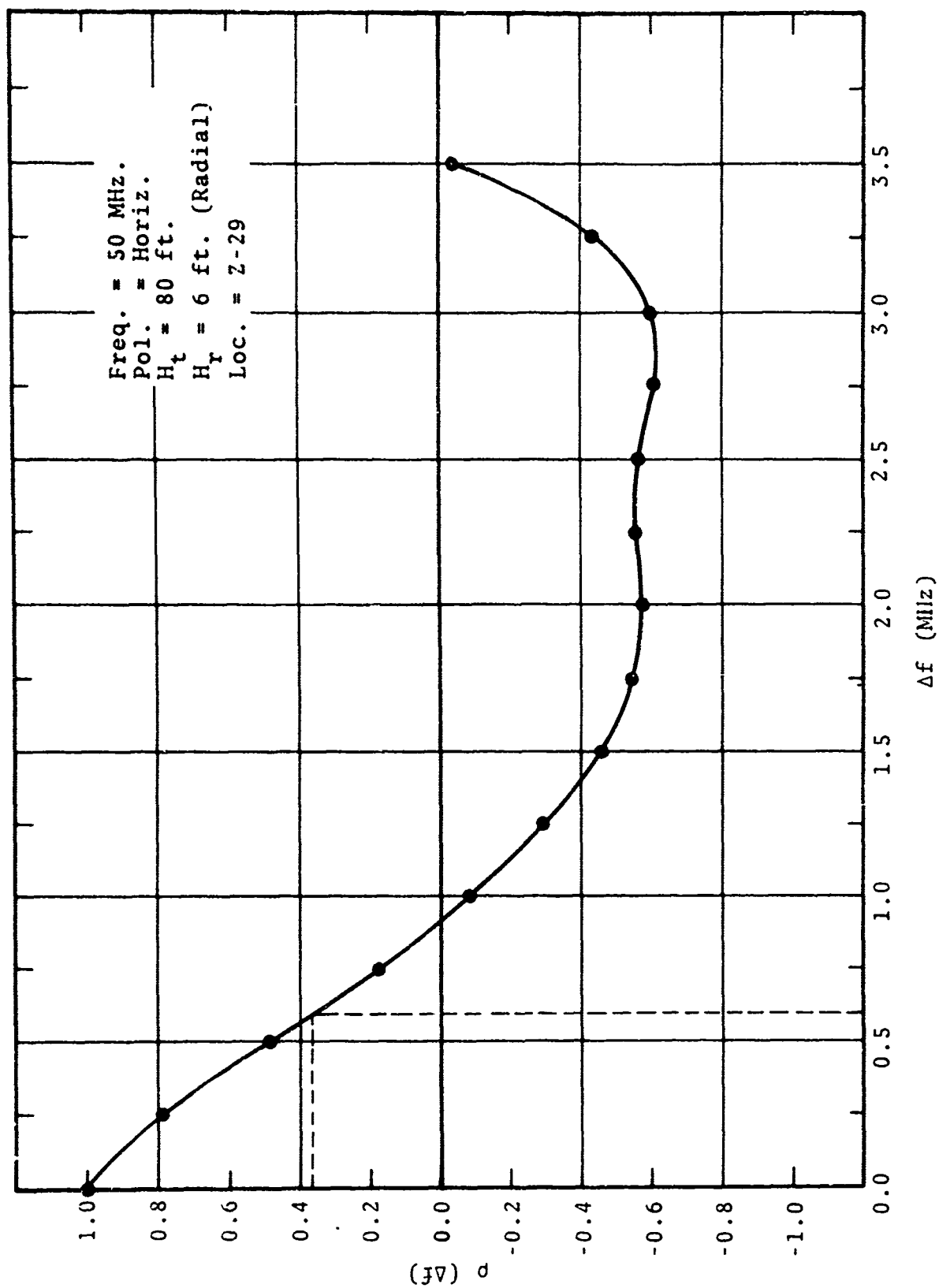


Figure 4.2.7 Normalized Frequency Correlation Coefficient

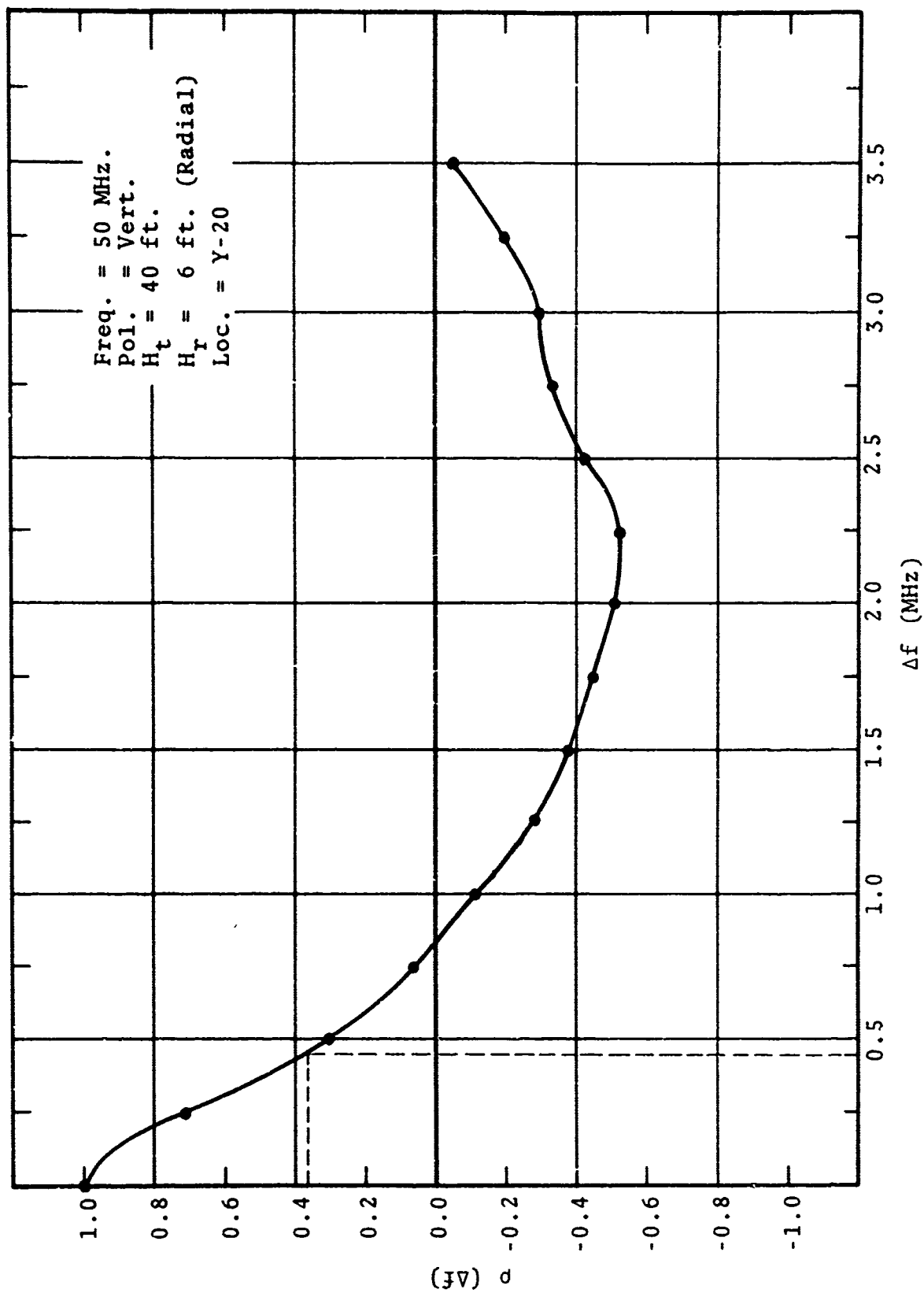


Figure 4.2.8 Normalized Frequency Correlation Coefficient

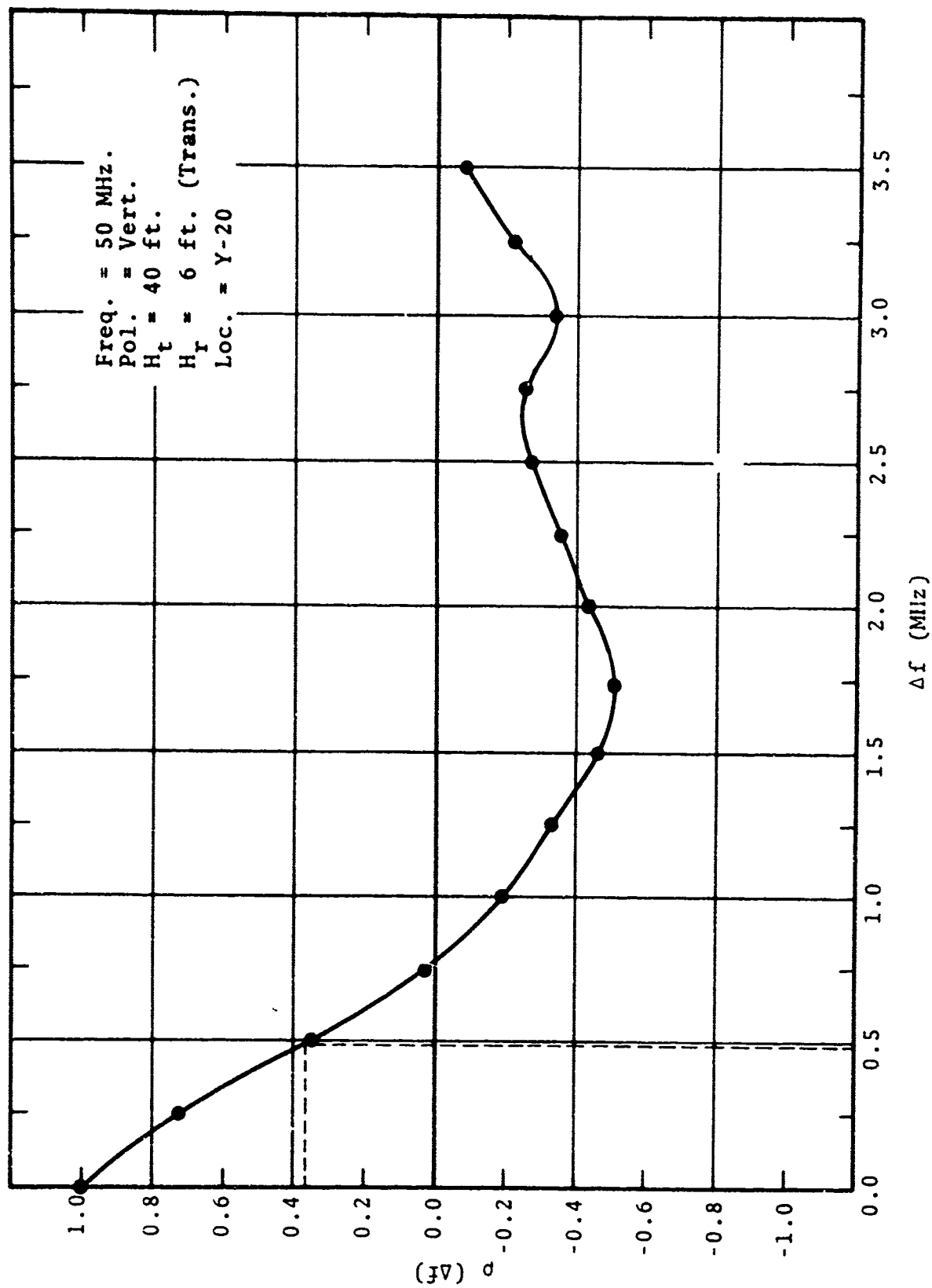


Figure 4.2.9 Normalized Frequency Correlation Coefficient

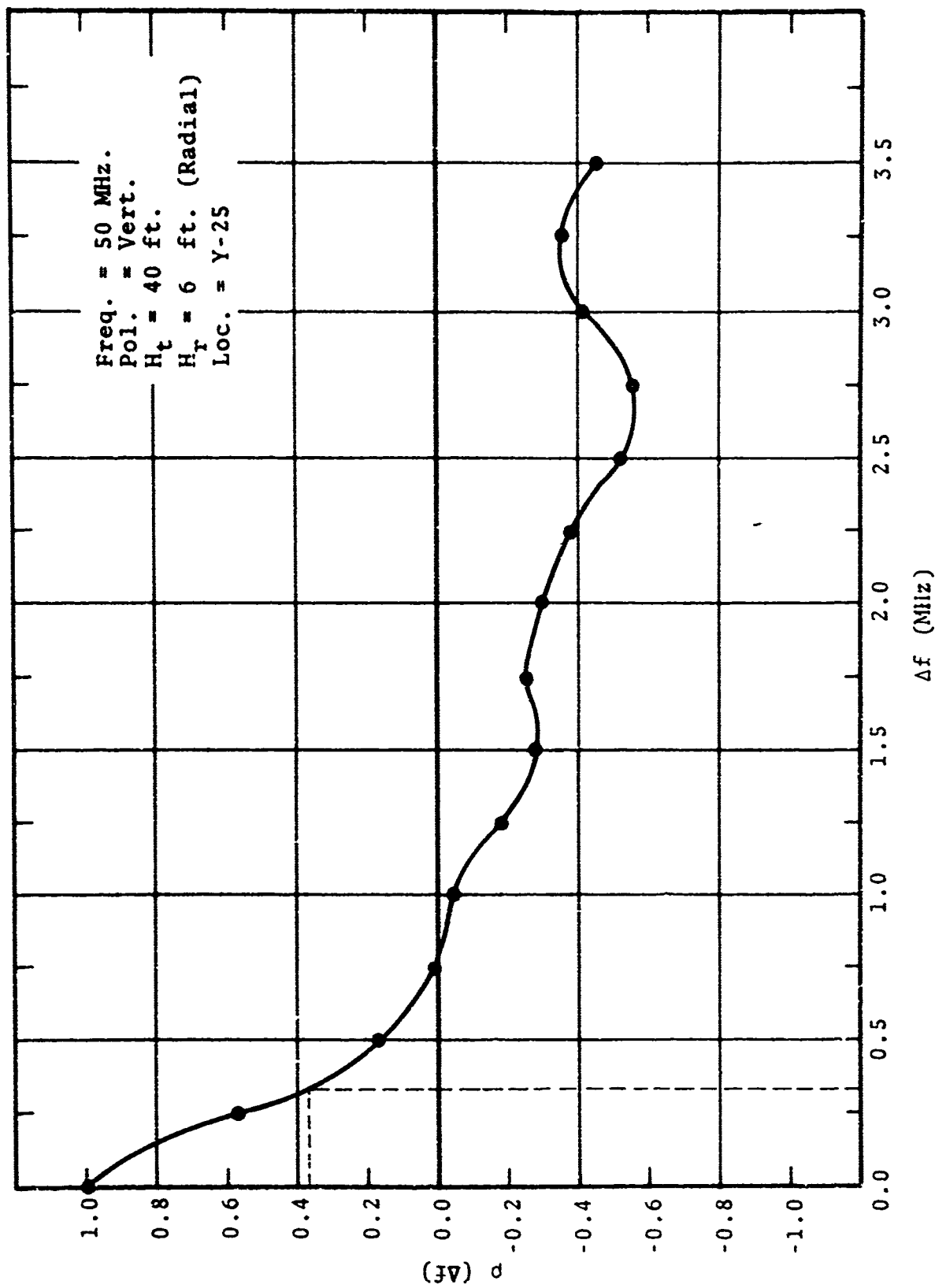


Figure 4.2.10 Normalized Frequency Correlation Coefficient

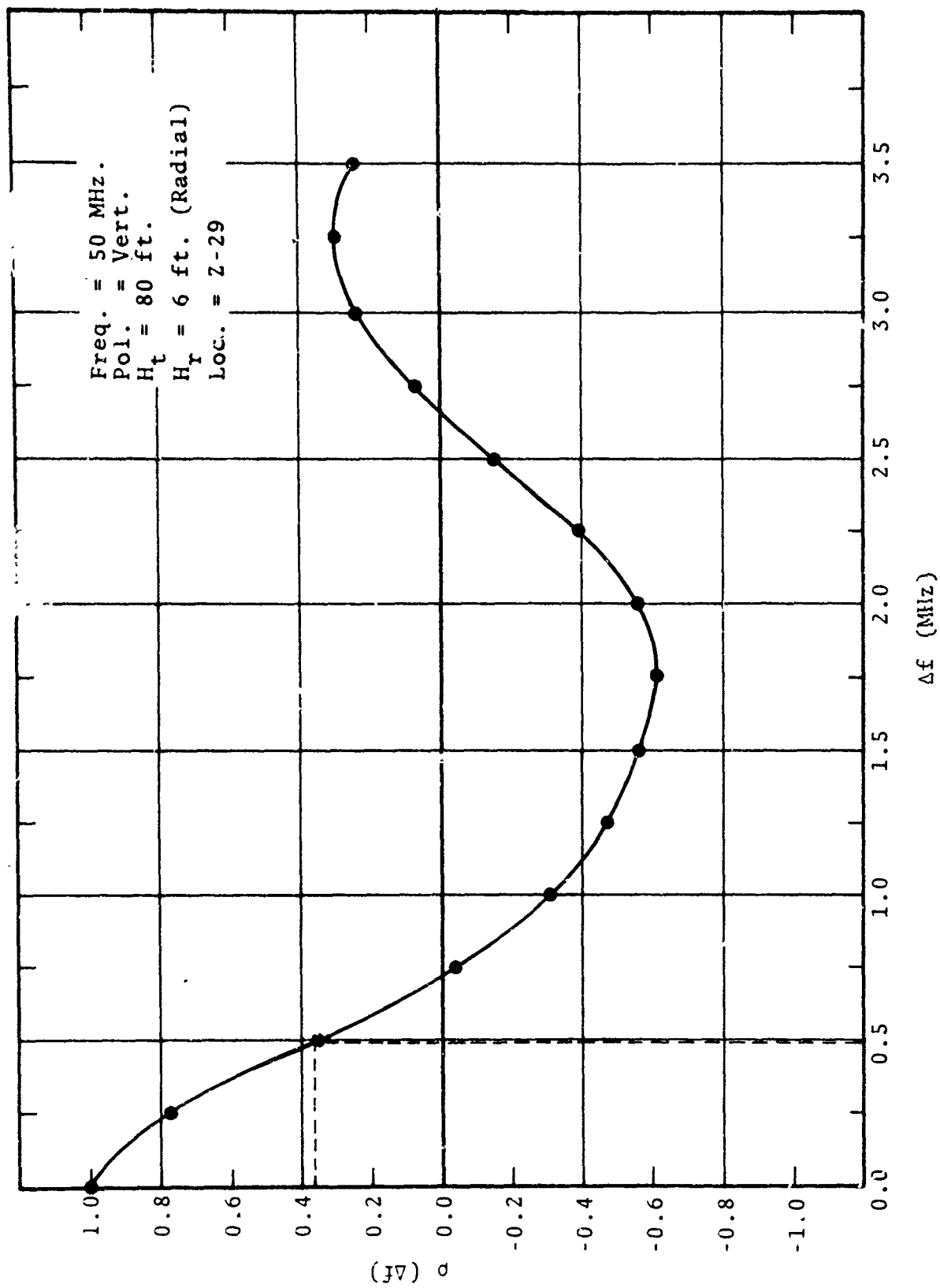


Figure 4.2.11 Normalized Frequency Correlation Coefficient

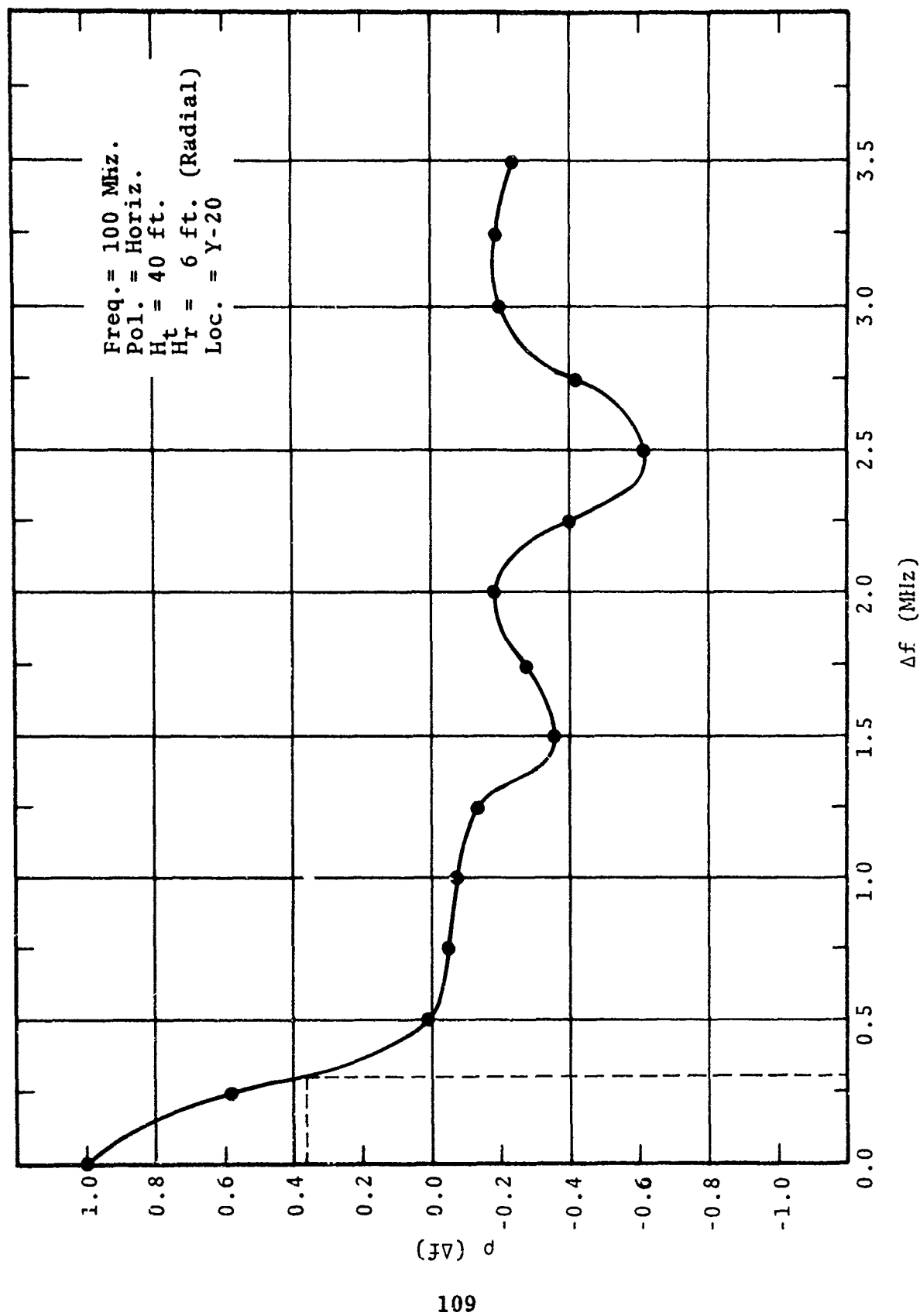


Figure 4.2.12 Normalized Frequency Correlation Coefficient

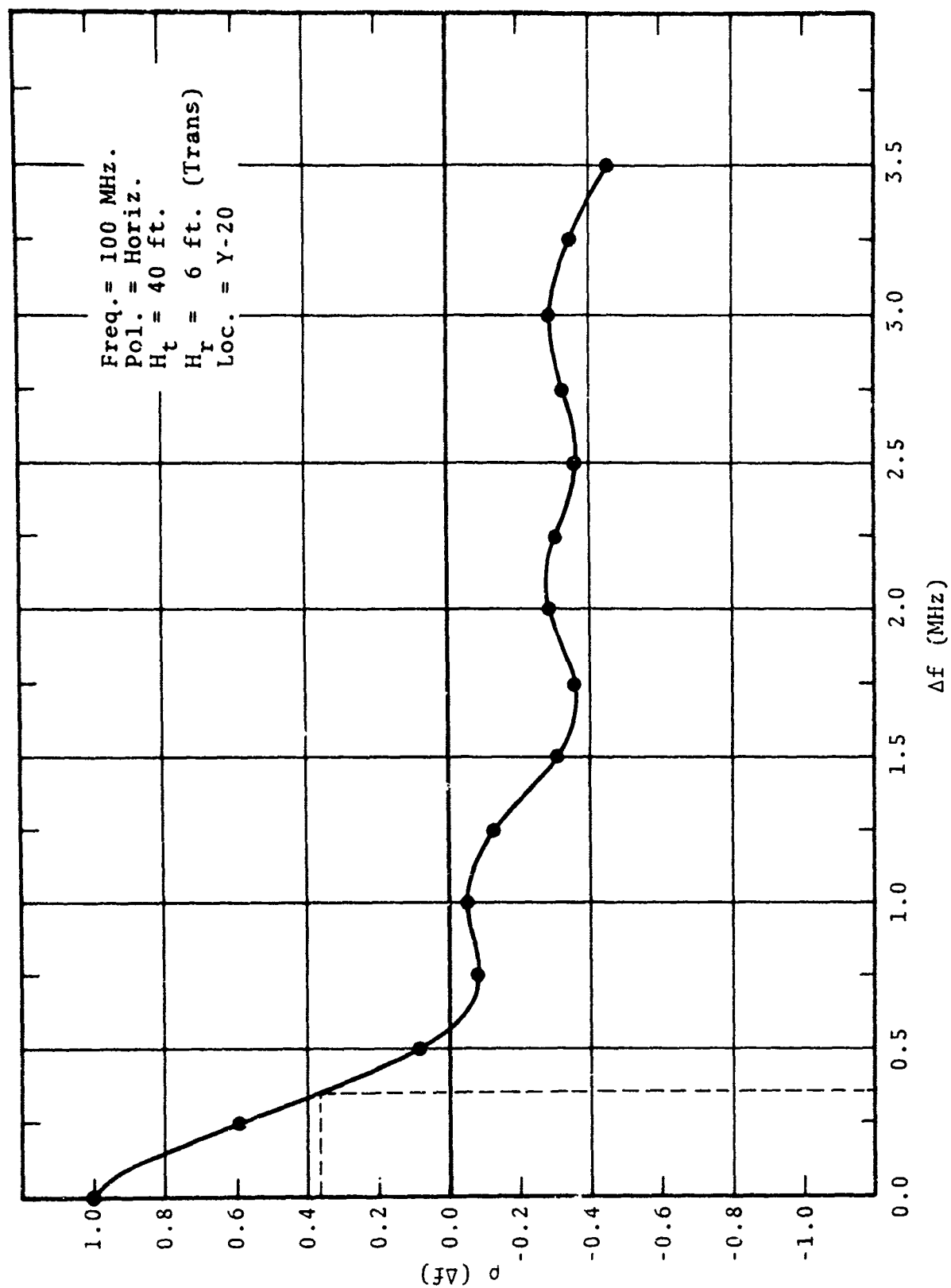


Figure 4.2.13 Normalized Frequency Correlation Coefficient

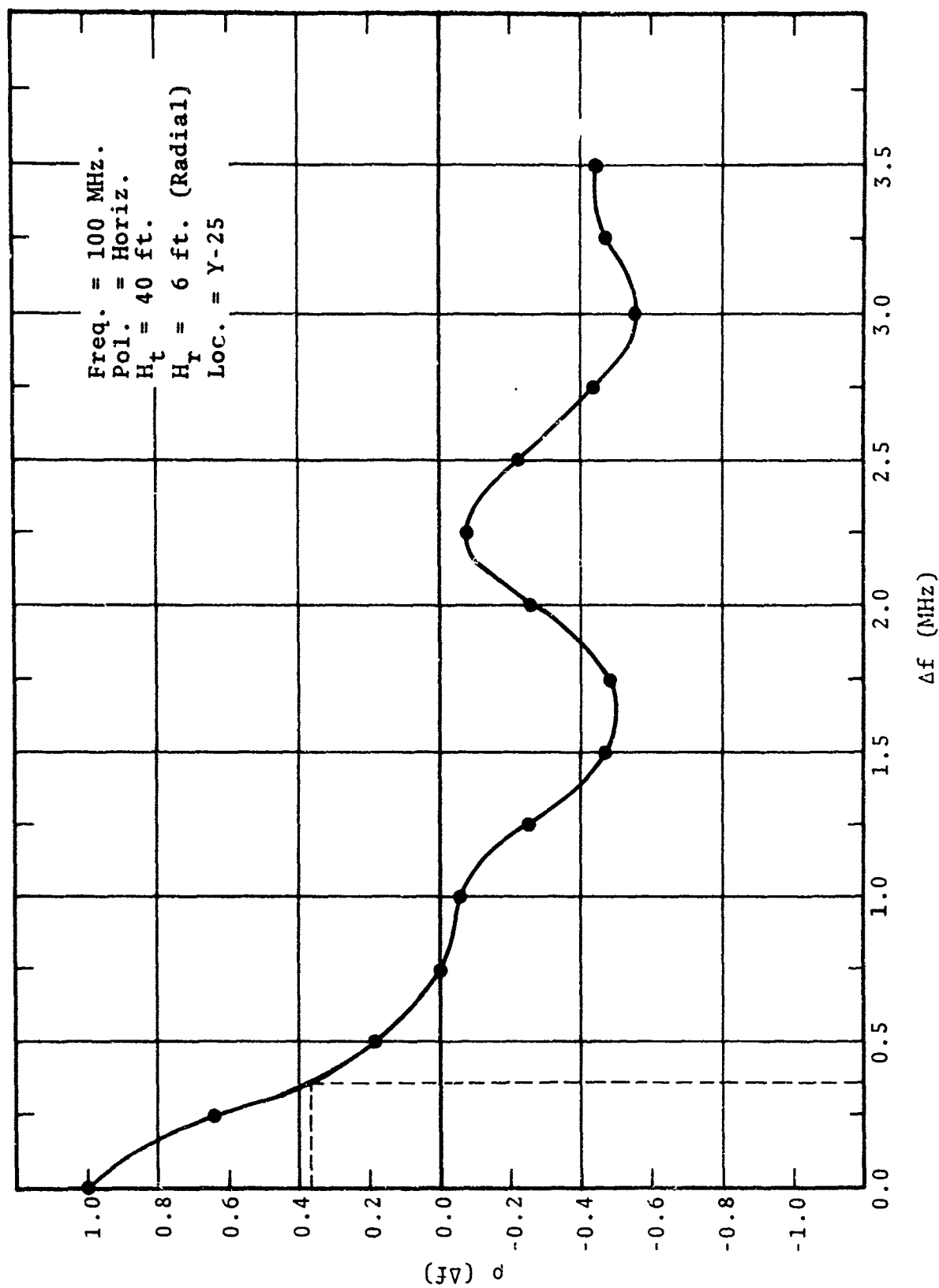


Figure 4.2.14 Normalized Frequency Correlation Coefficient

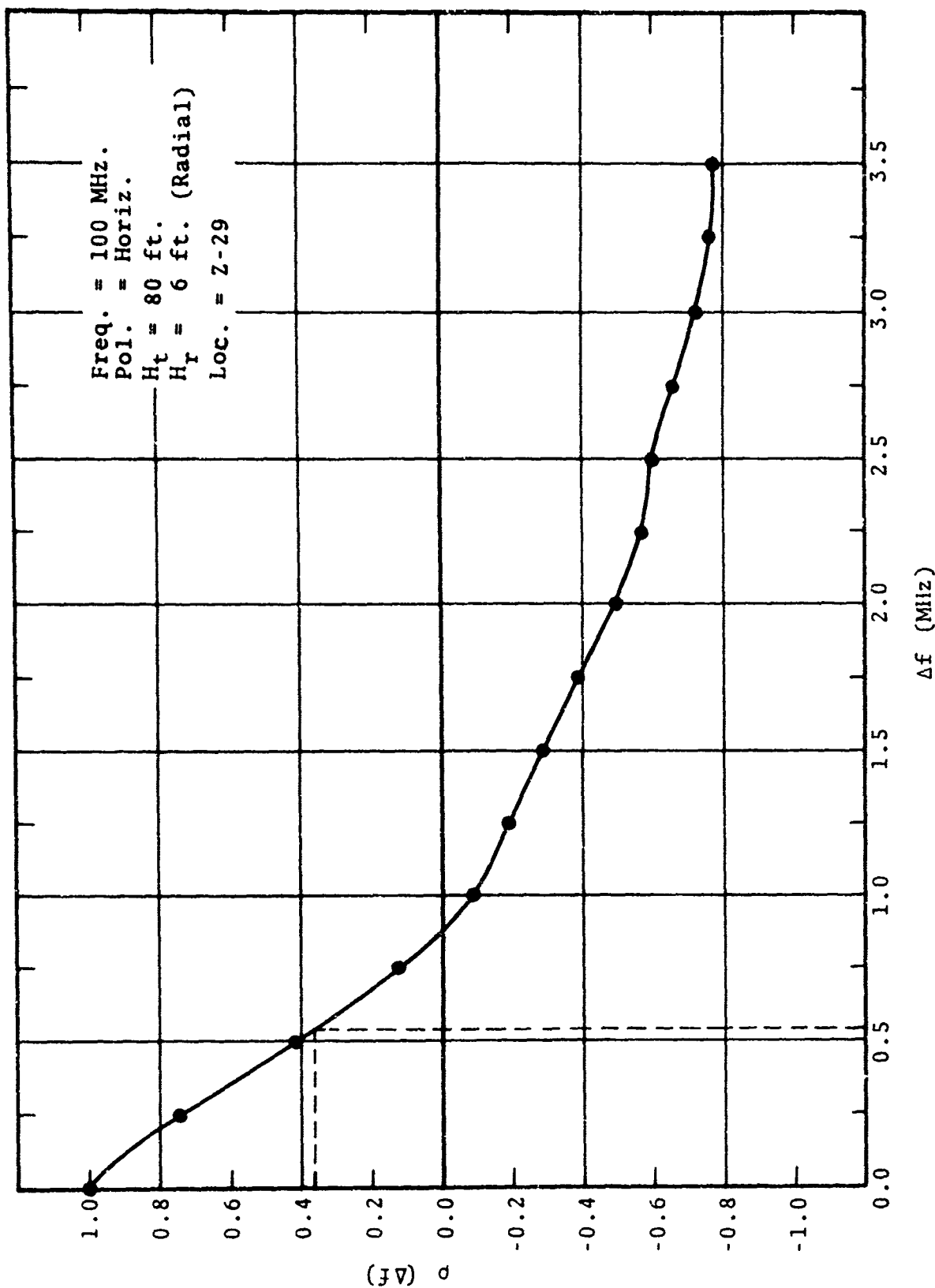


Figure 4.2.15 Normalized Frequency Correlation Coefficient

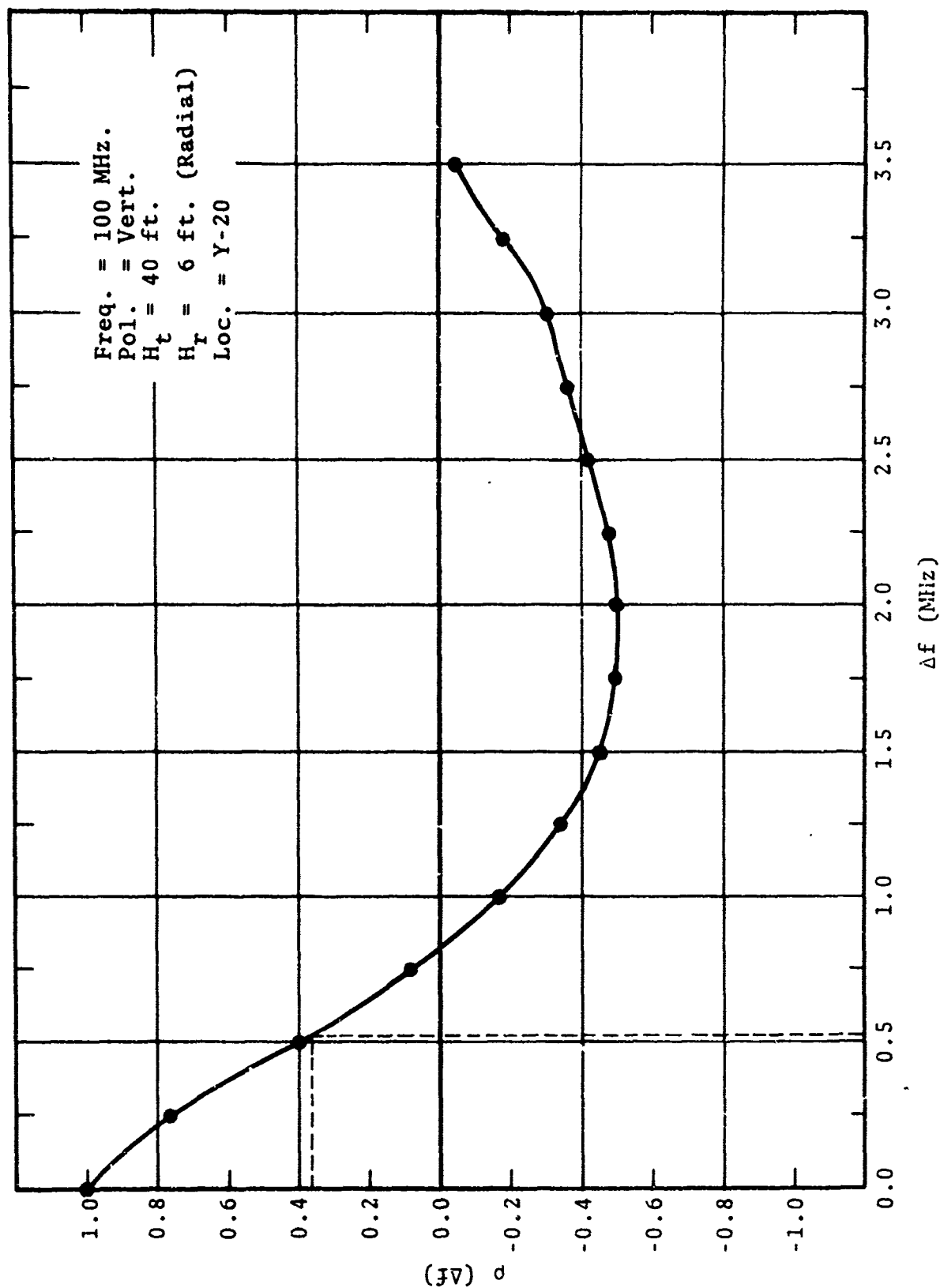


Figure 4.2.16 Normalized Frequency Correlation Coefficient

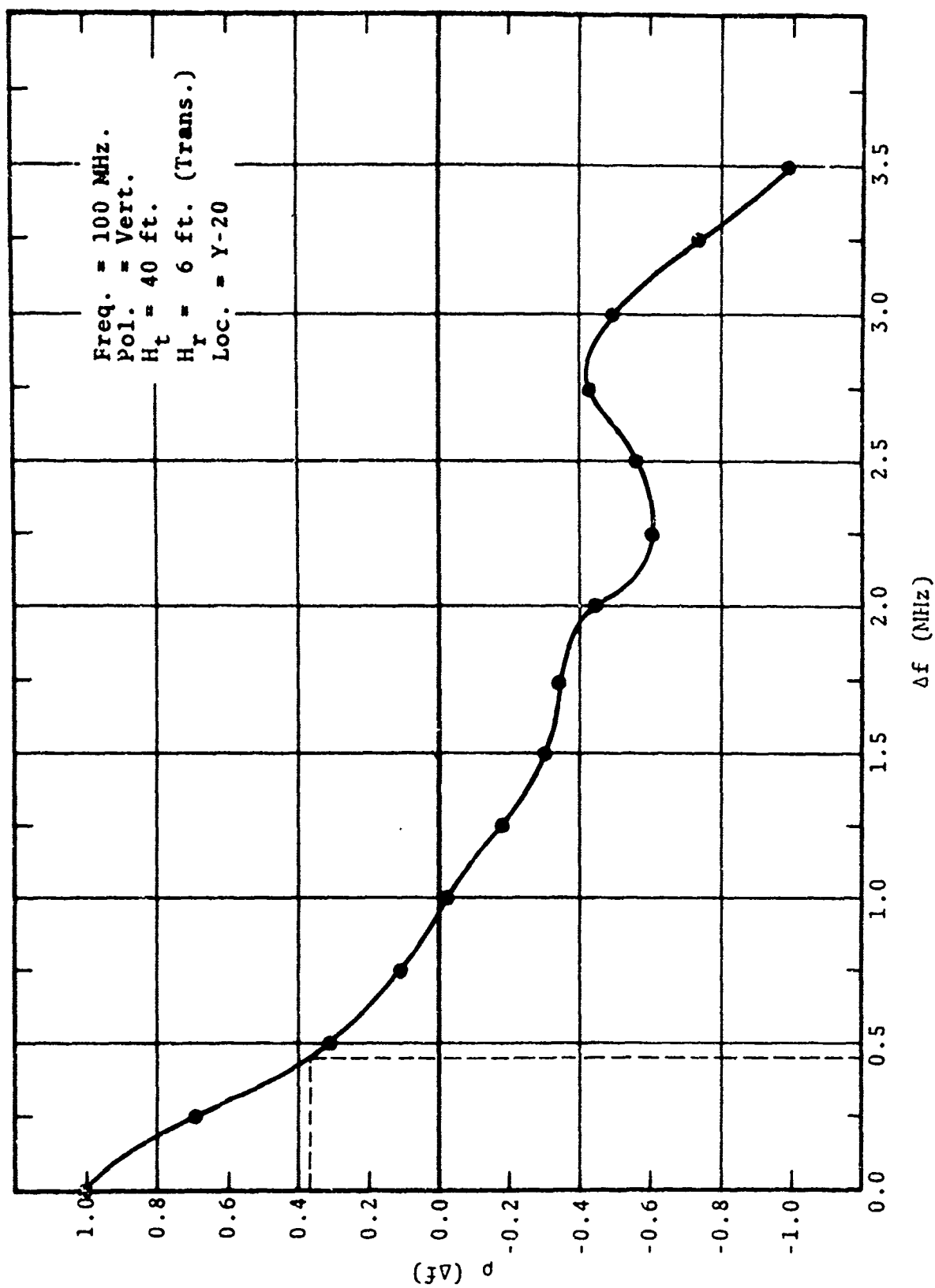


Figure 4.2.17 Normalized Frequency Correlation Coefficient

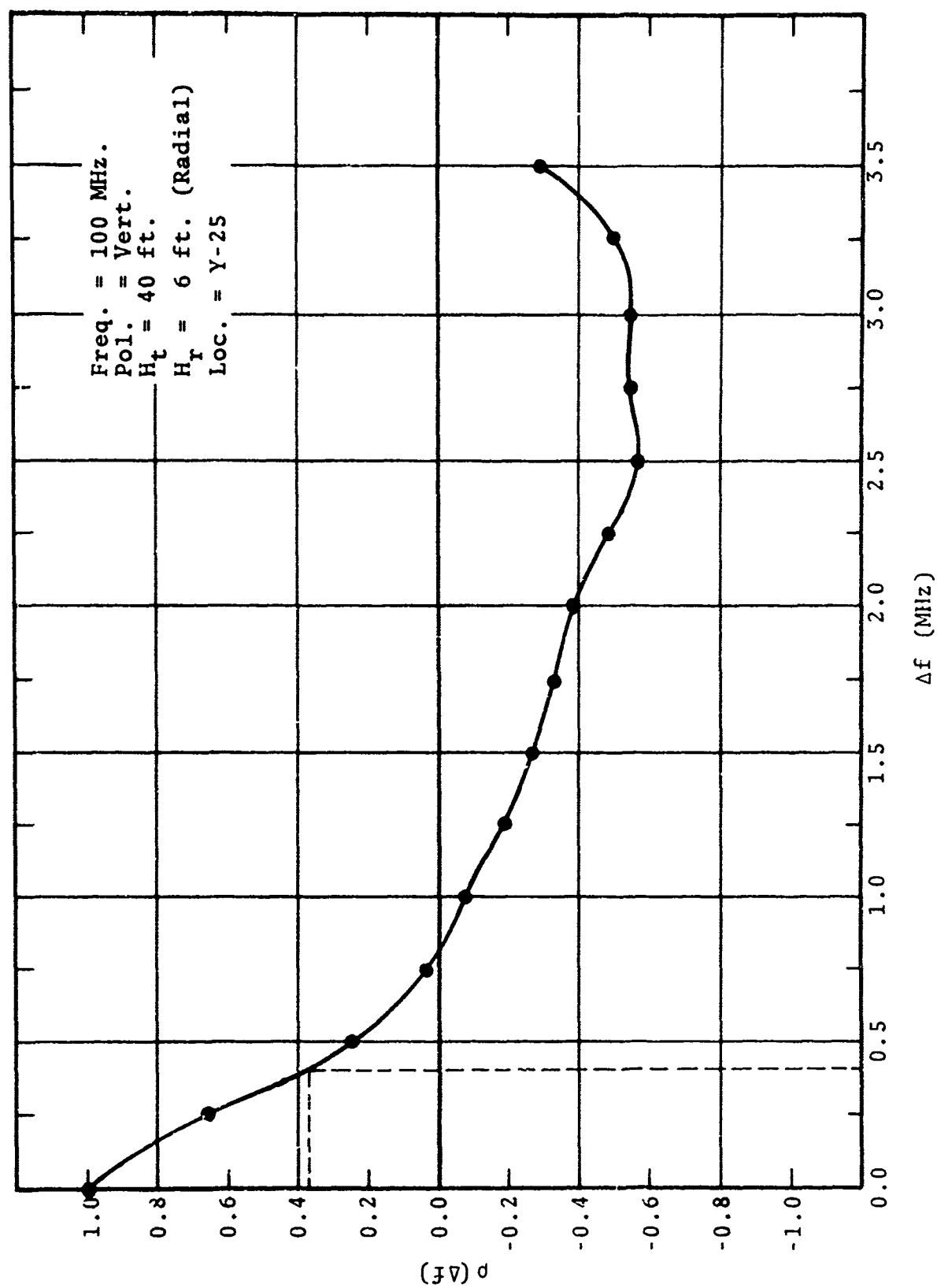


Figure 4.2.18 Normalized Frequency Correlation Coefficient

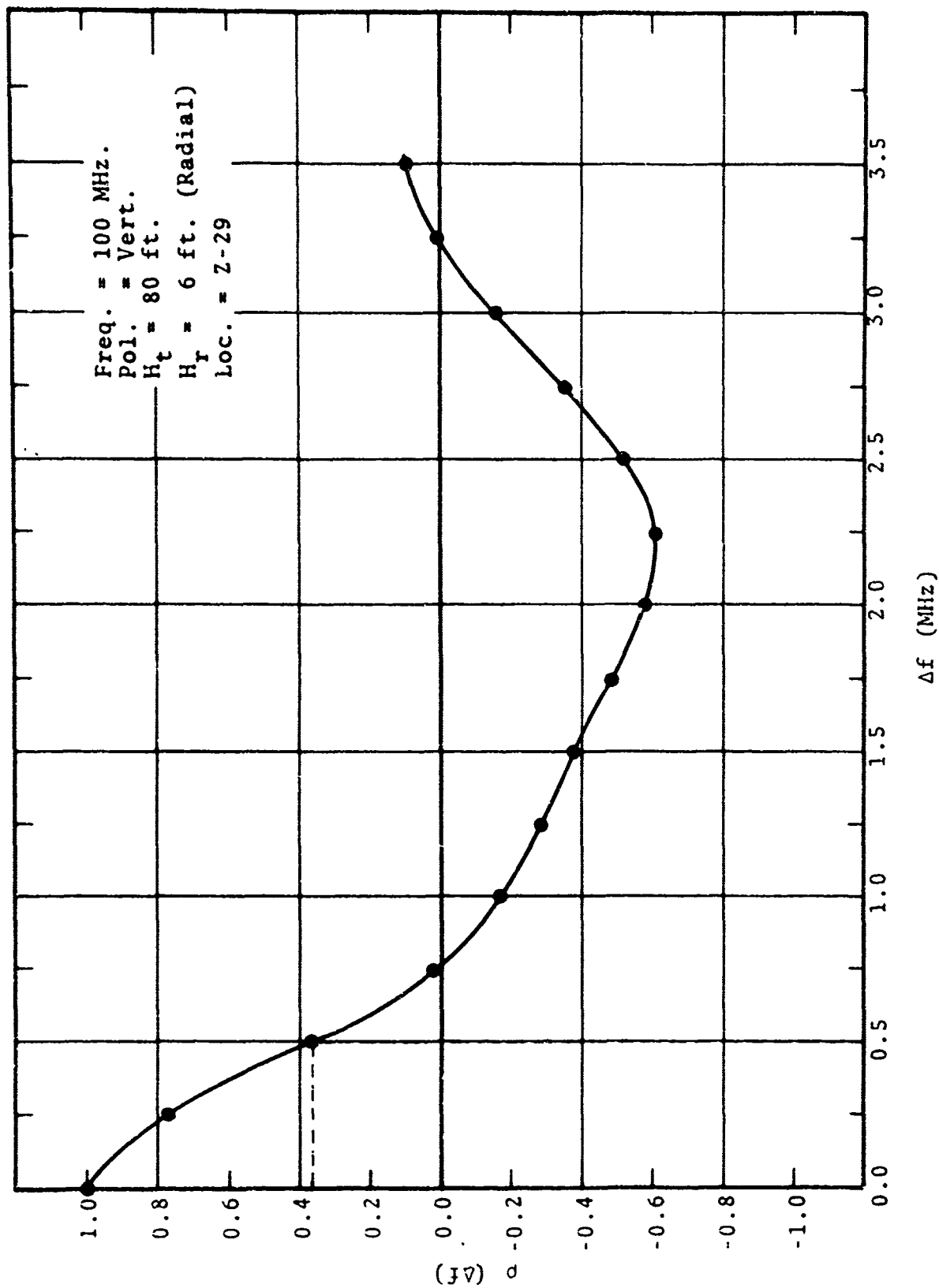


Figure 4.2.19 Normalized Frequency Correlation Coefficient

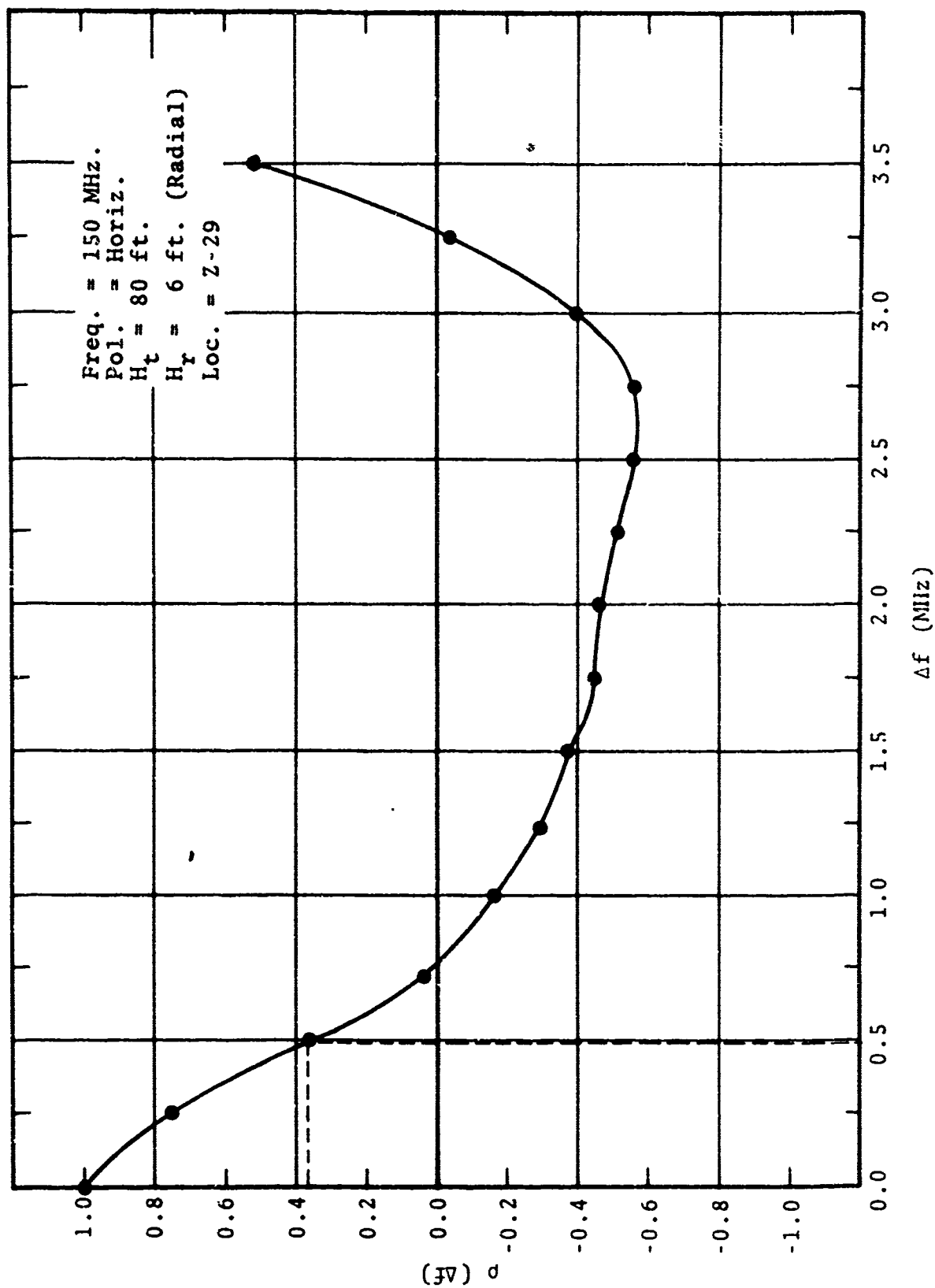


Figure 4.2.20 Normalized Frequency Correlation Coefficient

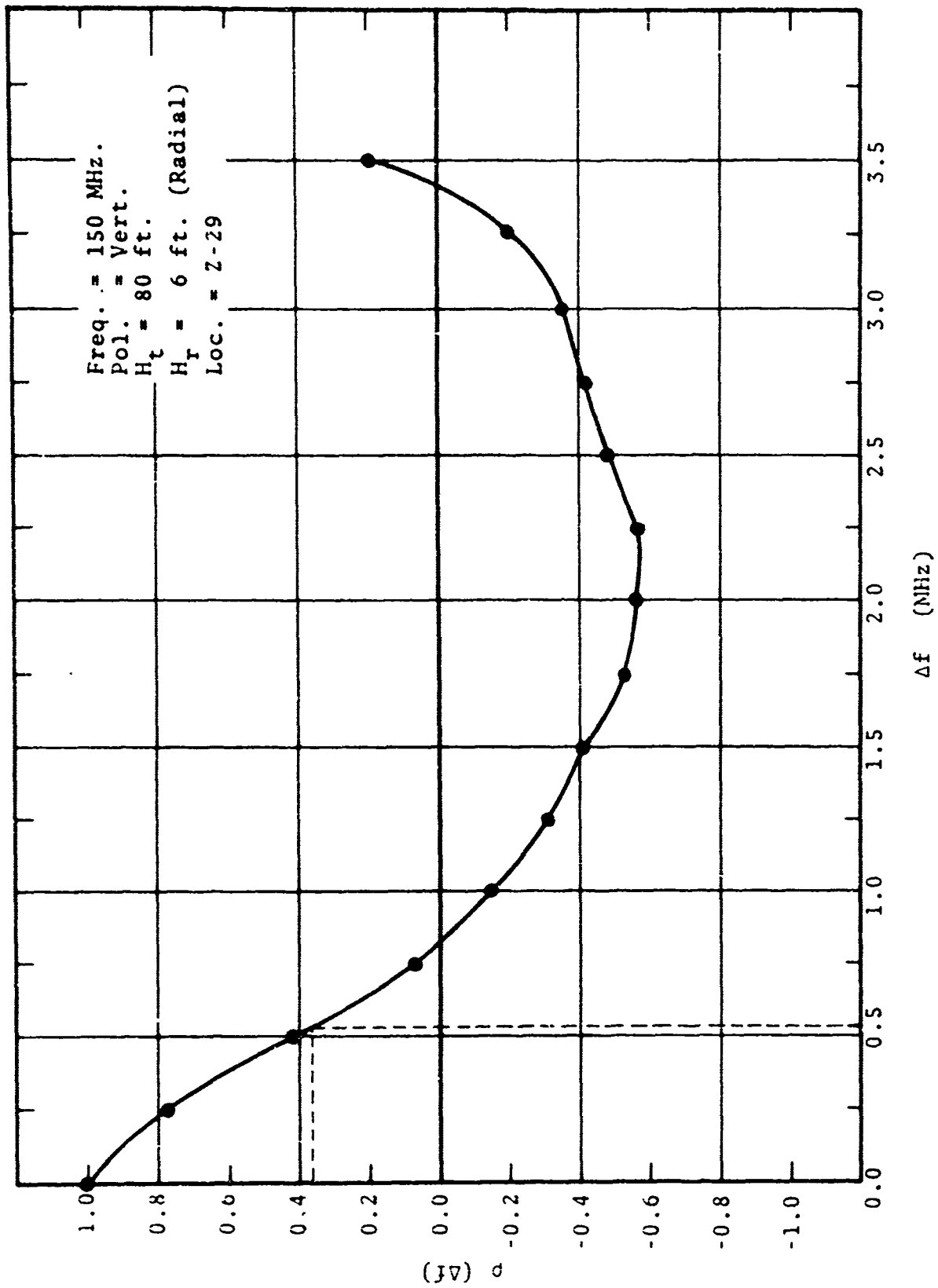


Figure 4.2.21 Normalized Frequency Correlation Coefficient

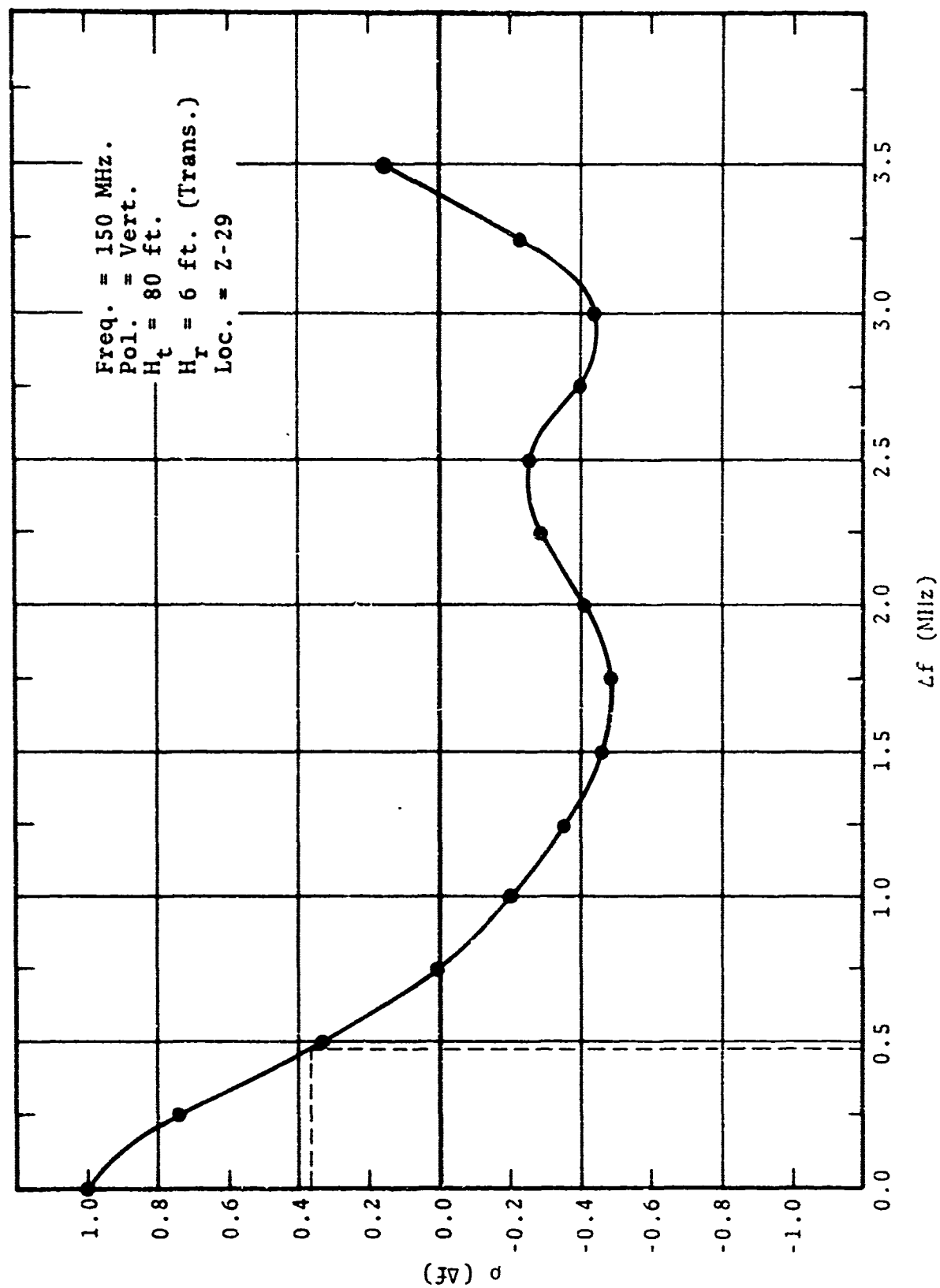


Figure 4.2.22 Normalized Frequency Correlation Coefficient

Table 4.2.1
Values of Coherent Bandwidth BW_C for Different Operational Configurations

Frequency (MHz)	Polarization H=Horiz. V=Vert.	Location of Receiver (Field Point)				Average BW _C (MHz)
		Y-20 BW _C (MHz)	Y-25		Z-29 BW _C (MHz)	
			BW _C (MHz)	BW _C (MHz)		
50	H	0.55	0.52		0.59	0.55
		0.48 (T)				0.48 (T)
50	V	0.44	0.33		0.49	0.42
		0.48 (T)				0.48 (T)
100	H	0.31	0.36		0.54	0.40
		0.36 (T)				0.36 (T)
100	V	0.52	0.41		0.50	0.48
		0.45 (T)				0.45 (T)
150	H				0.49	
150	V				0.53	0.53
					0.49 (T)	0.49 (T)
Average	BW _C (MHz)	0.45	0.41		0.53	0.46

(T) denotes transverse path; otherwise path was radial.

5. REFERENCES

1. Tropical Propagation Research, Jansky & Bailey Engineering Department, Atlantic Research Corporation, Final Report, Volume I, 1966.
2. A Conducting-Slab Model for Electromagnetic Propagation Within a Jungle Medium, by D. L. Sachs and P. J. Wyatt, General Research Corporation, Technical Memorandum, May, 1966 (AD 679-171). Also, Radio Science, pp 125-134, February, 1968.
3. A Conducting-Slab Model for Electromagnetic Propagation Within a Jungle Medium, II, by D. L. Sachs, General Corporation, Internal Memorandum 471, 30 Sept., 1966. Also, Theory of Radio Propagation in a Jungle Environment, by D. L. Sachs, General Research Corporation Technical Memorandum 1011, January, 1969.
4. On Radio-Wave Propagation in Forest Environments, by Theodor Tamir, IEEE Transactions on Antennas and Propagation, Volume AP-15, No. 6, November, 1967.
5. Tropical Propagation Research, Final Report, Volume II, by Hicks et al., Jansky & Bailey Engineering Department, Atlantic Research Corporation, Contract DA 36-039 SC-90889, 1969.
6. The Probability Distribution of the Amplitude of a Constant Vector Plus a Rayleigh-Distributed Vector, by K. A. Norton, L. E. Vogler, W. V. Mansfield, and P. J. Short, Proc. IRE, Volume 43, No. 10, October 1955.
7. Modern Communications Principles, by Seymour Stein and J. Jay Jones, McGraw-Hill, 1967, 382 pp.
8. Communications Systems and Techniques, by Mischa Schwartz, William R. Bennett and Seymour Stein, McGraw-Hill, 1966, 618 pp.
9. Tropical Propagation Research, Semiannual Reports 1 - 10, Jansky & Bailey Engineering Department, Atlantic Research Corporation, Contract DA 36-039 SC-90889.

10. Pulse Transmissions at VHF in a Tropical Rain Forest -
Tropical Propagation Research, Semiannual Report No. 11,
by John J. Hicks and Richard G. Robertson, Jansky & Bailey
Engineering Department, Atlantic Research Corporation,
Contract DA 36-039 SC-90889, 1969.
11. Binary Error Probability Due to an Adaptable Fading Model,
by M. Nesenbergs, IEEE Trans. on Comm. Systems, March,
1965.

UNCLASSIFIED

Security Classification

DOCUMENT CONTROL DATA - R & D

(Security classification of title, body of abstract and indexing annotation must be entered when the overall report is classified)

1. ORIGINATING ACTIVITY (Corporate author) Atlantic Research Corporation A Division of The Susquehanna Corporation J&B Engineering Department Shirley Hwy. at Edsall Rd. Alexandria, Va. 22314		2a. REPORT SECURITY CLASSIFICATION UNCLASSIFIED	
3. REPORT TITLE Tropical Propagation Research (U)		2b. GROUP	
4. DESCRIPTIVE NOTES (Type of report and inclusive dates) Final Report, Volume III			
5. AUTHOR(S) (First name, middle initial, last name) Richard G. Robertson John J. Hicks Charles B. Sykes Per A. Anti			
6. REPORT DATE	7a. TOTAL NO. OF PAGES 130	7b. NO. OF REFS 11	
8a. CONTRACT OR GRANT NO. DA 36-039 SC-90889 A. PROJECT NO.		8b. ORIGINATOR'S REPORT NUMBER(S)	
c. d.		8c. OTHER REPORT NO(S) (Any other numbers that may be assigned this report)	
10. DISTRIBUTION STATEMENT This document has been approved for public release and sale; its distribution is unlimited.			
11. SUPPLEMENTARY NOTES		12. SPONSORING MILITARY ACTIVITY Advanced Research Projects Agency Washington, D.C. and U.S. Army Electronics Command Fort Monmouth, N.J.	
13. ABSTRACT <p>This Final Report Volume III is sequential to Volumes I and II previously prepared on an extensive experimental and theoretical research program on the propagation of radio signals in tropical jungle environments. The over-all objective of this program is to collect and analyze radio propagation data from actual representative environments needed to advance the state-of-the-art in the design and development of improved radio communication systems in these environments.</p> <p>This Final Report summarizes the results of a series of specialized measurements, using pulse and swept-frequency transmitted signals. Various types of amplitude, frequency, and phase displays were recorded at the test receiver locations. The objective of these measurements was to obtain data which exhibit the multipath characteristics of the jungle path.</p> <p>This report discusses the methods of making these measurements, and the results of a limited analysis of the data. The probability distributions of signal amplitude at VHF in the tropical rain forest test area in Thailand are presented. These distributions are generally a prerequisite to the practical estimation of error rate performance of digital, or wideband, systems in this type of environment. An example is given in which the experimental probability distributions are used to obtain the error rate in an FSK modulation system in this type of environment.</p>			

DD FORM 1473

REPLACES DD FORM 1473, 1 JAN 64, WHICH IS OBSOLETE FOR ARMY USE.

UNCLASSIFIED

Security Classification

UNCLASSIFIED

Security Classification

14

KEY WORDS

LINK A

LINK B

LINK C

ROLE

WT

ROLE

WT

ROLE

WT

Propagation
Techniques
Tropical Environment
SEA - Southeast Asia
Thailand
SEACORE

UNCLASSIFIED

Security Classification